Advanced NMR & Imaging

Week 13: Solid-state NMR

Objectives

- Learn more about anisotropy
- Learn about coherent averaging
- Know what magic-angle-spinning (MAS) is

What's the Problem?

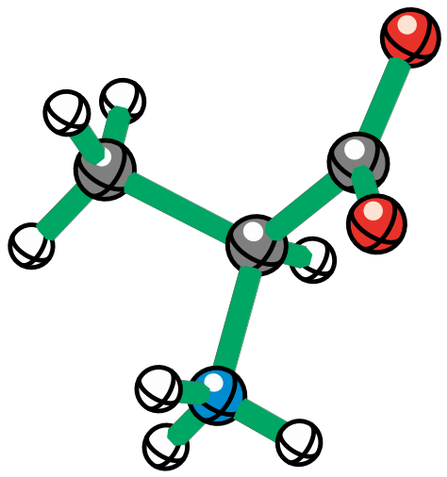

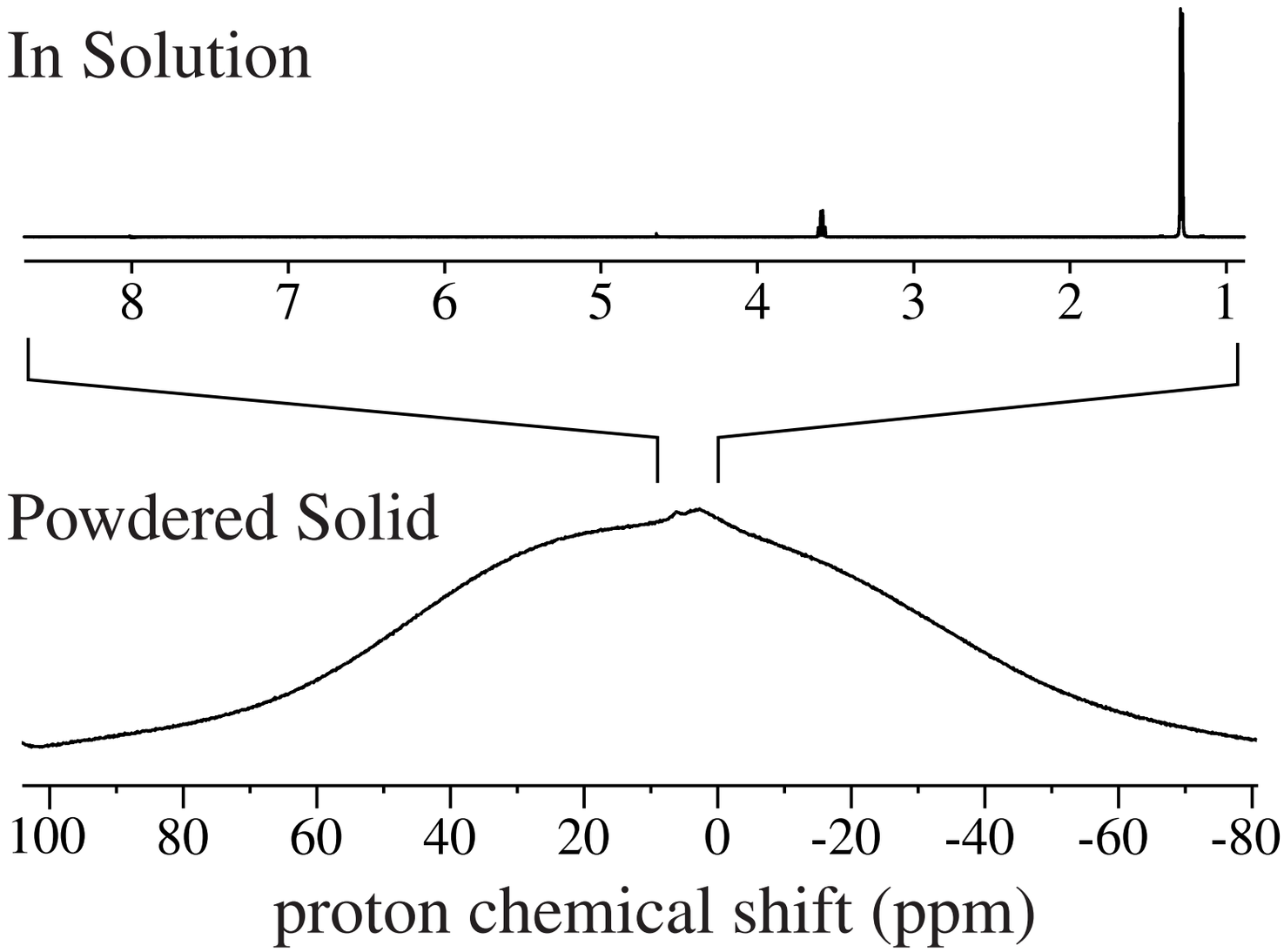

Solid-State NMR: Why is it different?

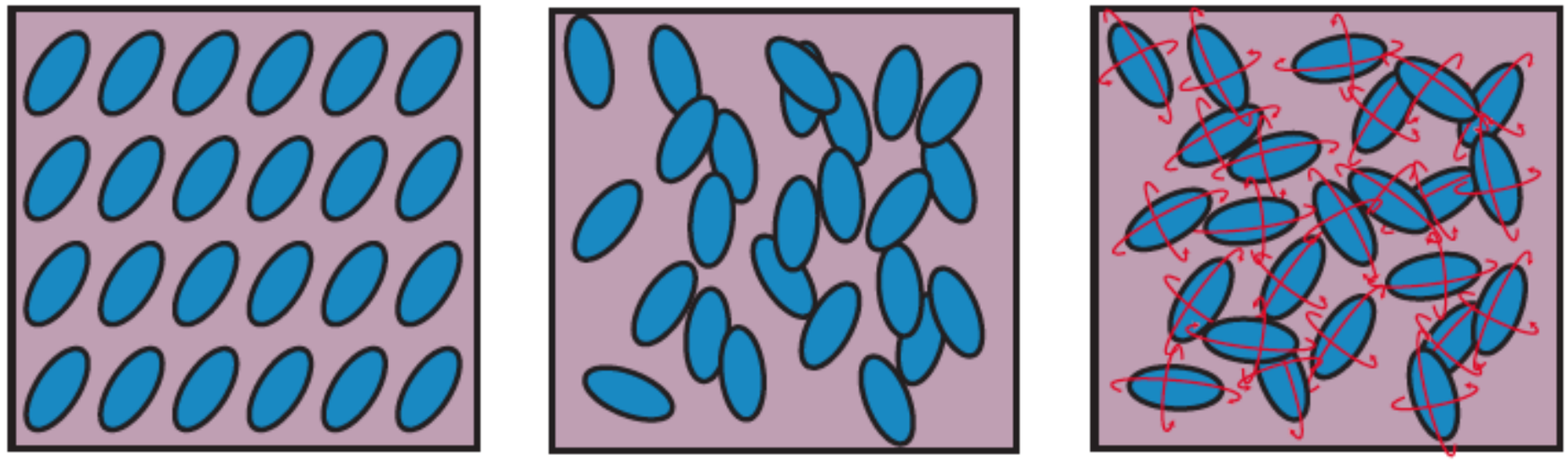

The only difference between solids and liquids, for NMR,
is the presence or absence of rapid molecular motion.

Recall Last Week: NMR interactions are anisotropic

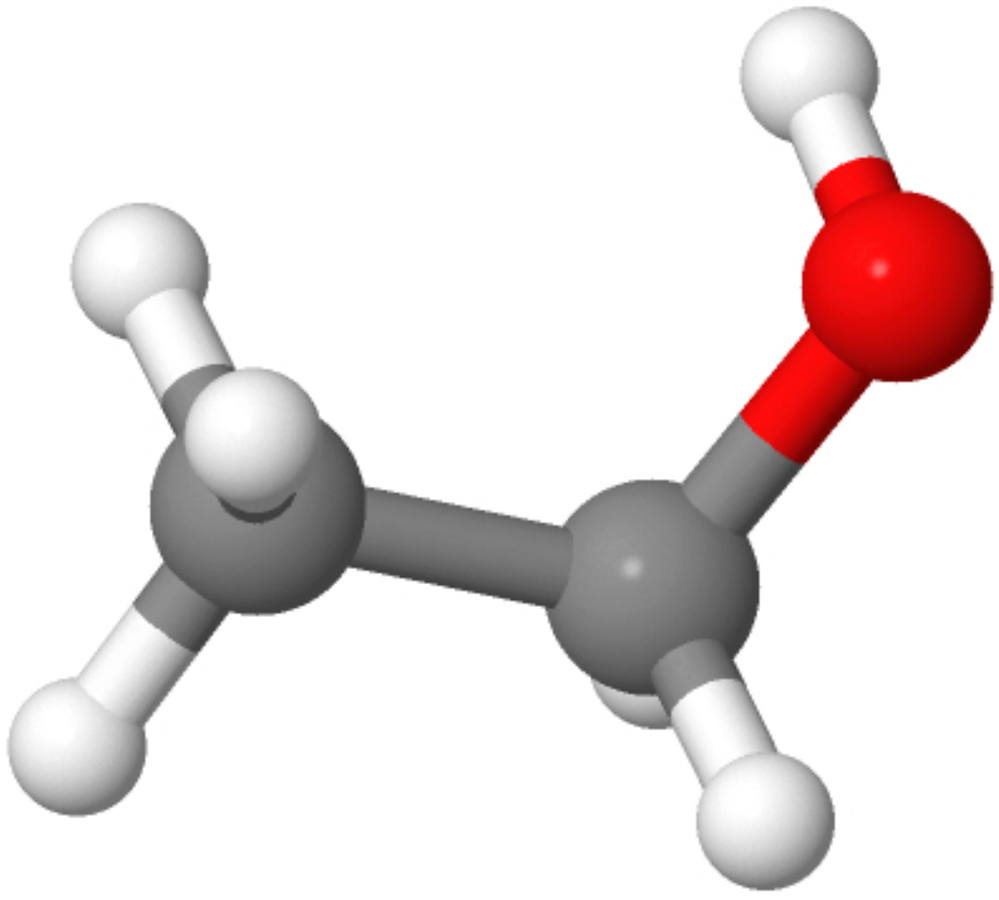

Consider the chemical shift of the CH_2 carbon resonance in ethanol

Recall Last Week: NMR interactions are anisotropic

	s ($\ell = 0$)	p ($\ell = 1$)			d ($\ell = 2$)					f ($\ell = 3$)						
	$m = 0$	$m = 0$	$m = \pm 1$		$m = 0$	$m = \pm 1$		$m = \pm 2$		$m = 0$	$m = \pm 1$		$m = \pm 2$		$m = \pm 3$	
	s	p_z	p_x	p_y	d_{z^2}	d_{xz}	d_{yz}	d_{xy}	$d_{x^2-y^2}$	f_{z^3}	f_{xz^2}	f_{yz^2}	f_{xyz}	$f_{z(x^2-y^2)}$	$f_{x(x^2-3y^2)}$	$f_{y(3x^2-y^2)}$
$n = 1$																
$n = 2$	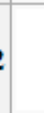															
$n = 3$	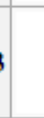		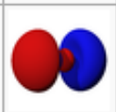					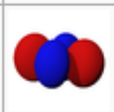								
$n = 4$	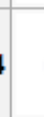		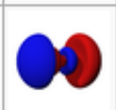			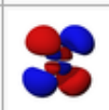		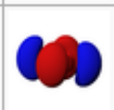	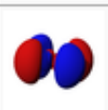				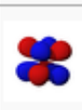		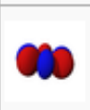	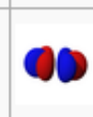
$n = 5$	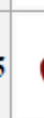			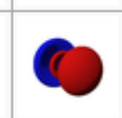		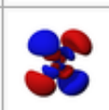		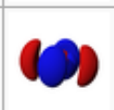	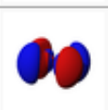	...	...	...	...	...	...	...
$n = 6$					...	...	...	...	...	...	...	...	...	...	...	...
$n = 7$		...	...	...	...	...	...	...	...	...	...	...	...	...	...	...

The chemical shift can be thought of as the shielding of the nucleus from the external magnetic field by the electrons.

The magnetic field is a vector quantity (the magnetic field has a well defined direction). The electronic distribution around the nucleus is highly ***anisotropic***.

Therefore the chemical shift must depend on the orientation of the molecule with respect to the magnetic field.

Recall Last Week: NMR interactions are anisotropic

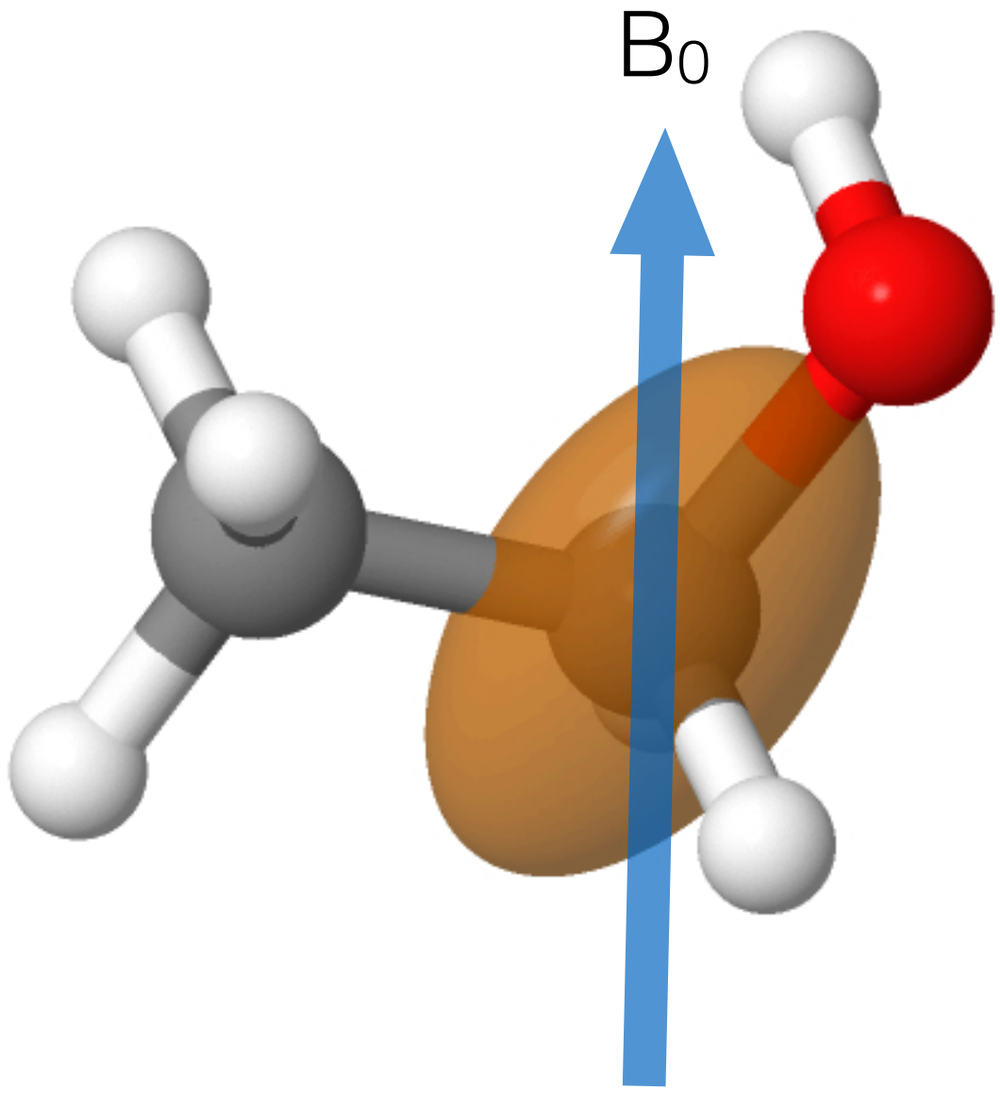

Here we show the chemical shift tensor as an ellipsoid superimposed on the molecular structure.

The shift tensor is fixed in the molecular frame.

Reminder: Shielding (σ) is related to chemical shift (δ) by:
$\delta \propto (1 - \sigma)$

The chemical shift is anisotropic. It is not described by a single number, but by a second rank spatial tensor, defined by the three principal values of the tensor and the angles that define the orientation of the principle values in the molecular reference frame.

Recall Last Week: NMR interactions are anisotropic

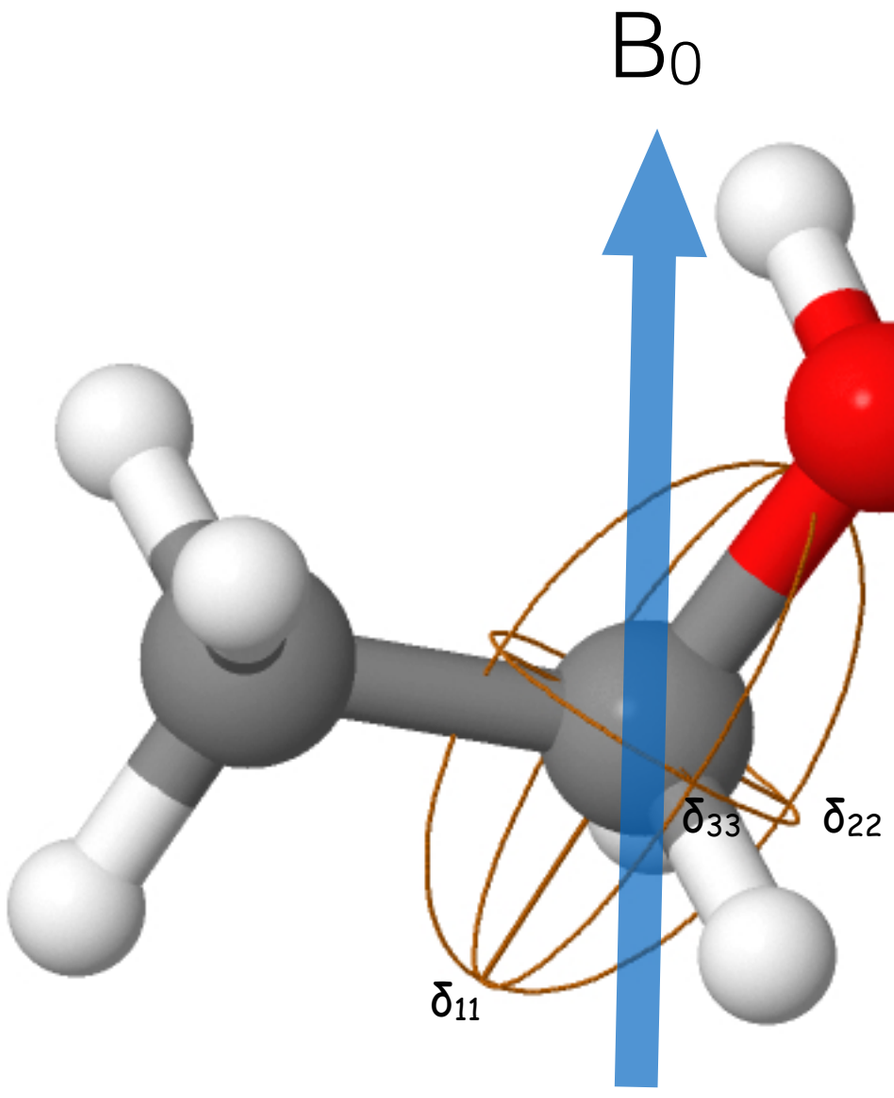

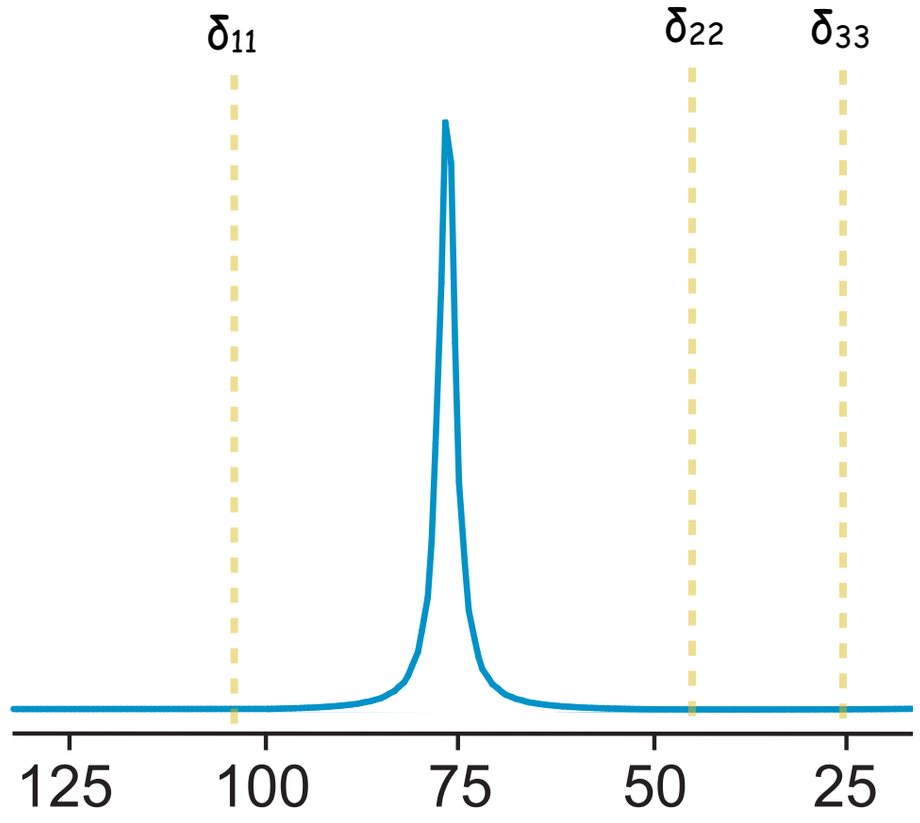

δ_{11} = 104 ppm ; δ_{22} = 44 ppm ; δ_{33} = 25 ppm (by convention $\delta_{11} > \delta_{22} > \delta_{33}$)

The chemical shift is anisotropic. It is not described by a single number, but by a second rank spatial tensor, defined by the three principal values of the tensor and the angles that define the orientation of the principle values in the molecular reference frame.

Single Crystal NMR

What are the chemical shifts for a single crystal of durene at a given orientation?

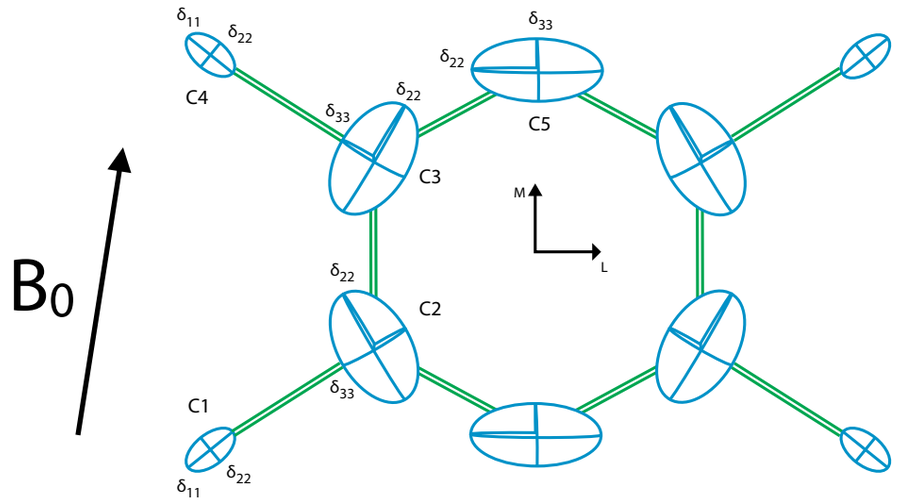

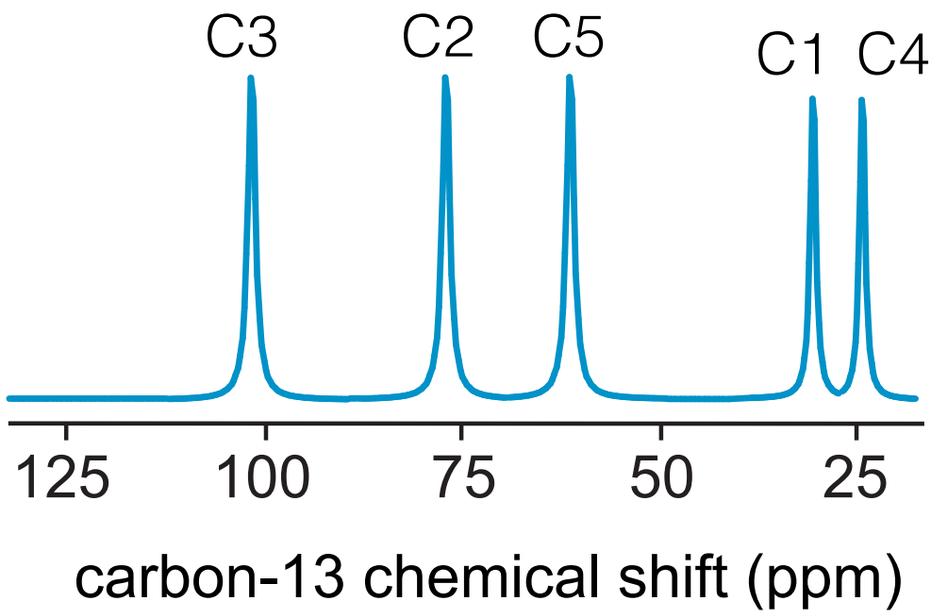

Single Crystal NMR

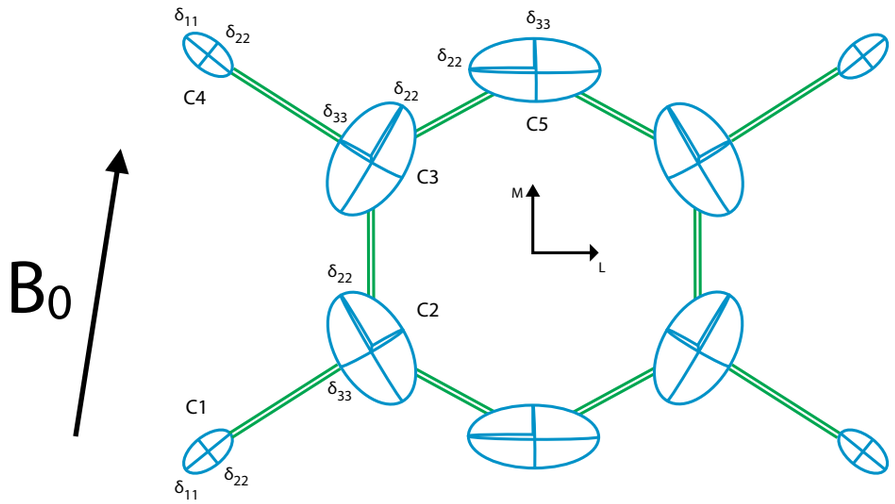

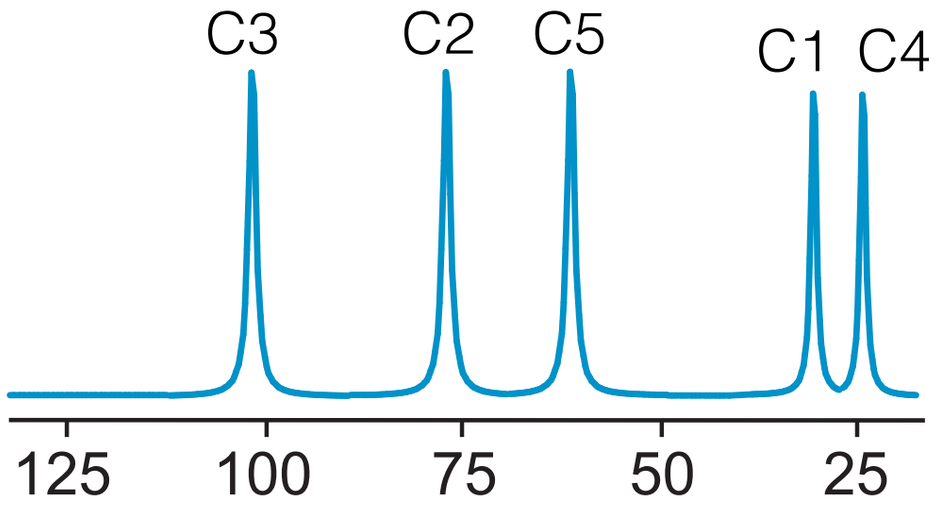

carbon-13 chemical shift (ppm)

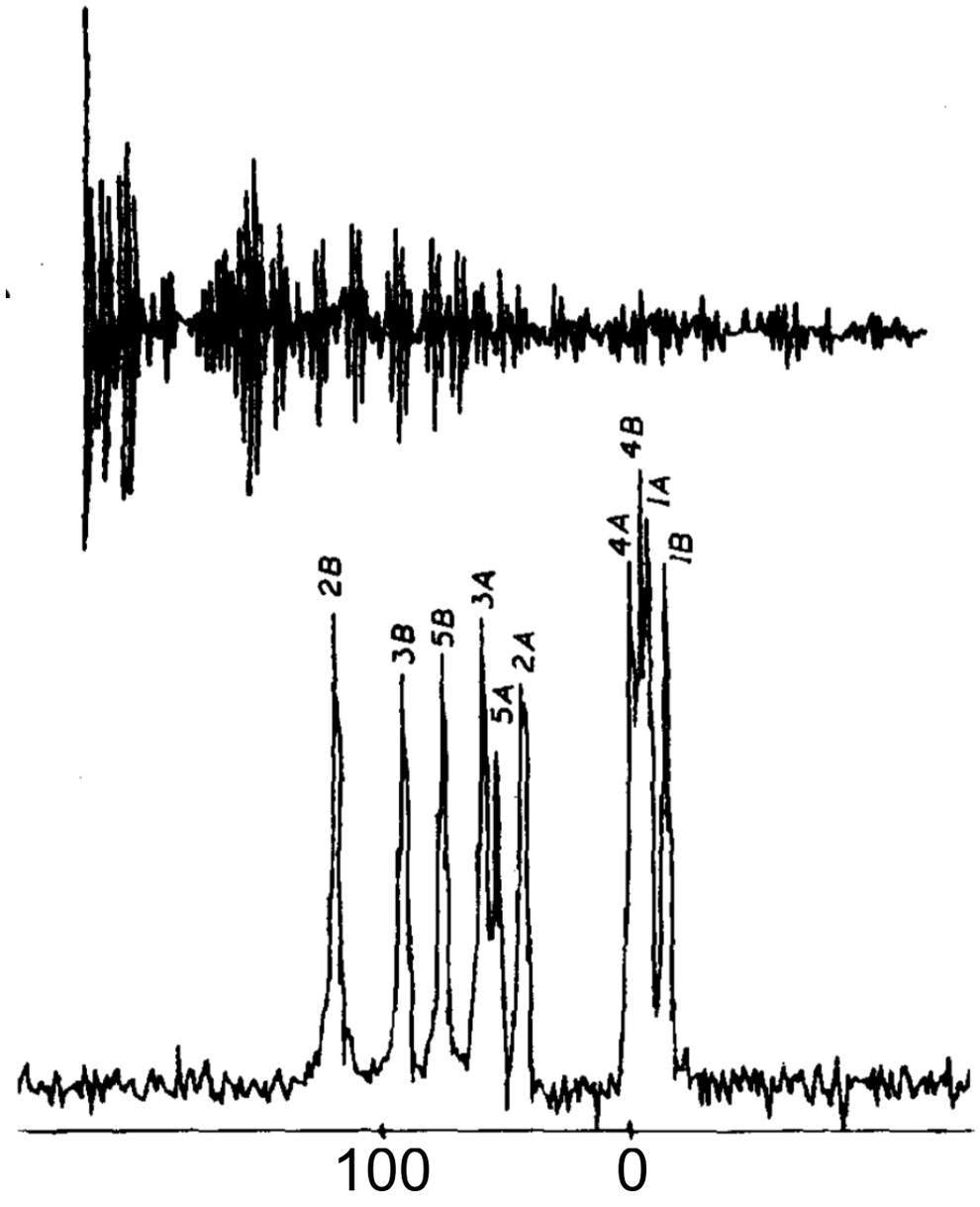

carbon-13 chemical shift (ppm)

Why are there 10 peaks in the experimental spectrum?

Powder Spectra

What does the spectrum of a powder look like?

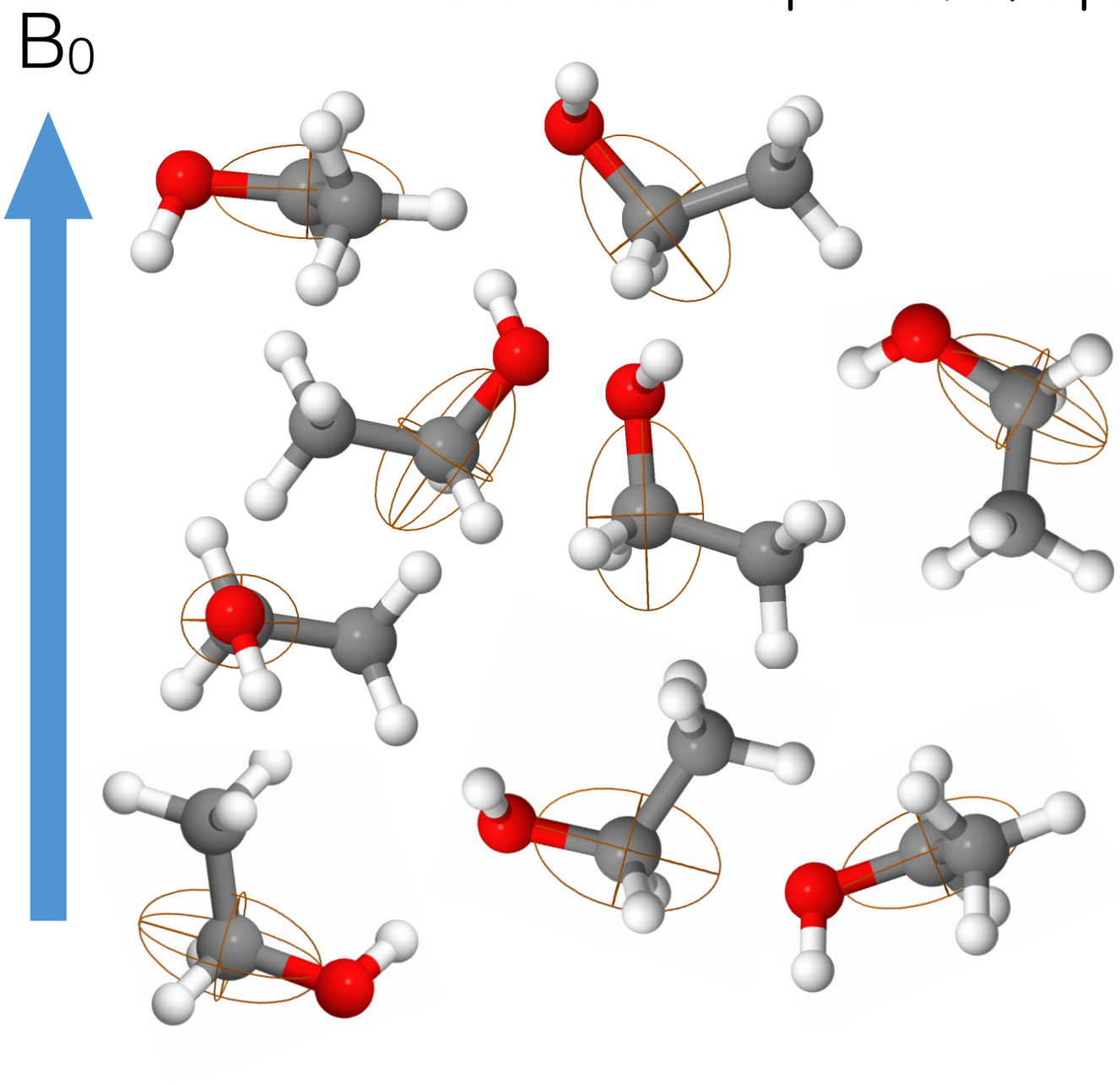

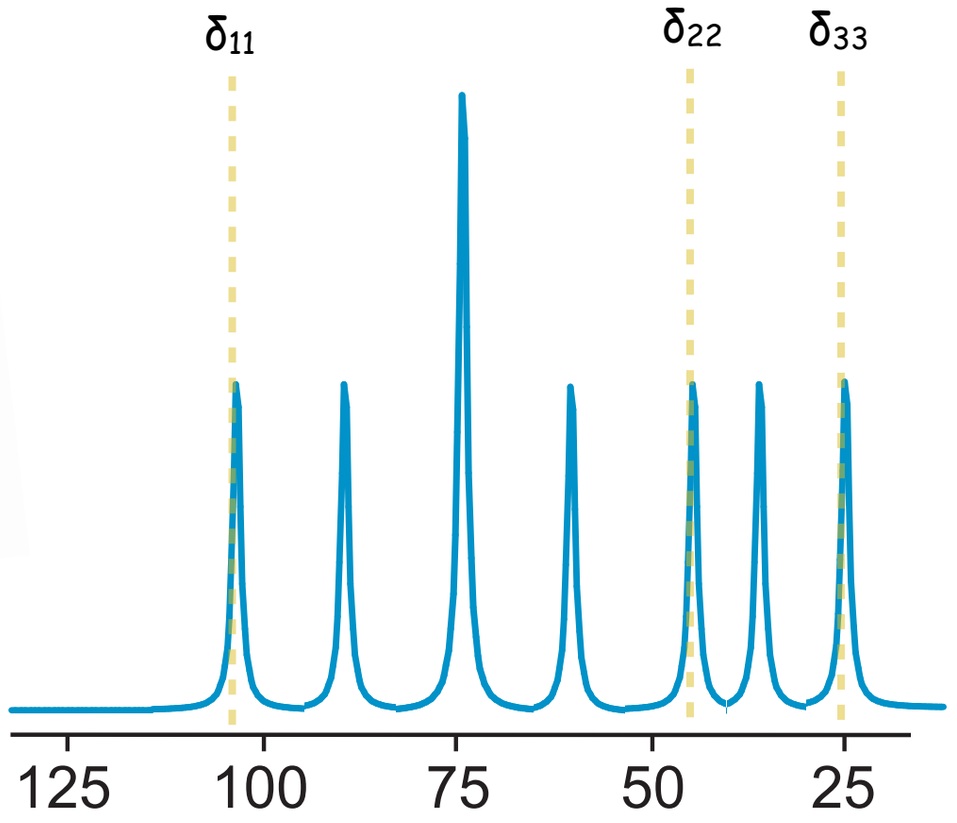

Powder Spectra

$$I(\omega) = \int_0^{2\pi} \int_0^{\pi} \delta(\omega - \omega_{zz}) p(\Omega) d\alpha \sin\beta d\beta$$

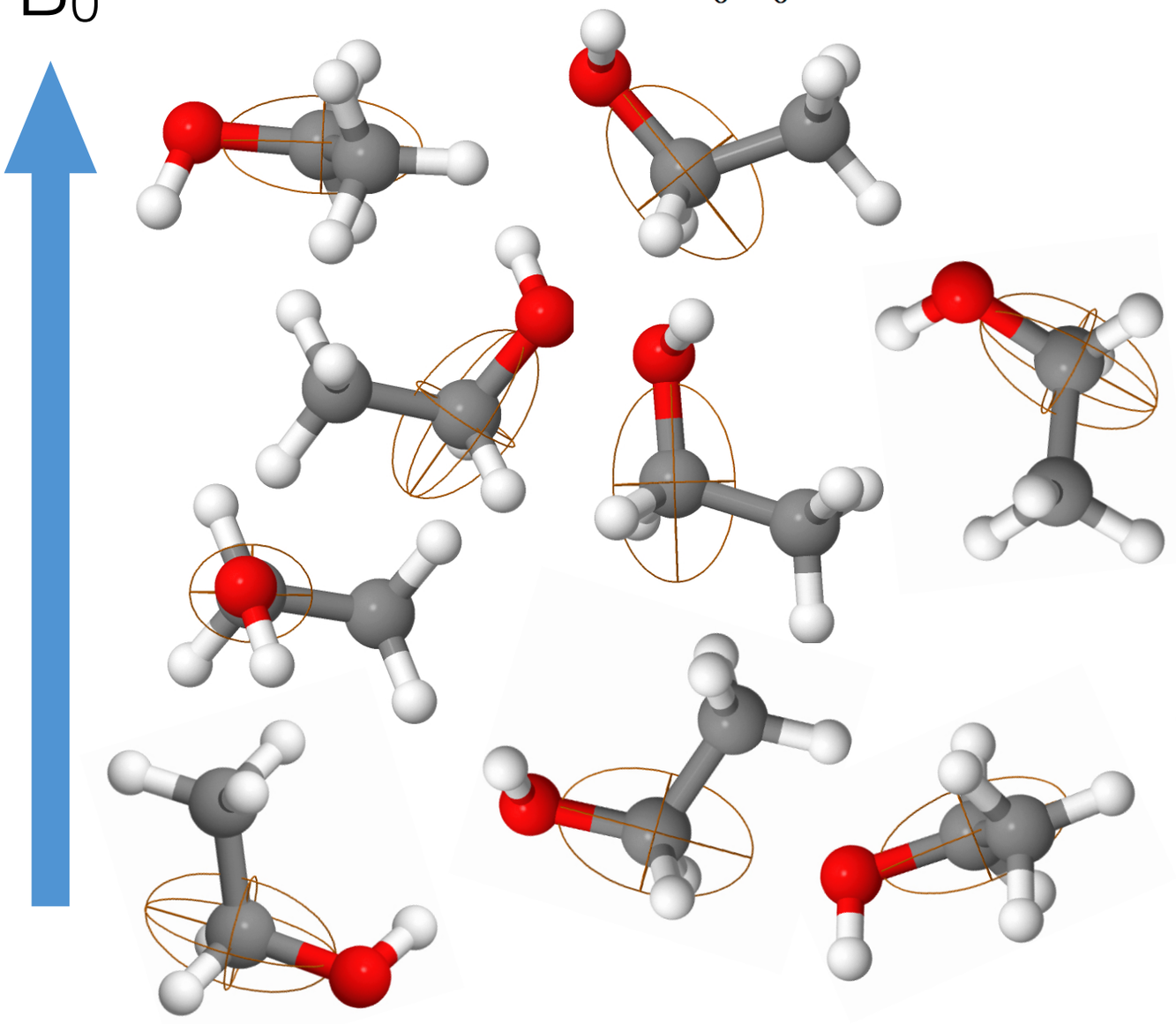

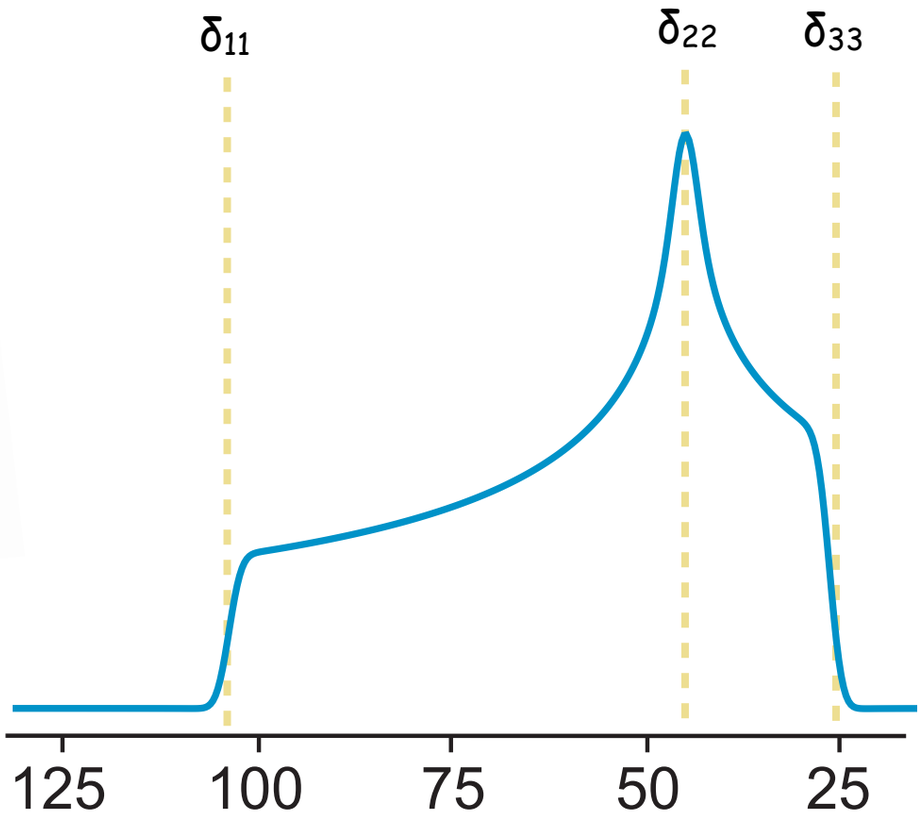

where $p(\Omega)$ is the probability of finding a particular crystallite orientation and ω_{zz} is the observed frequency for that orientation. In a powder sample, all orientations are present with equal probability.

Powder Spectra

$$I(\omega) = \int_0^{2\pi} \int_0^{\pi} \delta(\omega - \omega_{zz}) p(\Omega) d\alpha \sin\beta d\beta$$

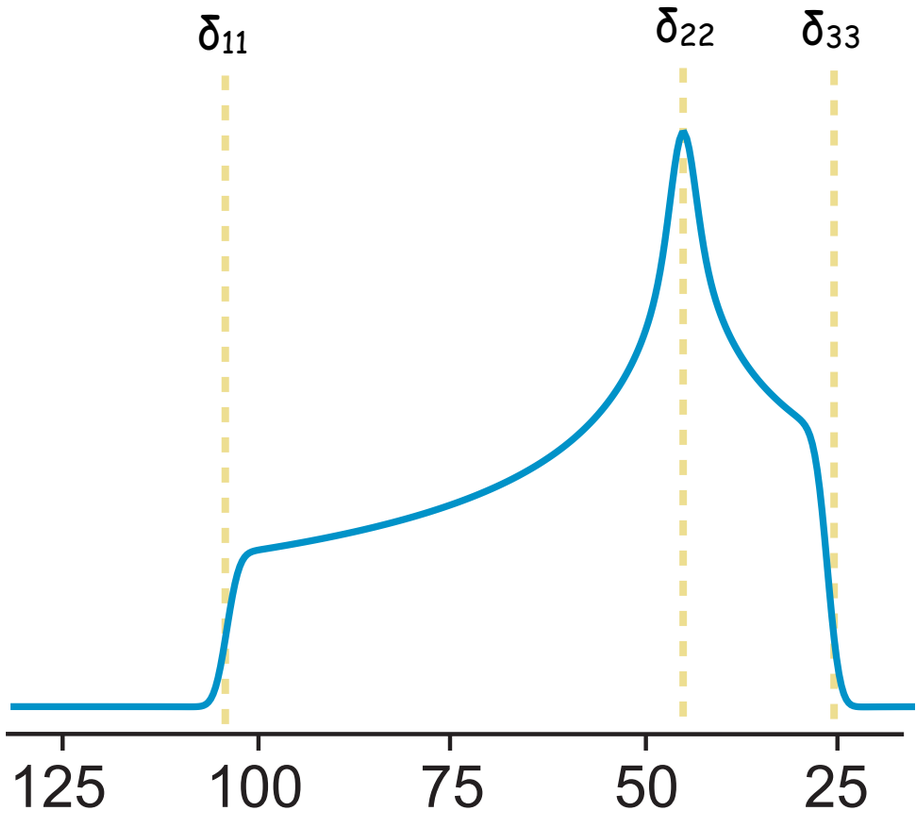

Chemical shift principle values (but not orientations) are available from powder spectra by simple inspection.

Powder Spectra

Chemical shift principle values (but not orientations) are available from powder spectra by simple inspection.

We refer to the special cases where $\delta_{11} = \delta_{22}$ or $\delta_{22} = \delta_{33}$ as axially symmetric tensors.

The CSA tensor principle values are often expressed in terms of the isotropic shift, δ_{iso}, span, Ω, and skew, κ :

$$\delta_{iso} = (\delta_{11} + \delta_{22} + \delta_{33})/3$$

$$\Omega = \delta_{11} - \delta_{33}$$

$$\kappa = 3(\delta_{22} - \delta_{iso})/\Omega$$

Ω will always be larger than or equal to 0. It measures the overall degree of anisotropy. κ will range from -1 to 1 and it measures the deviation from axial symmetry.

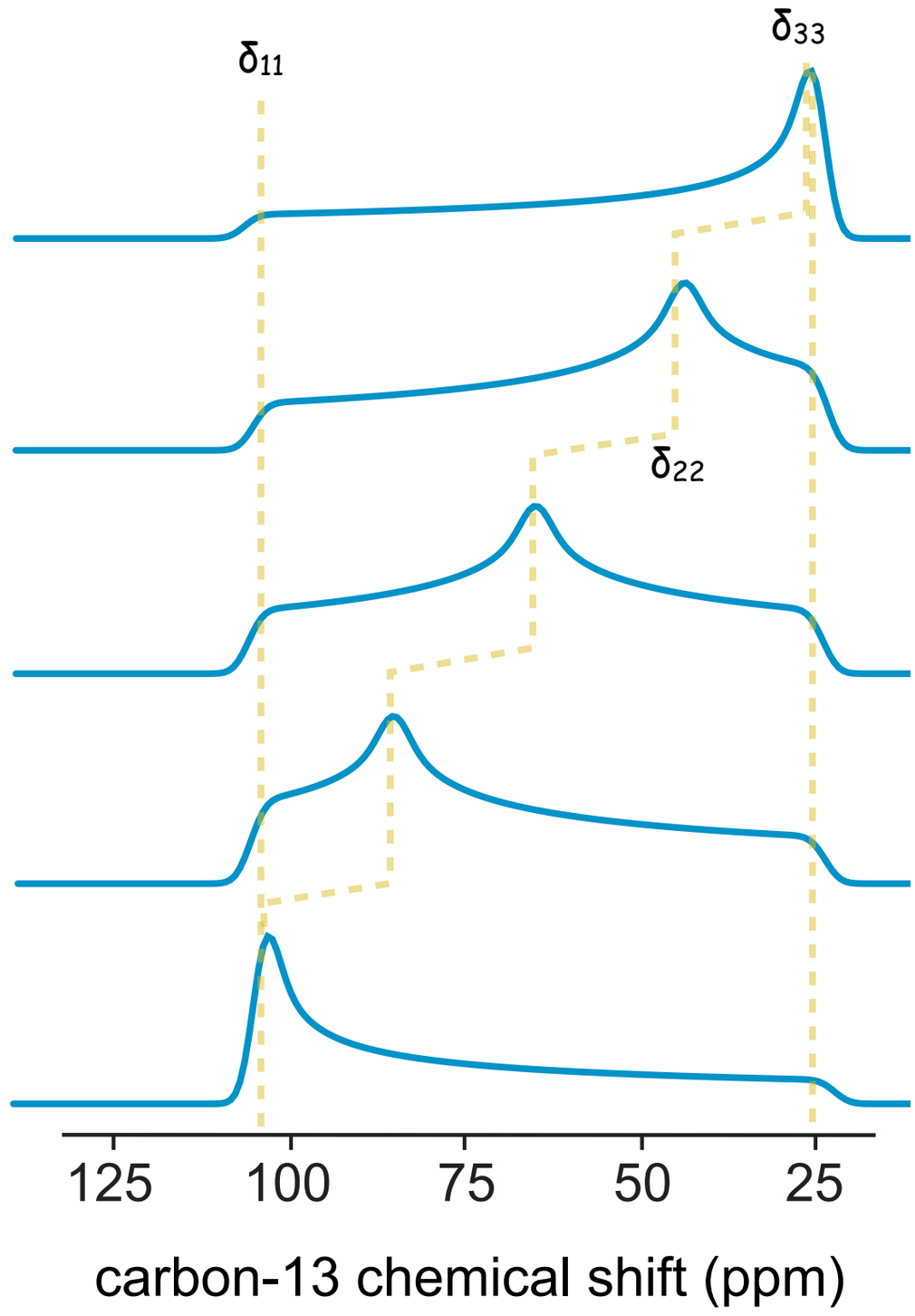

Powder Spectra

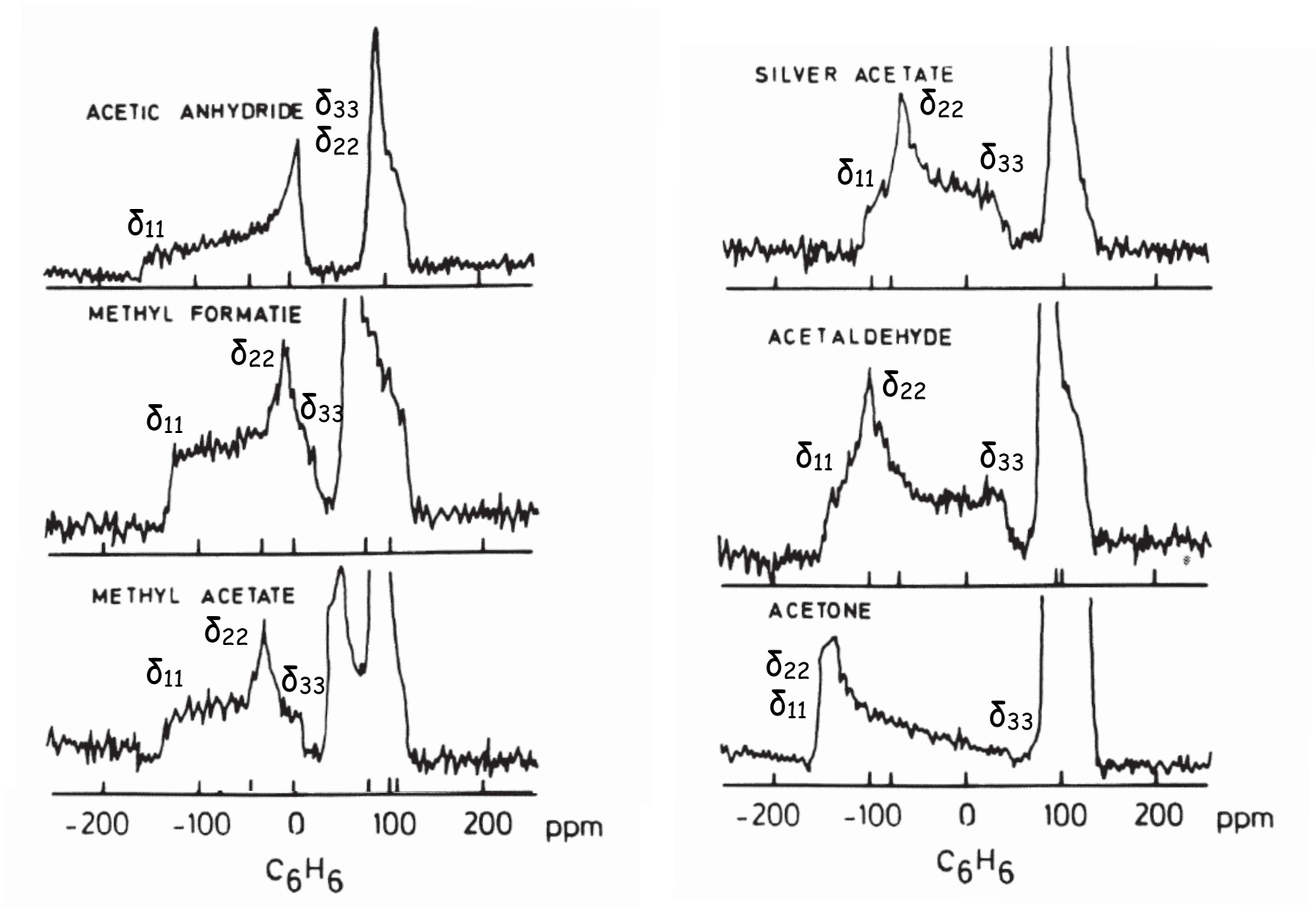

carbon-13 chemical **shielding** from C_6H_6 (ppm)

Chemical shift anisotropy is a sensitive reporter of electronic structure.

homework: work out the chemical basis for the difference in CSA between acetic anhydride and acetone

Figure: adapted from M. Mehring, "High Resolution NMR Spectroscopy in Solids," Springer, 1976

Powder Spectra Have Low Resolution

Cyclosporin A
a cyclic 11 amino acid peptide

polycrystalline powder

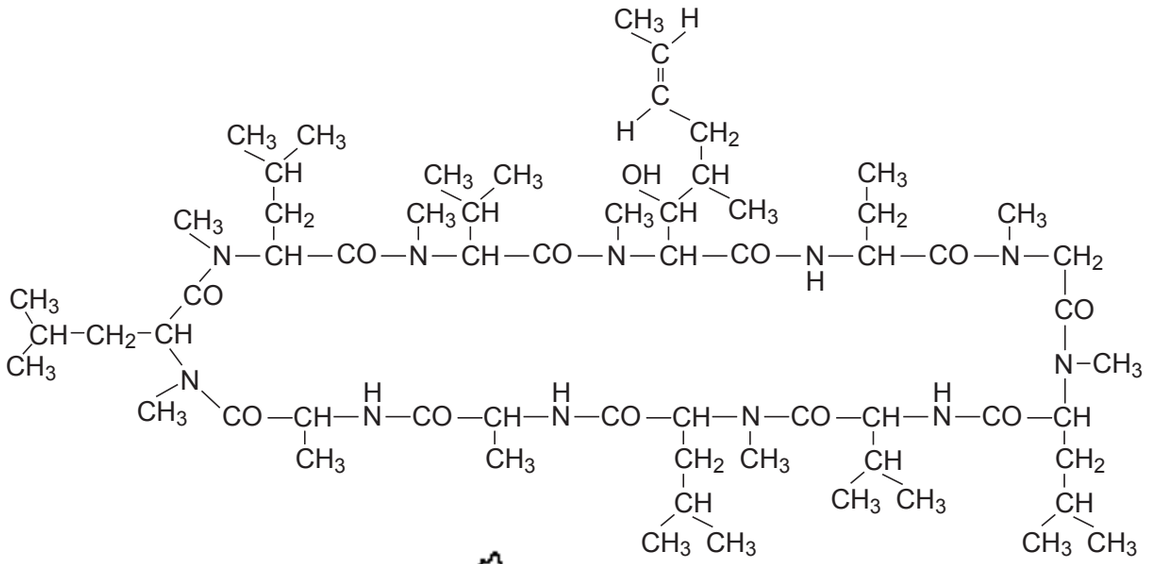

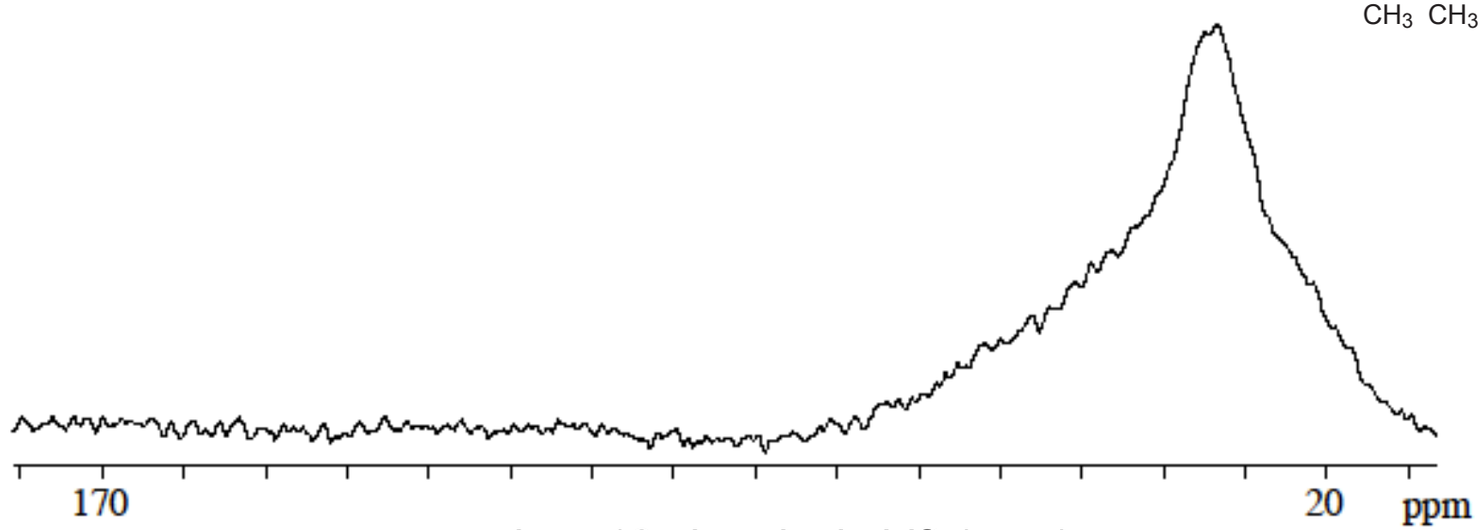

carbon-13 chemical shift (ppm)

In molecules with many different nuclei, powder spectra will overlap, and resolution is lost.
Many overlapping powder patterns make spectra unreadable.
No access to pertinent chemical information.

How can we regain high-resolution?

Cyclosporin A
a cyclic 11 amino acid peptide

polycrystalline powder

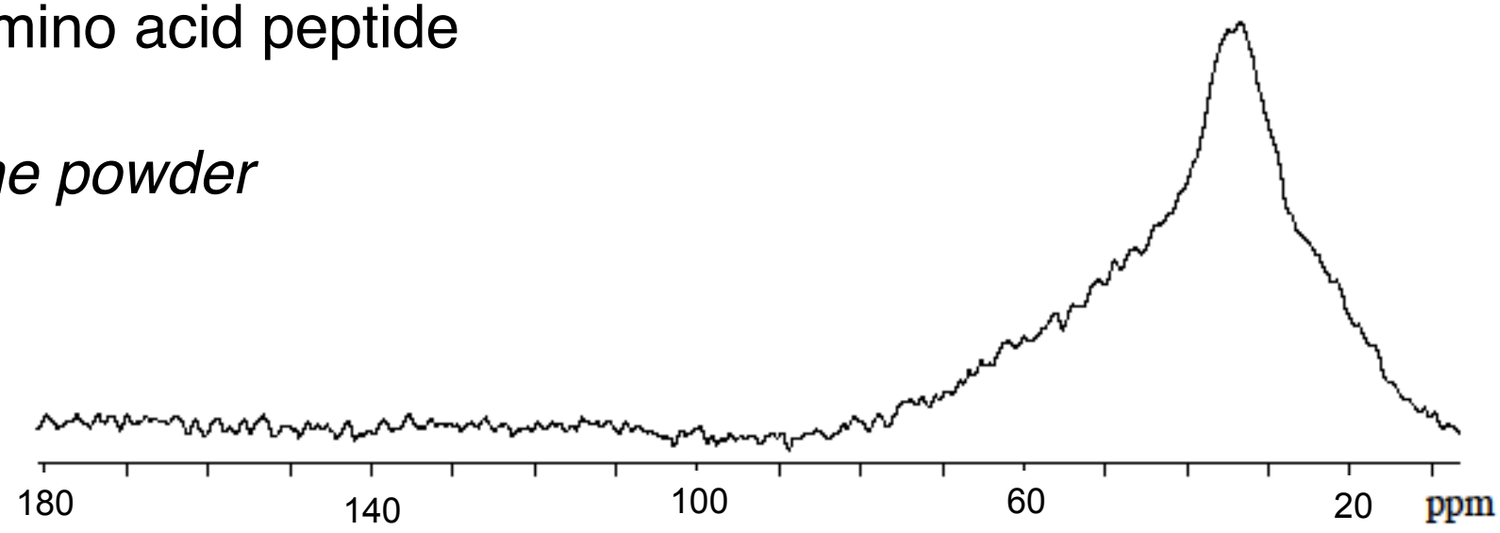

$CDCl_3$ solution

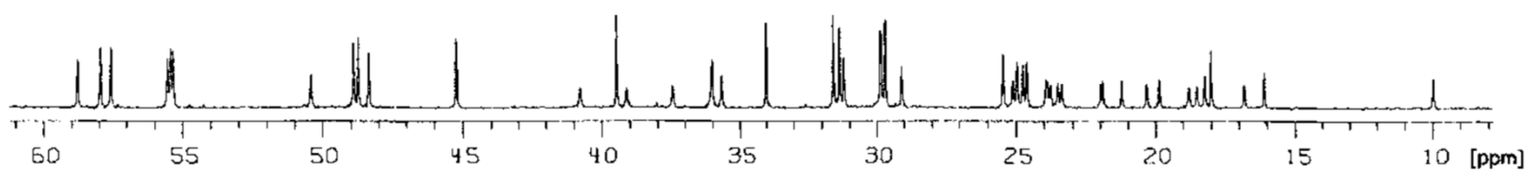

carbon-13 chemical shift (ppm)

One simple way to gain resolution is by dissolving the sample in a liquid. **Why?**

Solution spectrum from Helv. Chim. Acta **68**, 661 (1985)

How can we regain high-resolution?

Cyclosporin A
a cyclic 11 amino acid peptide

polycrystalline powder

Molecular motion with a correlation time τ_c much faster than $1/\Omega$ will result in a spectrum in which only the average value of the chemical shift is observed. (Think of it as rapid exchange between all orientations.) For each type of nucleus, it will be the same for all the molecules in the sample δ_{iso}.

Idea: Impose motions on the sample, which will average the anisotropic component to zero. Do these motions have to be low symmetry? (SO(3)?)

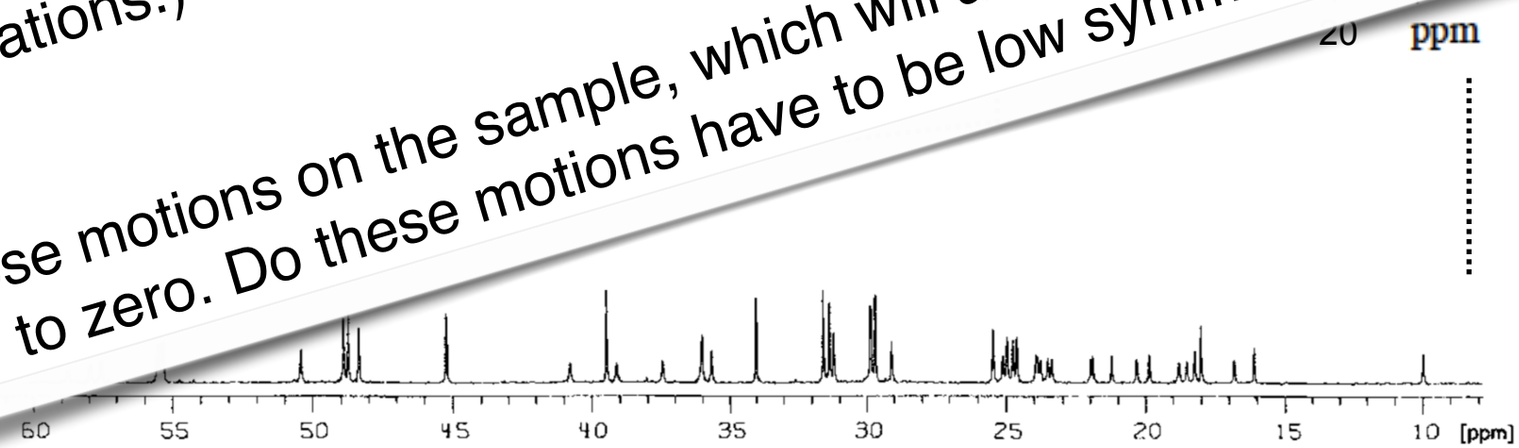

carbon-13 chemical shift (ppm)

One simple way to gain resolution is by dissolving the sample in a liquid. **Why?**

Solution spectrum from Helv. Chim. Acta **68**, 661 (1985)

Coherent Averaging

What is the simplest motion that will remove the anisotropic part of the interaction? Does it have to be random isotropic motion?

By comparing the symmetry of the interaction (here 2nd rank spherical harmonics) and the symmetry of a given motion, we can determine to what extent that motion will average the interaction. Group theory gives us the answer.

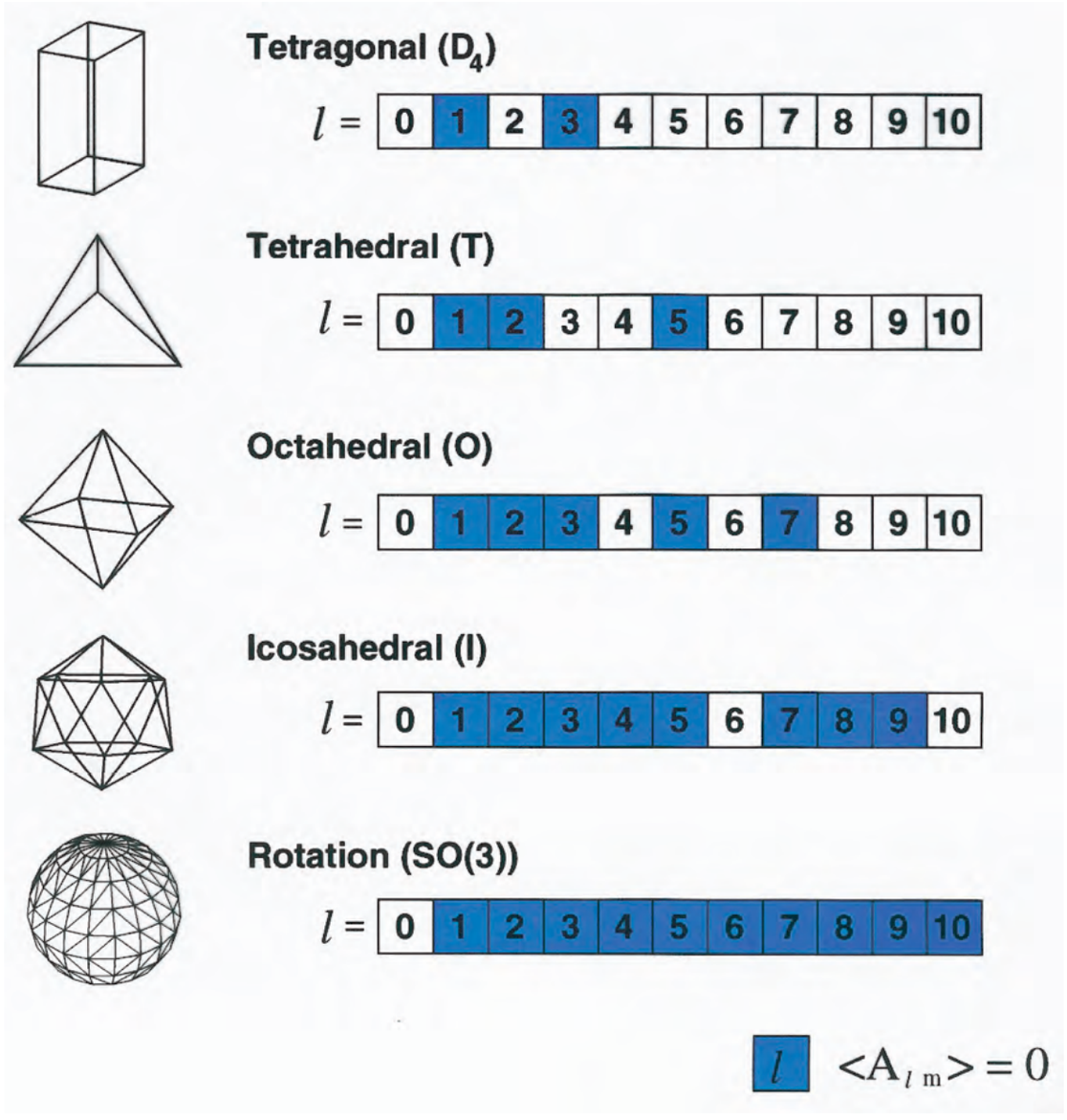

Coherent Averaging: Magic Angle Spinning

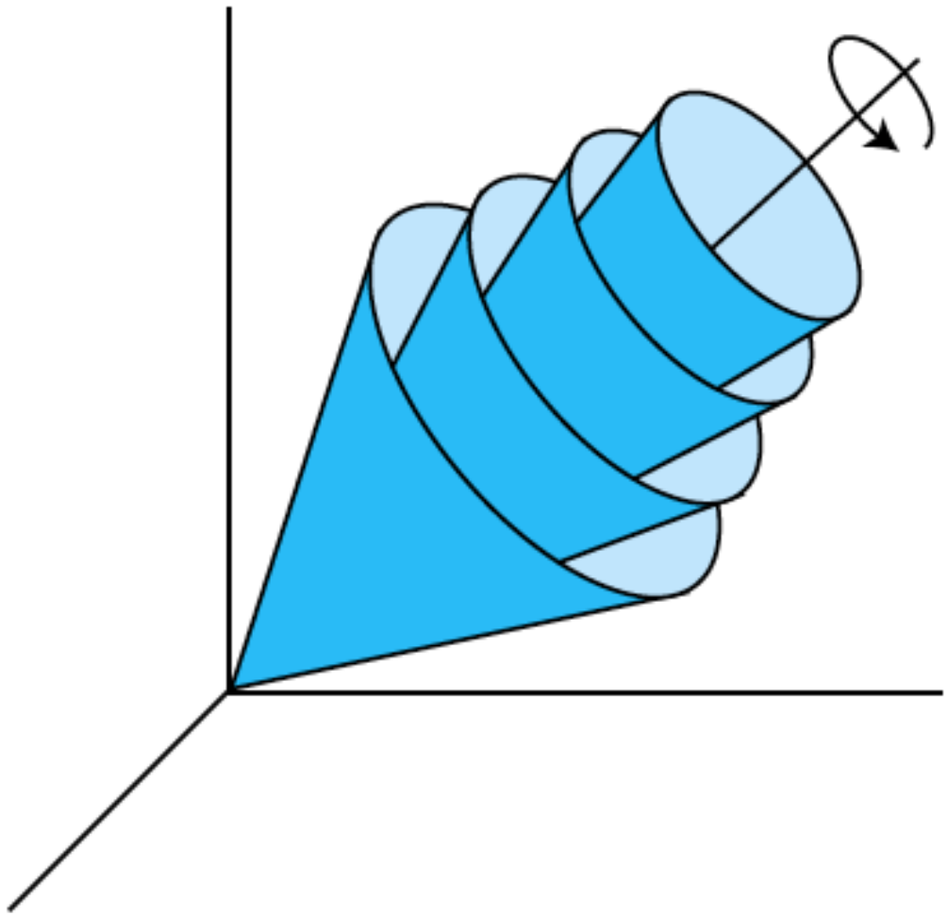

Spinning the sample produces an **average orientation** that is aligned with the spinning axes for any given initial orientation of the interaction.

Coherent Averaging: Magic Angle Spinning

For an axially symmetric tensor (i.e. either with $\delta_{22} = \delta_{33} = \delta_{xx}$ and $\delta_{11} = \delta_{zz}$ or with $\delta_{11} = \delta_{22} = \delta_{xx}$ and $\delta_{33} = \delta_{zz}$) the chemical shift is given by:

$$\delta = \delta_{iso} + \quad (\delta_{zz} - \delta_{iso}) \left(\frac{3cos^2\beta - 1}{2} \right)$$

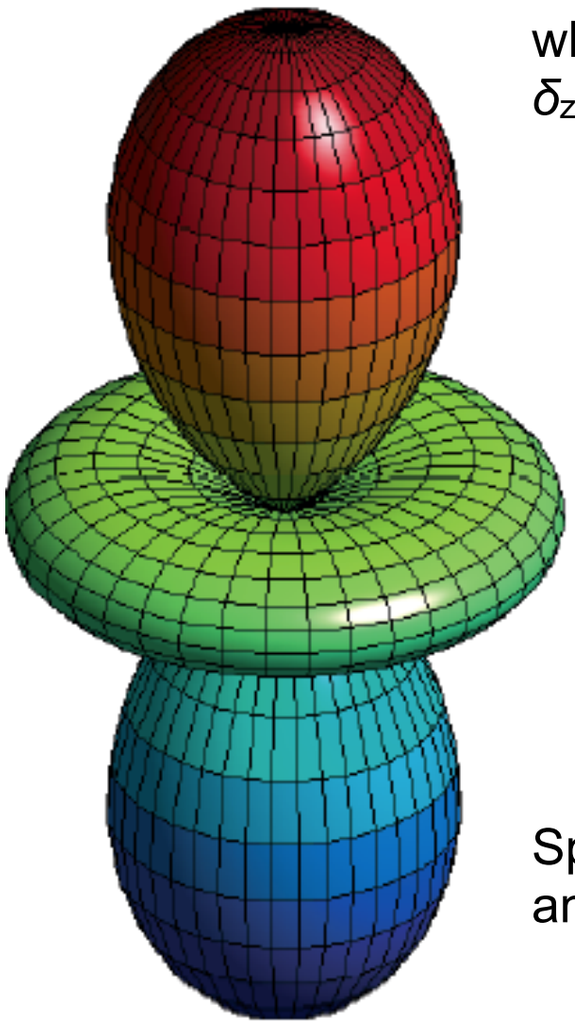

where β is the angle between the δ_{zz} axis and the magnetic field.

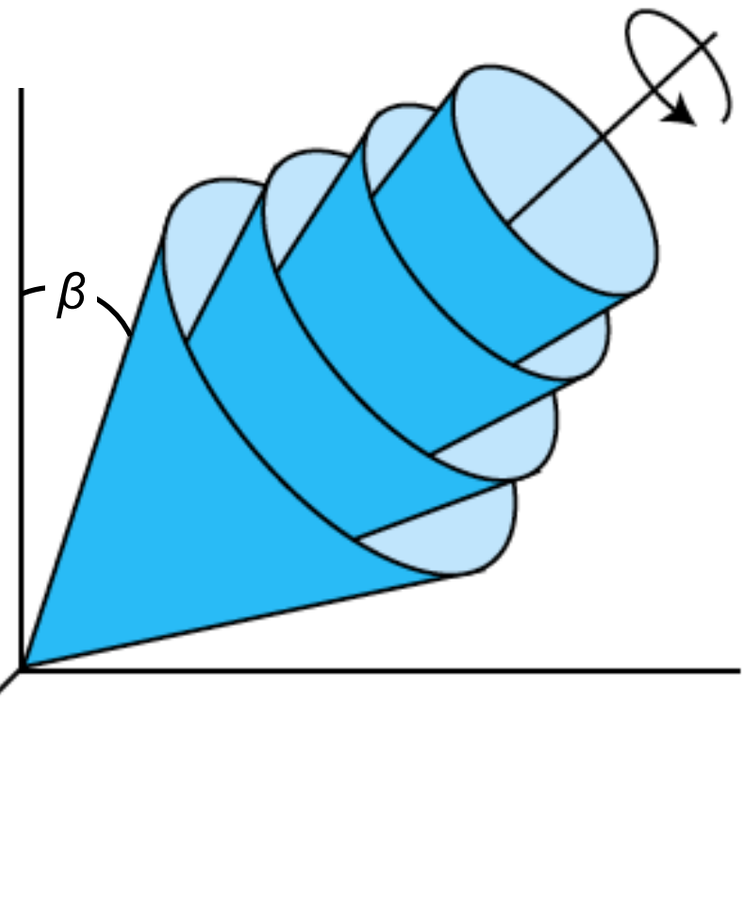

Spinning the sample makes all crystallites appear to have an average β angle $\langle\beta\rangle$ that is oriented along the spinning axis.

Magic Angle Spinning

If the angle of the spinning axes is set to 54.7° wrt to B_0, then
all orientations will have the same average frequency.
It is the center of gravity of the powder pattern: **the isotropic chemical shift**

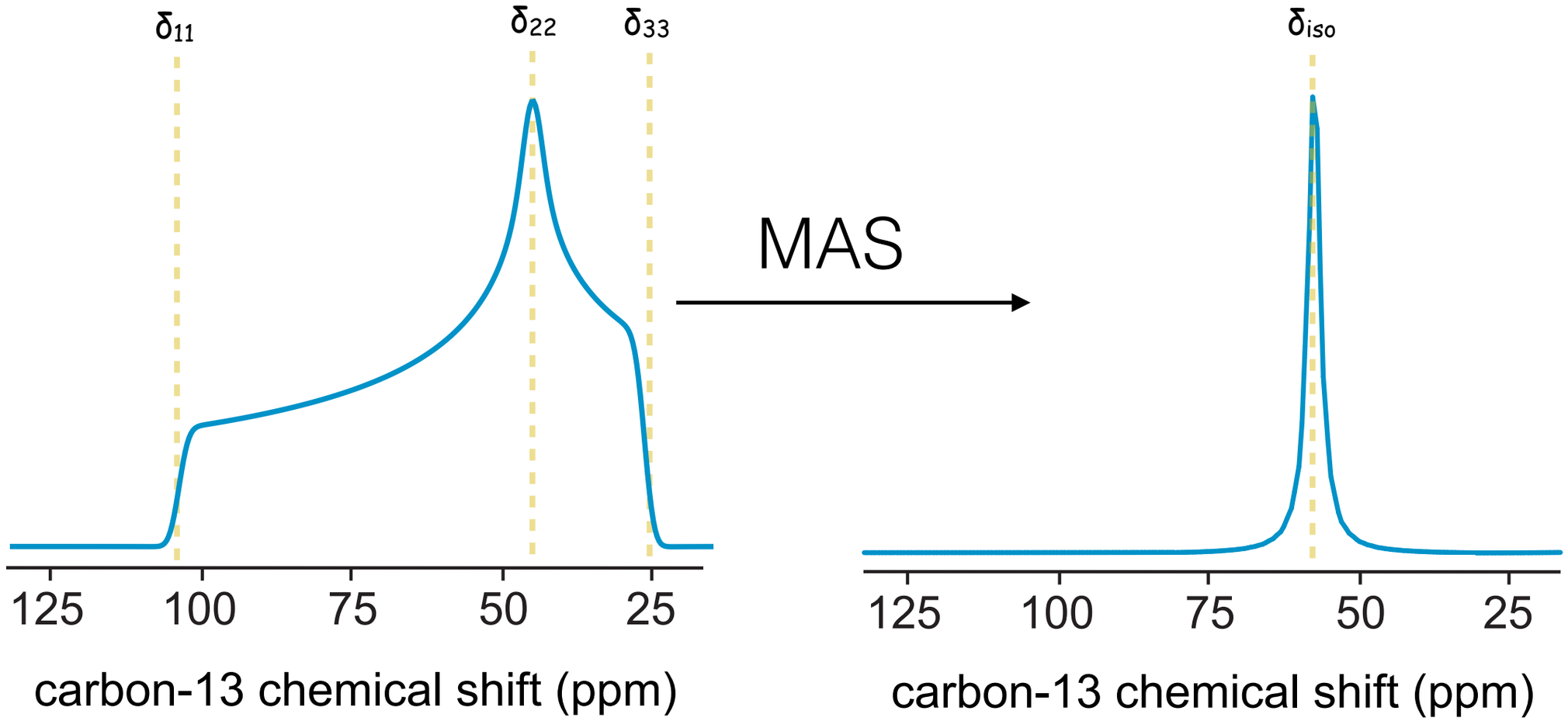

$$\delta_{iso} = (\delta_{11} + \delta_{22} + \delta_{33})/3$$

Magic Angle Spinning

isotropic solid-state spectroscopy

Cyclosporin A
a cyclic 11 amino acid peptide

polycrystalline powder

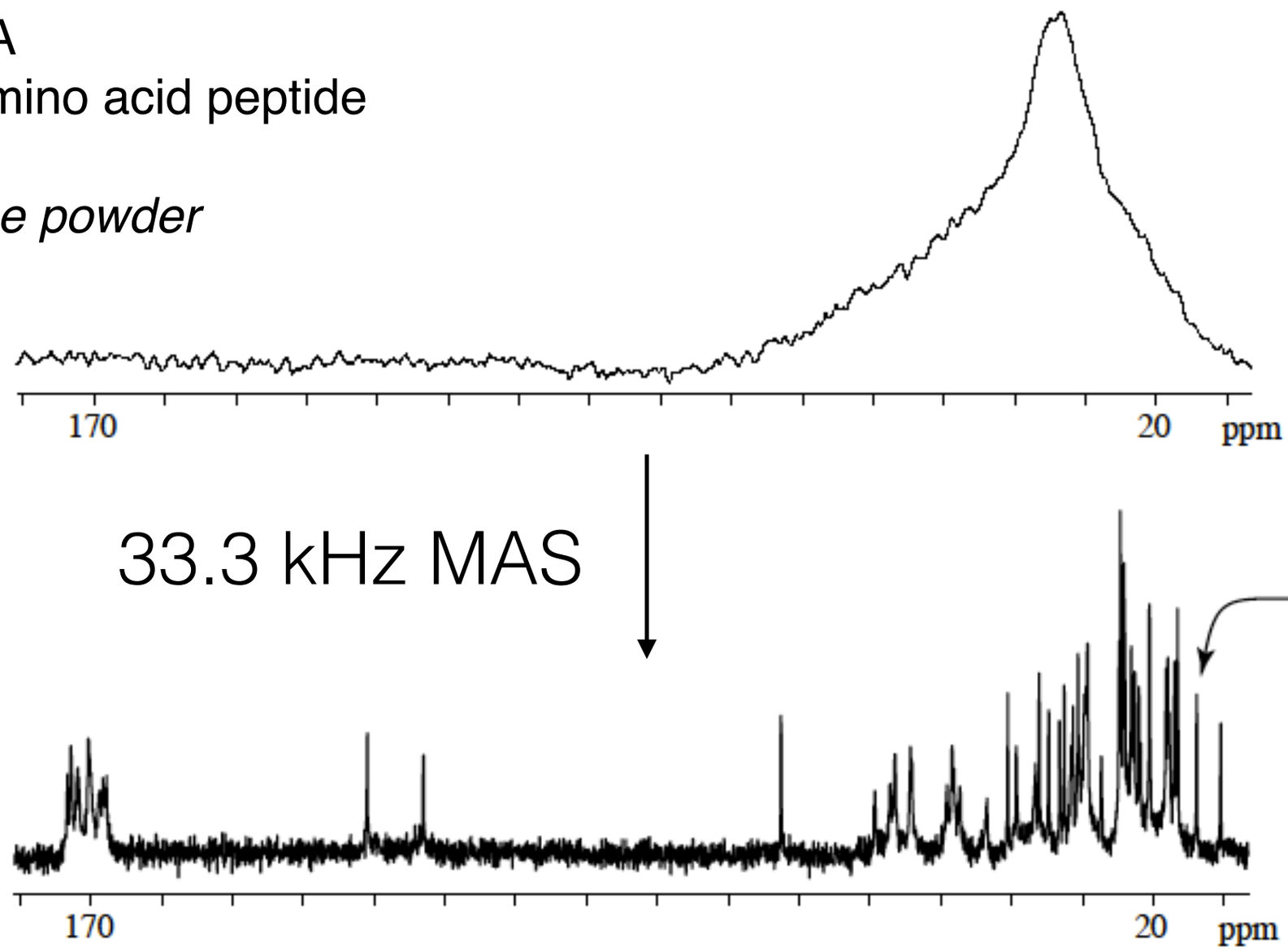

Magic Angle Spinning

Note that the isotropic chemical shift can change between the solid and liquid phases

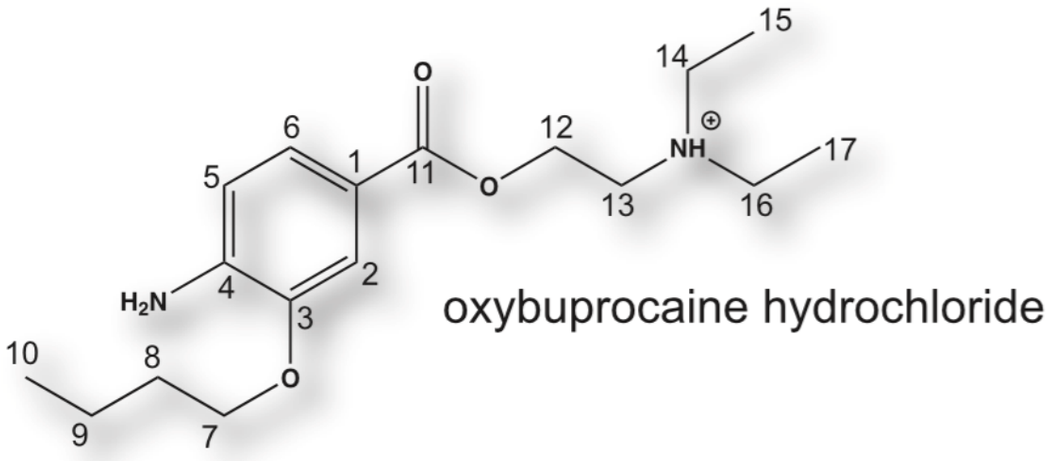

oxybuprocaine hydrochloride

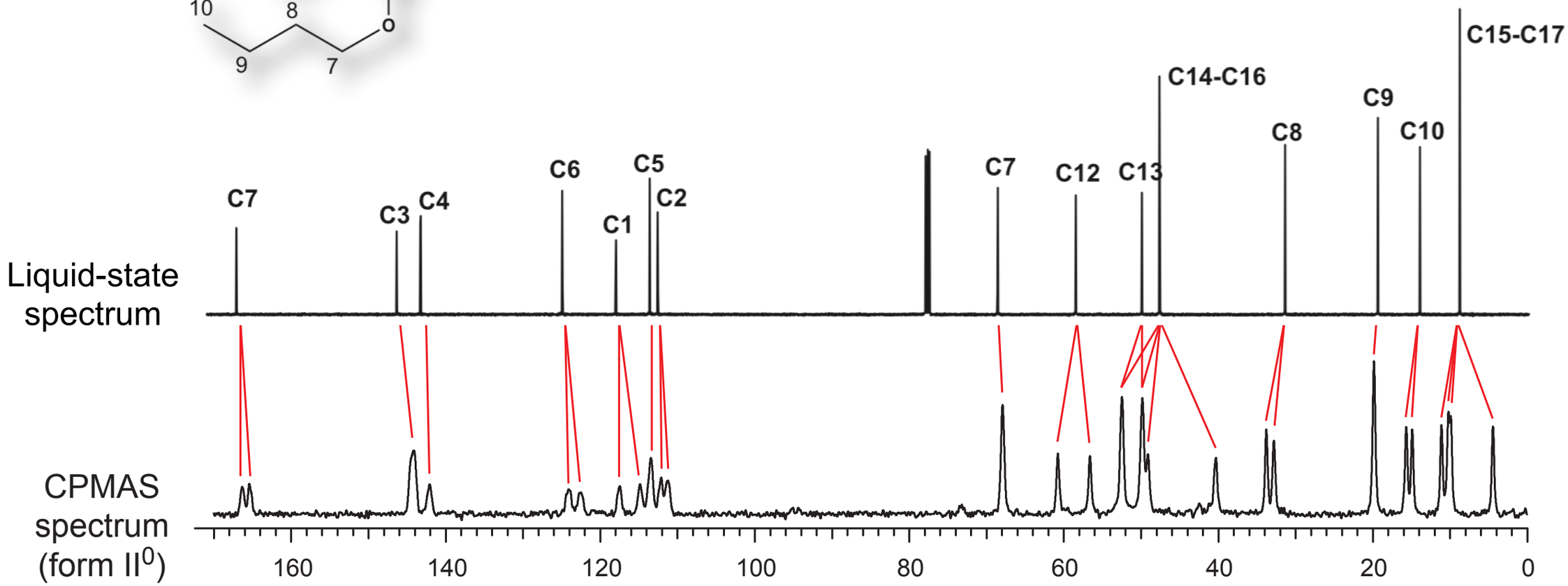

Chemical shifts are exquisite reporters of chemical structure and dynamics

Conclusions

- The chemical shift is anisotropic. The NMR frequency depends on the orientation of the molecule with respect to the magnetic field.

- Anisotropic interactions are described by a tensor. The CSA tensor is second rank, and has three principle values in an axes system described by three angles with respect to a reference frame fixed in the molecule.

- The full CSA tensor can be determined from NMR of single crystals.

- Powder spectra are the sum of spectra from all orientations. Line shapes are characteristic of the tensor principle values.

- By rapidly spinning the sample around an axes at an angle of 54.7° with respect to the main field, the anisotropy can be averaged to the isotropic value for any crystallite orientation. We refer to this as coherent averaging. Magic angle spinning yields a high-resolution isotropic spectrum from a powder.

Objective

- What happens for spin I > 1/2?

The NMR Hamiltonian: The Key to the Spectrum

Reminder:

$$\rho(t) = \exp(-i\mathcal{H}t)\rho(0)\exp(+i\mathcal{H}t).$$

$$\mathcal{H} = \mathcal{H}_z + \mathcal{H}_Q + \mathcal{H}_D + \mathcal{H}_{cs} + \mathcal{H}_J$$

Zeeman Interaction
(~100 MHz)

Quadrupolar Interaction
(0-100 MHz)

Dipolar Interaction
(0-20 kHz)

Chemical Shift
(0-2000 ppm)

Scalar Coupling
(0-200 Hz)

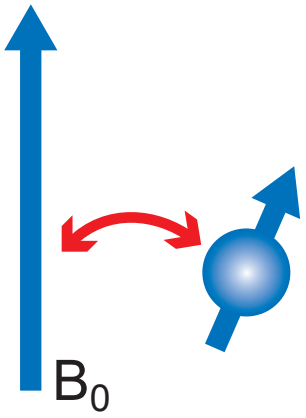

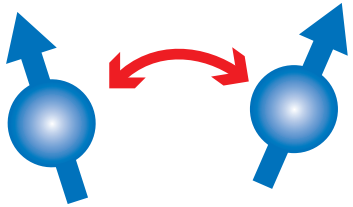

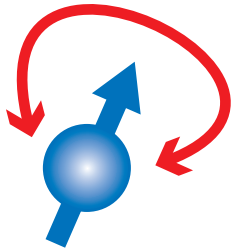

Quadrupolar Nuclei

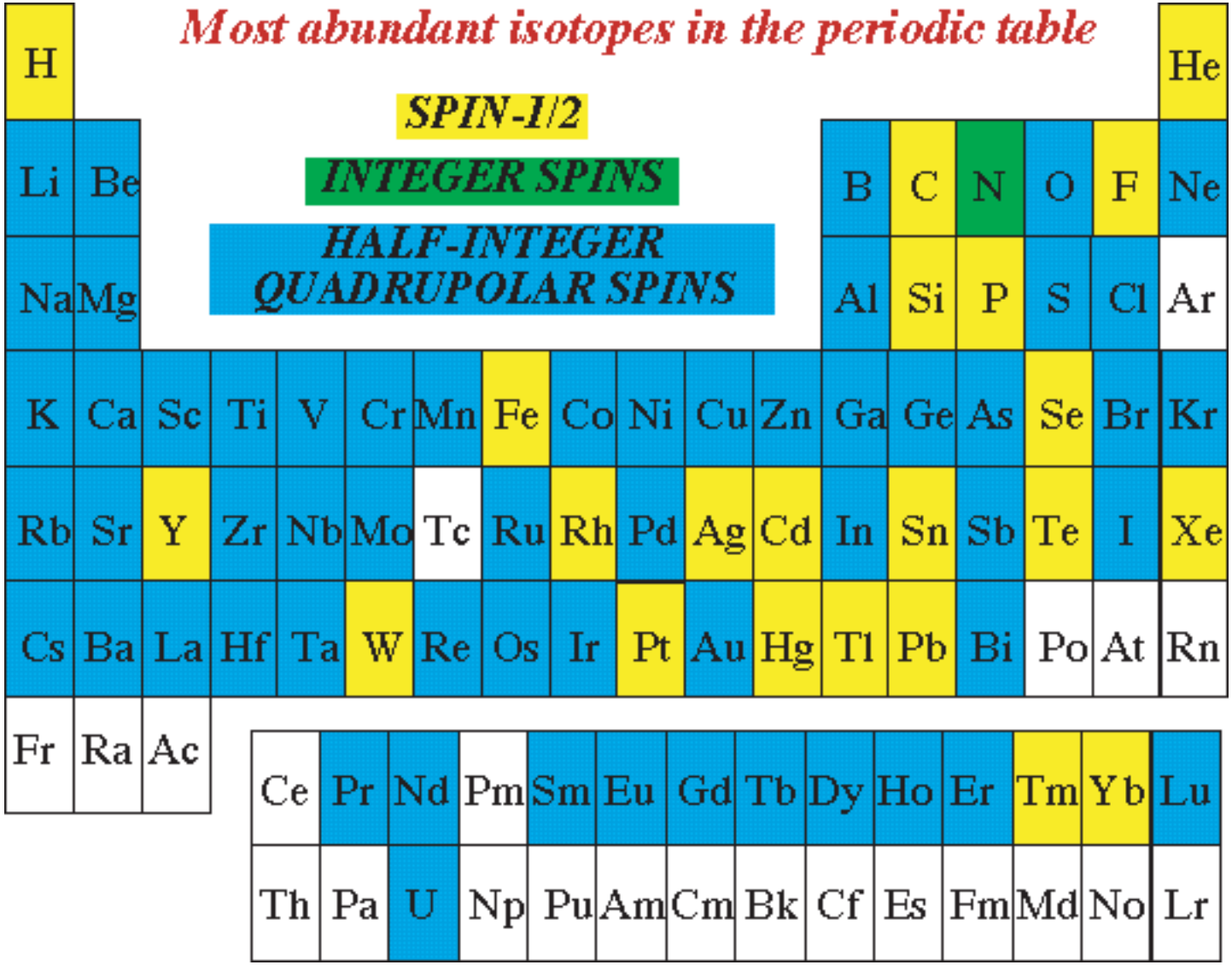

L. Frydman
http://www.weizmann.ac.il/chemphys/Frydman_group/home.html

The Quadrupolar Interaction

The quadrupolar interaction arises from the presence of an electric field gradient at the nucleus interacting with a non-spherical charge distribution. We will not go into more detail. We will just note that $\mathcal{H}_Q = 0$ for spin $I = \frac{1}{2}$, but that it is normally not zero for $I > \frac{1}{2}$. The Hamiltonian is expressed as

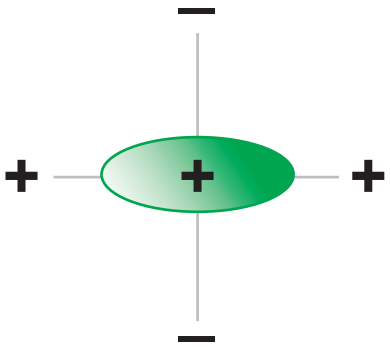

$$\mathcal{H}_Q = \frac{eQ}{6I(2I-1)h} \sum_{\alpha,\beta=x,y,z} V_{\alpha\beta}\left[\tfrac{3}{2}\left(I_\alpha I_\beta + I_\beta I_\alpha\right) - \delta_{\alpha\beta} I(I+1)\right]$$

$$\mathcal{H}_Q = \frac{eQ}{6I(2I-1)h} I \cdot V \cdot I$$

where eQ is the *nuclear quadrupole moment* and V is the electric field gradient tensor. We define a quadrupolar coupling constant

$$\chi_Q = \frac{3e^2 qQ}{4I(2I-1)h}$$

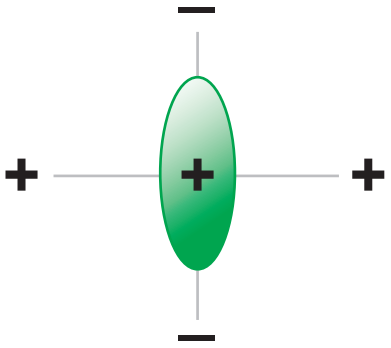

where eq represents the field gradient component V_{zz}, and with an asymmetry parameter given by $\eta = \left(V_{xx} - V_{yy}\right)/V_{zz}$, and the secular Hamiltonian becomes

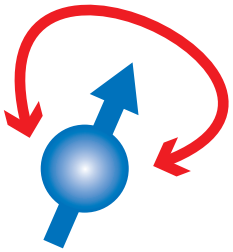

$$\mathcal{H}_Q = \frac{\chi_Q}{3}\left(3I_z^2 - I^2 + \eta\left(I_x^2 - I_y^2\right)\right)\left(\tfrac{1}{2}\left(3\cos^2\beta - 1\right) + \tfrac{1}{2}\eta\sin^2\beta\cos 2\alpha\right)$$

The Quadrupolar Interaction

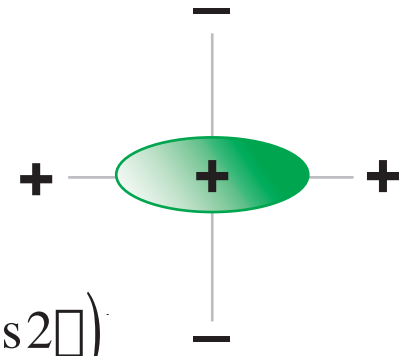

$$\mathcal{H}_Q = \frac{\delta_Q}{3}\left(3I_z^2 - I^2 + \eta\left(I_x^2 - I_y^2\right)\right)\left(\tfrac{1}{2}\left(3\cos^2\theta - 1\right) + \tfrac{1}{2}\eta\sin^2\theta\cos 2\phi\right)$$

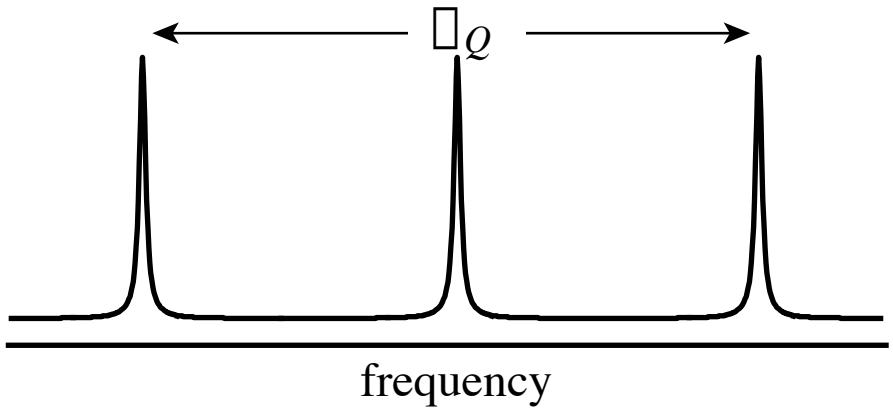

For spin $I = 1$, e.g. ^{2}H, we obtain a doublet with an orientation dependent splitting. For higher spins we see more lines, e.g. for spin $I = \frac{3}{2}$ (^{23}Na) we see an orientation independent central transition and two orientation dependent outer lines, as shown in the figure. In general there are $2I$ non-degenerate transitions.

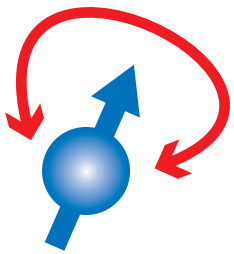

In conclusion, we have clearly seen that the secular parts of $\mathcal{H}_{cs}$, $\mathcal{H}_D$ and $\mathcal{H}_Q$ are all orientation dependent with respect to $\mathcal{H}_z$. They all have a tensorial nature.

First Order Quadrupolar Spectra: MAS

measurement of quadrupolar couplings

^{27}Al MAS spectrum of □-Al_2O_3

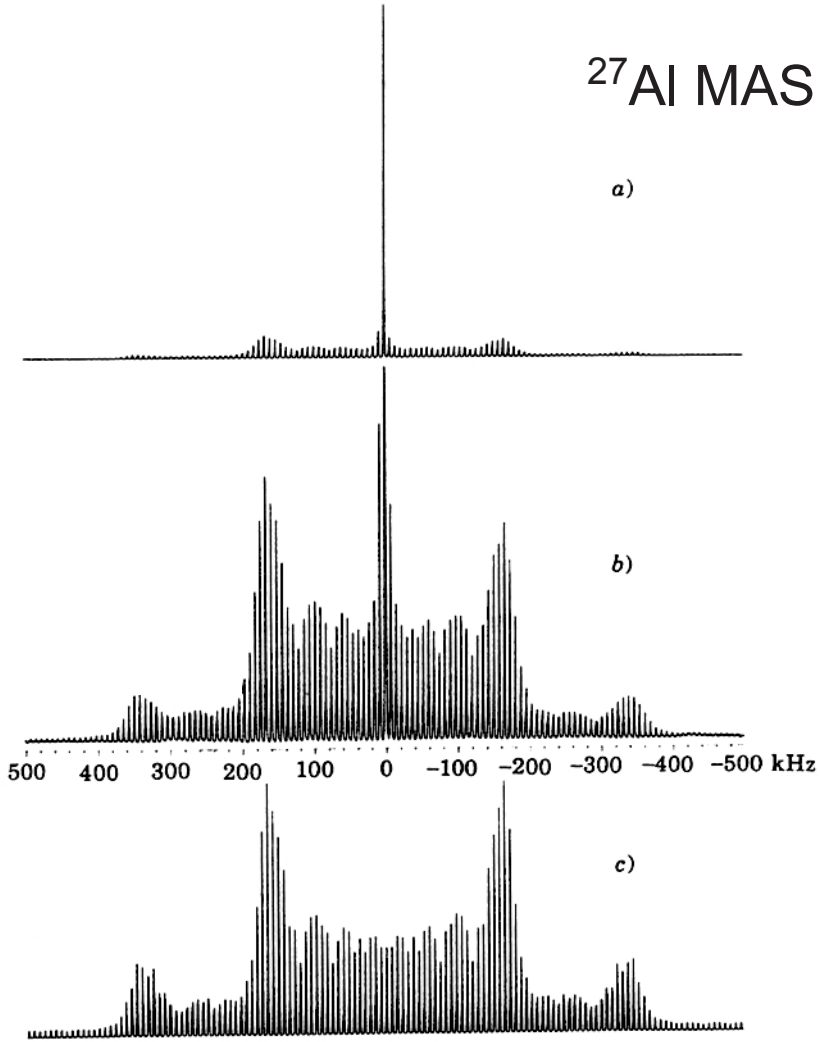

Fig. 2.4. – ^{27}Al MAS NMR spectra of the central and satellite transitions for α-Al_2O_3 spinning at 7.525 kHz. *a*) Experimental spectrum showing the relative intensities of the central and satellite transitions. *b*) Spectrum in *a*) with the vertical scale expanded by a factor of ten.

c)

Simulated spectrum for the satellite transitions obtained using a quadrupolar coupling $C_Q = 2.38$ MHz and $\eta = 0.00$. (Adapted from *J. Magn. Reson.*, 85, 173 (1989), with permission.)

J. AM. CHEM. SOC. 2004, 126, 4926- 4933

The Complete ^{51}V MAS NMR Spectrum of Surface Vanadia Nanoparticles on Anatase (TiO_2): Vanadia Surface Structure of a $DeNO_x$ Catalyst

Ulla Gro Nielsen,[†,§] Nan-Yu Topsˇe, Michael Brorson, Jˇrgen Skibsted,[†] and Hans J. Jakobsen*[,†]

Contribution from the Instrument Centre for Solid-State NMR Spectroscopy, Department of Chemistry, UniVersity of Aarhus, DK-8000 Aarhus C, Denmark, and Haldor Topsˇe A/S, Nymˇlle Vej 55, DK-2800 Lyngby, Denmark

Abstract: The first observations of the complete manifold of spinning sidebands (ssbs) including both the central and satellite transitions in ^{51}V MAS NMR spectra of surface vanadia nanoparticles on titania in $DeNO_x$ catalysts are presented. ^{51}V quadrupole coupling and chemical shift anisotropy parameters for the dominating vanadia structure are determined from ^{51}V MAS NMR spectra recorded at 9.4 and 14.1 T. Based on correlations previously established between ^{51}V NMR parameters and crystal structure data for inorganic vanadates, the NMR data are consistent with vanadium in a distorted octahedral oxygen coordination environment for the so-called strongly bonded vanadia species on the surface. The investigation includes two vanadia- titania model catalysts and six industrial-type $DeNO_x$ catalysts.

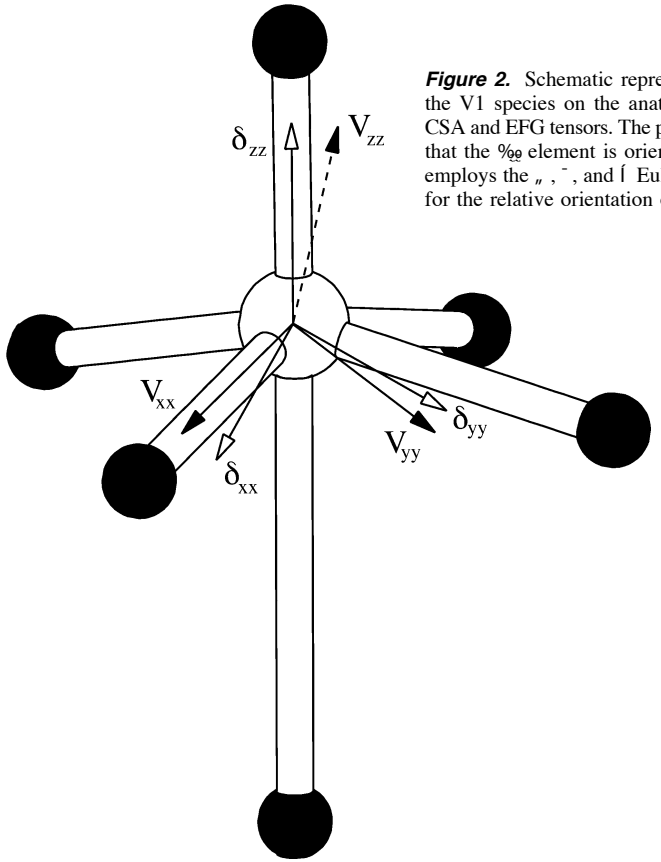

Figure 2. Schematic representation of the distorted VO_6 octahedron for the V1 species on the anatase surface, illustrating the orientation of the CSA and EFG tensors. The projection of these tensors upon this unit assumes that the %ϱϱ element is oriented along the short Vd O bond (see text) and employs the „ , ¯, and Í Euler angles determined experimentally (Table 1) for the relative orientation of the two tensors.

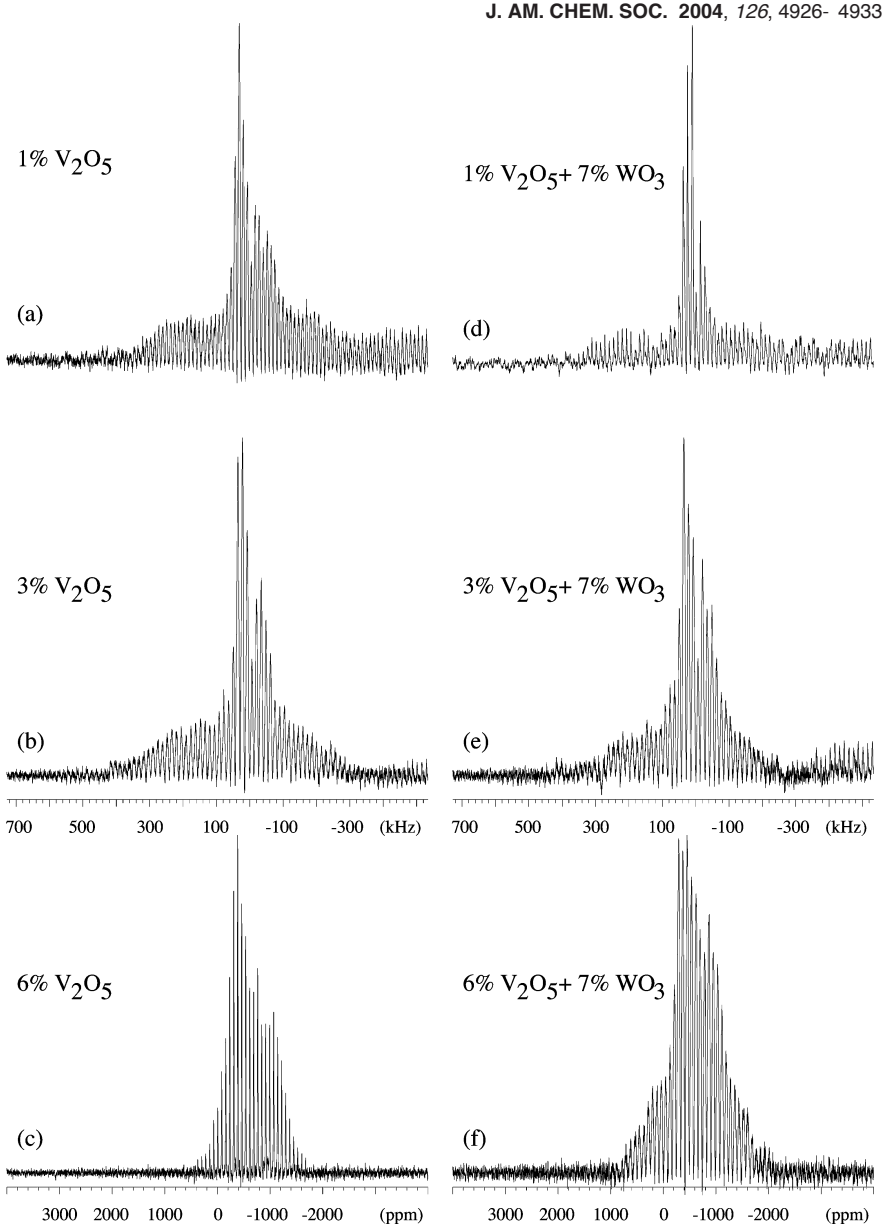

Figure 4. ^{51}V MAS NMR spectra of six different vanadia- titania catalysts. All samples are removed from their mechanical supports (glass-fiber mats) which have vanadia loadings corresponding to (a) 1 wt % V_2O_5 (Ó¿) 12.0 kHz, 300 000 scans), (b) 3 wt % V_2O_5 (Ó¿) 14.0 kHz, 333 000 scans), (c) 6 wt % V_2O_5 (Ó¿) 12.0 kHz, 67 000 scans), and, finally, loadings corresponding to 7 wt % WO_3 and (d) 1 wt % V_2O_5 (Ó¿) 13.0 kHz, 313 000 scans), (e) 3 wt % V_2O_5 (Ó¿) 14.0 kHz, 311 000 scans), and (f) 6 wt % V_2O_5 (Ó¿) 13.0 kHz, 153 000 scans). All spectra are shown on the same spectral width. The kHz scales are relative to the isotropic peak for V_2O_5, and the ppm scales are referenced relative to neat $VOCl_3$. Spinning sidebands from ^{27}Al in aluminum oxide from the residual glass-fiber contaminations are observed in the low-frequency part (Óe 300 kHz) for most of the spectra.

Biochemistry **2000,** *39,* 4939−4946

The Dynamic Impact of CpG Methylation in DNA†

Karen B. Geahigan,‡ Gary A. Meints, Mary E. Hatcher,§ John Orban,|| and Gary P. Drobny*

Departments of Chemistry and Physics, University of Washington, Seattle, WA 98195

Received July 28, 1999; Revised Manuscript Received December 6, 1999

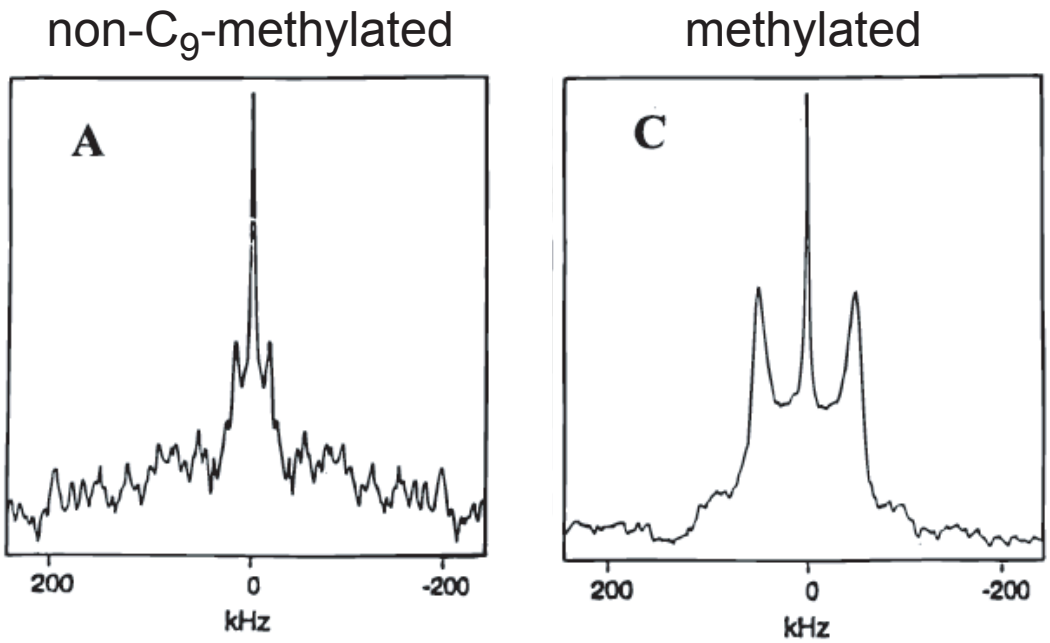

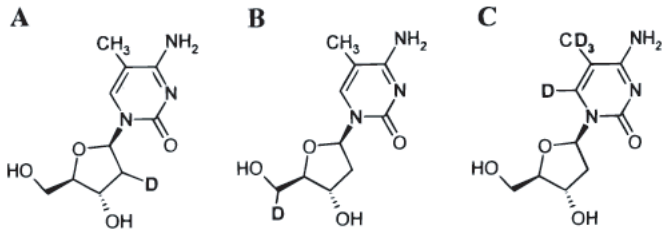

FIGURE 3: Location of deuterium labels in this study. (A) [2″-^{2}H]-5-methyl-2′-deoxycytidine. (B) [5′/5″-^{2}H]-5-methyl-2′-deoxycytidine (C) [d_6, methyl-^{2}H]-5-methyl-2′-deoxycytidine.

FIGURE 2: DNA sequence containing the *Eco*RI restriction site -GAATTC-, with C5-methyl-2′-deoxycytidine at the C_9 position. The binding site is in bold, with the cleavage sites indicated by the arrows.

ABSTRACT: Solid-state deuterium NMR is used to investigate perturbations of the local, internal dynamics in the *Eco*RI restriction binding site, -GAATTC- induced by cytidine methylation. Methylation of the cytidine base in this sequence is known to suppress hydrolysis by the *Eco*RI restriction enzyme. Previous solid-state deuterium NMR studies have detected large amplitude motions of the phosphate−sugar backbone at the AT−CG junction of the unmethylated DNA sequence. This study shows that methylation of the cytidine base in a CpG dinucleotide reduces the amplitudes of motions of the phosphate−sugar backbone. These observations suggest a direct link between suppression of the amplitudes of localized, internal motions of the sugar−phosphate backbone of the DNA and inhibition of restriction enzyme cleavage.

Effects of Na^+ on Dynamics of *p*-Nitroaniline Molecules in Zeolite ZSM-5 Studied by Solid-State NMR

Bull. Chem. Soc. Jpn., **77**, 673–679 (2004)

Yoshihiko Komori and Shigenobu Hayashi*

Institute for Materials & Chemical Process, National Institute of Advanced Industrial Science and Technology (AIST), Tsukuba Central 5, 1-1-1 Higashi, Tsukuba, Ibaraki 305-8565

Received September 3, 2003; E-mail: hayashi.s@aist.go.jp

The dynamics of deuterated *p*-nitroaniline (*p*NA-*d*) molecules in zeolite ZSM-5 including Na^+ (NaZSM-5) were investigated by means of ^2H and ^{13}C solid-state NMR to clarify the effects of Na^+ and hydrated Na^+. The adsorbed amount of *p*NA-*d* was four molecules per unit cell of NaZSM-5. ^2H NMR spectra of a dehydrated sample indicated that the motion of *p*NA-*d* in the micropore is a 180° flip-flop around the C_2 axis of the molecule. Another species with a faster flip-flop motion was distinguishable and assigned to *p*NA-*d* on the outer surface. When the sample adsorbed water molecules, ^2H spectra showed that the flip-flop motion of *p*NA-*d* was largely suppressed in the micropore and that *p*NA-*d* on the outer surface underwent an isotropic motion. These results indicated that the dynamics of *p*NA-*d* in NaZSM-5 depended on the interactions with Na^+ and hydrated Na^+ as well as on the location.

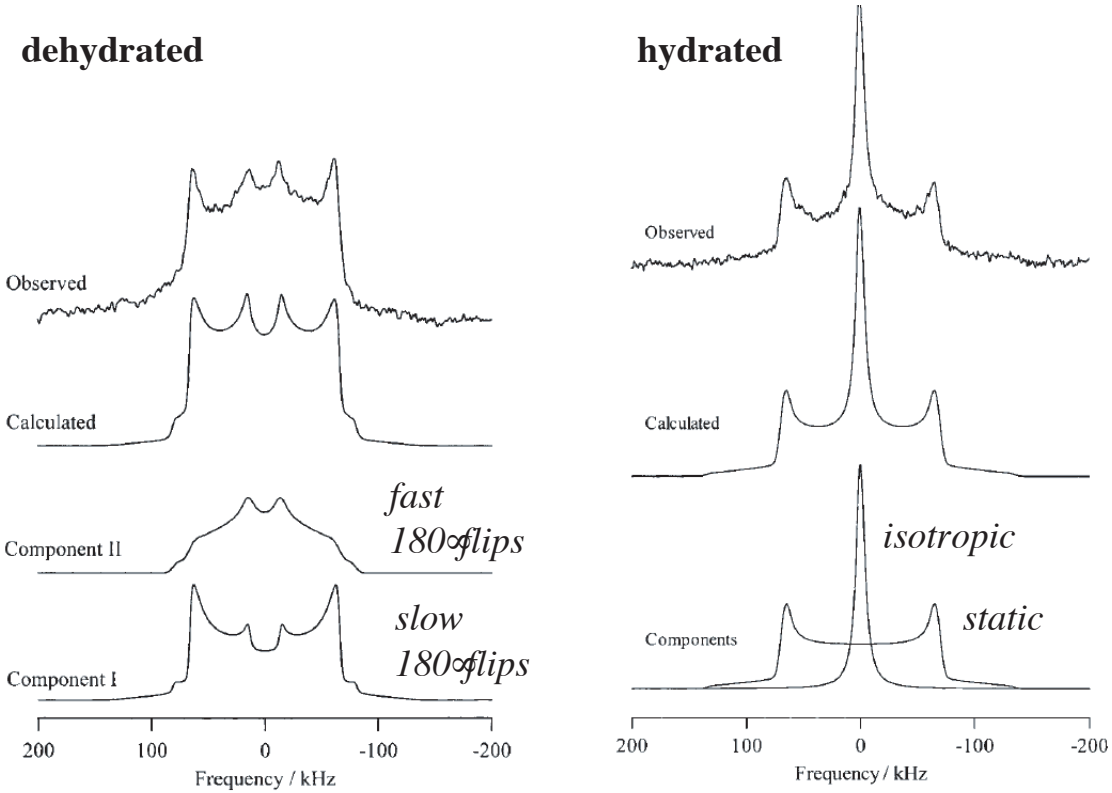

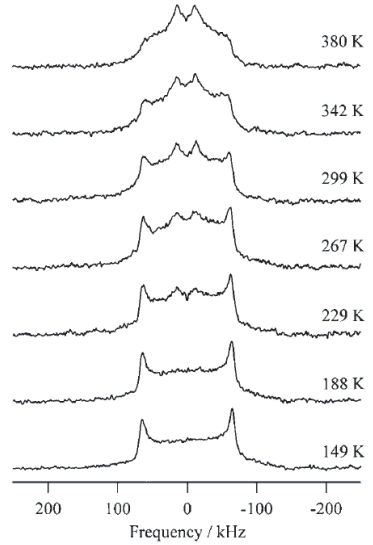

Fig. 1. Temperature dependence of ^2H NMR spectra of dehydrated NaZSM-5/*p*NA-*d*. Recycle times are 3 s.

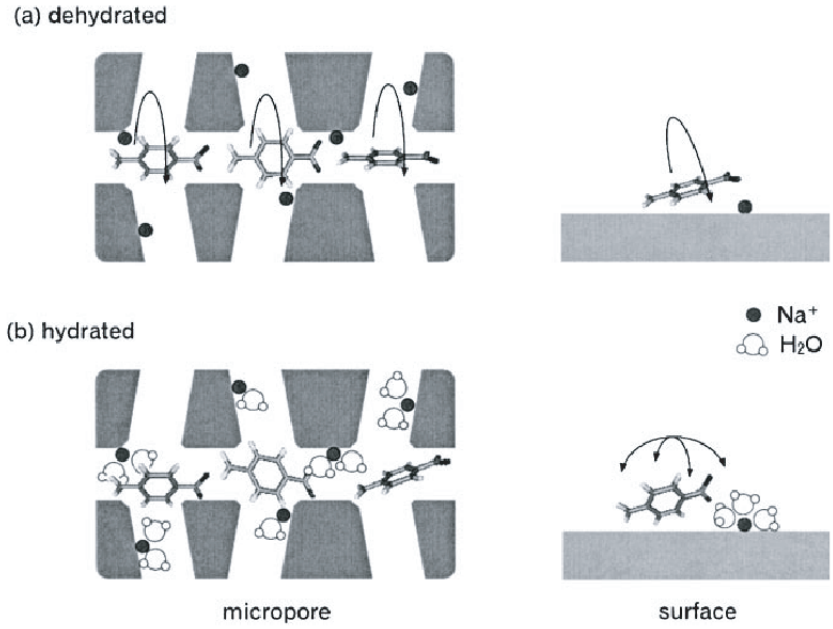

Ultra-Slow Motions
2D Deuterium Exchange Spectra:
Molecular Dynamics

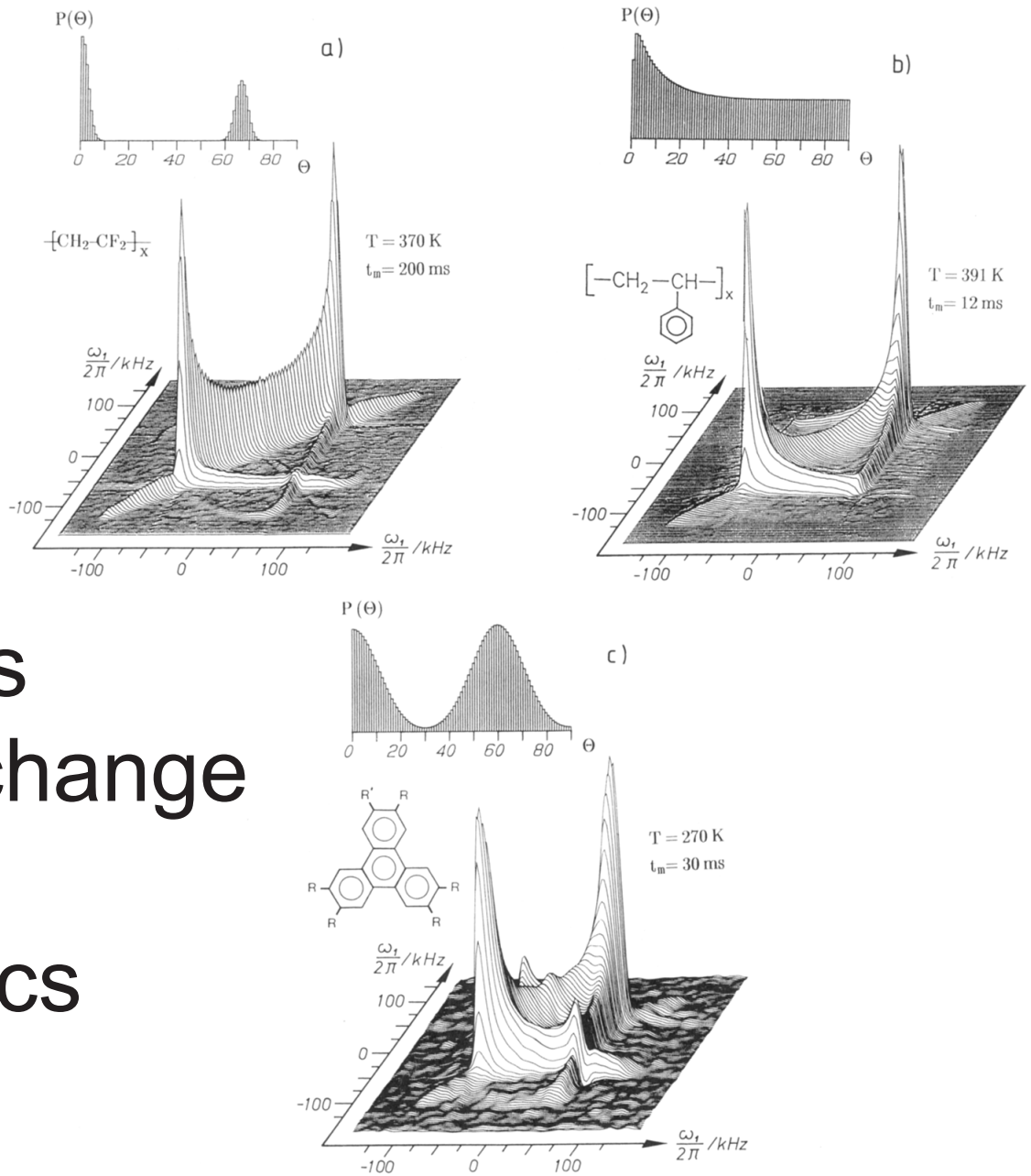

Figure 8. Experimental ^2H 2D exchange spectra: (a) poly(vinylidene fluoride) crystalline α-phase,[57] (b) chain deuterated polystyrene above its glass transition,[22] and (c) columnar liquid crystal based on a triphenylene core above its glass transition,[62] (R = OC_5H_{11}, R_1 = $OCOCHClCHCH_3C_2H_5$). The insets show the RADs derived from the analysis of the 2D spectra.

Proc. Natl. Acad. Sci. USA
Vol. 94, pp. 14237±14242, December 1997
Chemistry

Solid and liquid phase ^{59}Co NMR studies of cobalamins and their derivatives

ALES MEDEK, VERONICA FRYDMAN, AND LUCIO FRYDMAN *

Department of Chemistry, University of Illinois, Chicago, IL 60607

ABSTRACT We describe the application of ^{59}Co NMR to the study of naturally occurring cobalamins. Targets of these investigations included vitamin B_{12}, the B_{12} coenzyme, methylcobalamin, and dicyanocobyrinic acid heptamethylester. These measurements were carried out on solutions and powders of different origins, and repeated at a variety of magnetic field strengths. Particularly informative were the solid-state central transition NMR spectra, which when combined with numerical line shape analyses provided a clear description of the cobalt coupling parameters. These parameters showed a high sensitivity to the type of ligands attached to the metal and to the crystallization history of the sample. ^{59}Co NMR determinations also were carried out on synthetic cobaloximes possessing alkyl, cyanide, aquo, and nitrogenated axial groups, substituents that paralleled the coordination of the natural compounds. These analogs displayed coupling anisotropies comparable to those of the cobalamins, as well as systematic up-field shifts that can be rationalized in terms of their stronger binding affinity to the cobalt atom. Cobaloximes also displayed a higher regularity in the relative orientations of their quadrupole and shielding coupling tensors, reflecting a higher symmetry in their in-plane coordination. For the cobalamines, poor correlations were observed between the values measured for the quadrupole couplings in the solid and the line widths observed in the corresponding solution ^{59}Co NMR resonances.

FIG. 4. Superimposed experimental (thick lines) and simulated (thin lines) ^{59}Co solid-state NMR spectra corresponding to the indicated B_{12} derivatives. (Left) Spectra recorded on the samples as purchased. (Right) Spectra recorded on samples crystallized by slow evaporation. Line shapes were fitted at all magnetic fields simultaneously as described in the text, by using the coupling parameters summarized in Table 1.

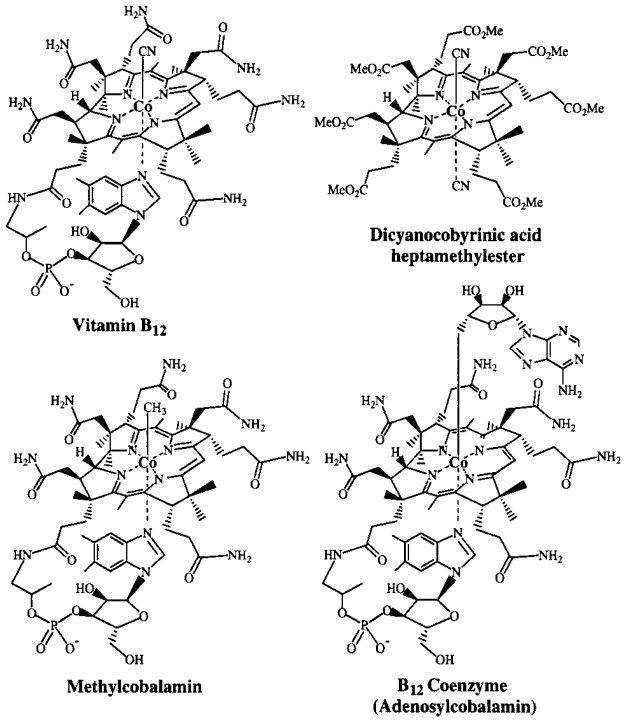

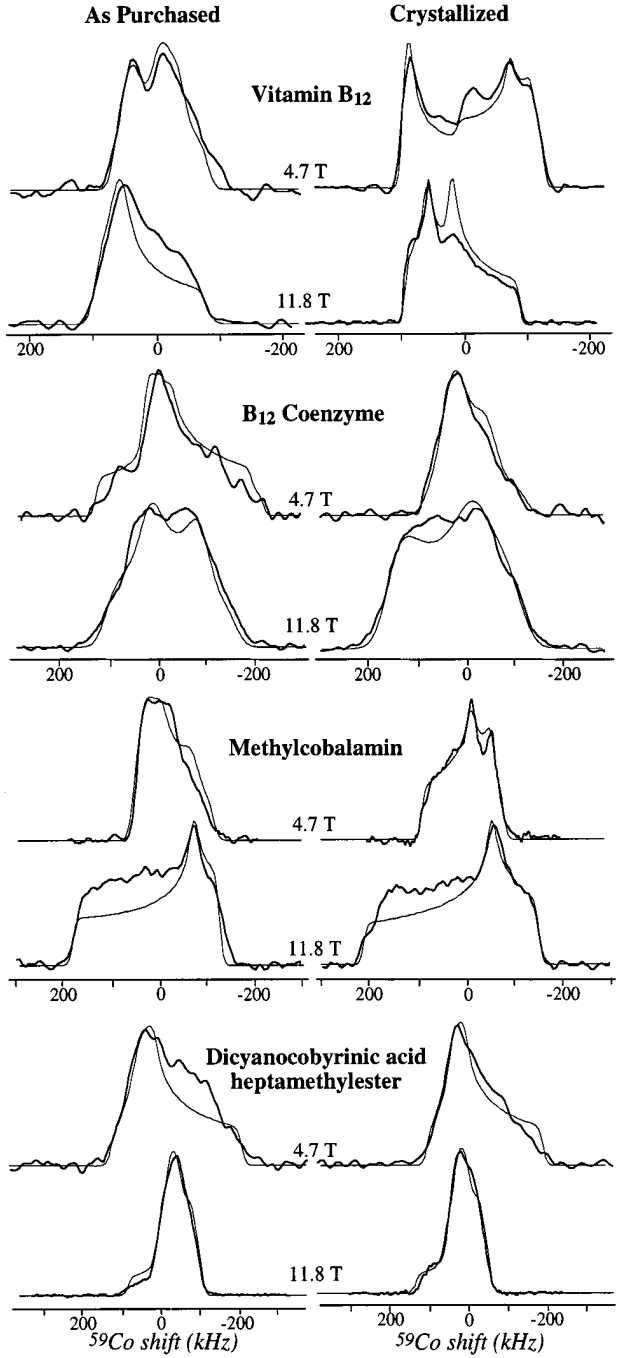

The Quadrupolar Interaction: Second Order

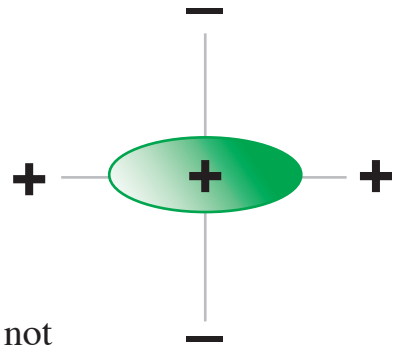

If the Quadrupolar coupling is large, then the first order perturbation we have used so far is not sufficient, and second order contributions to the perturbation on the Zeeman interaction must be considered.

The second order treatment generates the appearance of products of second-rank tensors, leading to an *overall fourth rank contribution to the anisotropy*, which also affects the central transition.

We find that the resonance frequency is proportional to:

$$f \propto d_{ij}^{(0)} + a_{ij}^{(2)} P_2[\cos\theta] + a_{ij}^{(4)} P_4[\cos\theta]$$

with

$$P_2[\cos\theta] = \tfrac{1}{2}\left(3\cos^2\theta - 1\right)$$

and

$$P_4[\cos\theta] = \tfrac{1}{8}\left(35\cos^4\theta - 30\cos^2\theta + 3\right).$$

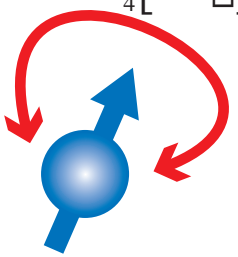

The Quadrupolar Interaction: Second Order

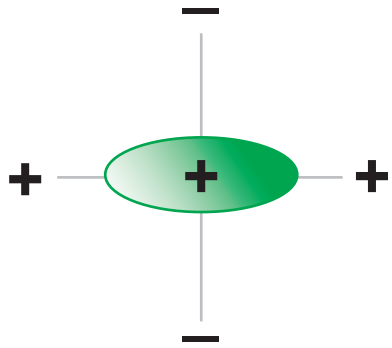

The result is that for large quadrupole couplings we expect to see an orientation dependent central transition, with second and fourth rank spatial anisotropy.

The satellite transitions will be so broad as to be unobservable in most cases.

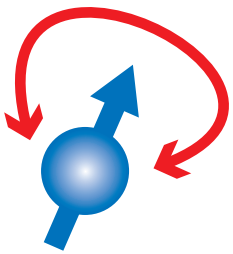

Proc. Natl. Acad. Sci. USA
Vol. 94, pp. 14237±14242, December 1997
Chemistry

Solid and liquid phase ^{59}Co NMR studies of cobalamins and their derivatives

ALES MEDEK, VERONICA FRYDMAN, AND LUCIO FRYDMAN *

Department of Chemistry, University of Illinois, Chicago, IL 60607

ABSTRACT We describe the application of ^{59}Co NMR to the study of naturally occurring cobalamins. Targets of these investigations included vitamin B_{12}, the B_{12} coenzyme, methylcobalamin, and dicyanocobyrinic acid heptamethylester. These measurements were carried out on solutions and powders of different origins, and repeated at a variety of magnetic field strengths. Particularly informative were the solid-state central transition NMR spectra, which when combined with numerical line shape analyses provided a clear description of the cobalt coupling parameters. These parameters showed a high sensitivity to the type of ligands attached to the metal and to the crystallization history of the sample. ^{59}Co NMR determinations also were carried out on synthetic cobaloximes possessing alkyl, cyanide, aquo, and nitrogenated axial groups, substituents that paralleled the coordination of the natural compounds. These analogs displayed coupling anisotropies comparable to those of the cobalamins, as well as systematic up-field shifts that can be rationalized in terms of their stronger binding affinity to the cobalt atom. Cobaloximes also displayed a higher regularity in the relative orientations of their quadrupole and shielding coupling tensors, reflecting a higher symmetry in their in-plane coordination. For the cobalamines, poor correlations were observed between the values measured for the quadrupole couplings in the solid and the line widths observed in the corresponding solution ^{59}Co NMR resonances.

FIG. 4. Superimposed experimental (thick lines) and simulated (thin lines) ^{59}Co solid-state NMR spectra corresponding to the indicated B_{12} derivatives. (Left) Spectra recorded on the samples as purchased. (Right) Spectra recorded on samples crystallized by slow evaporation. Line shapes were fitted at all magnetic fields simultaneously as described in the text, by using the coupling parameters summarized in Table 1.

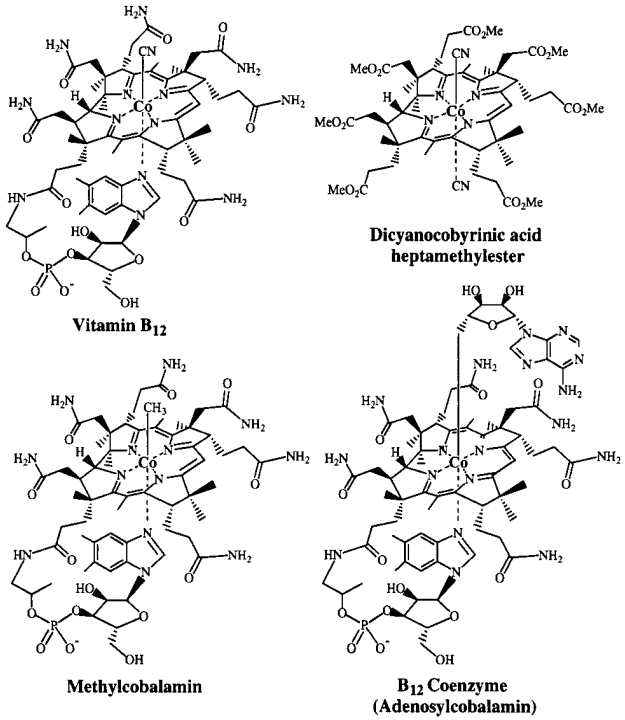

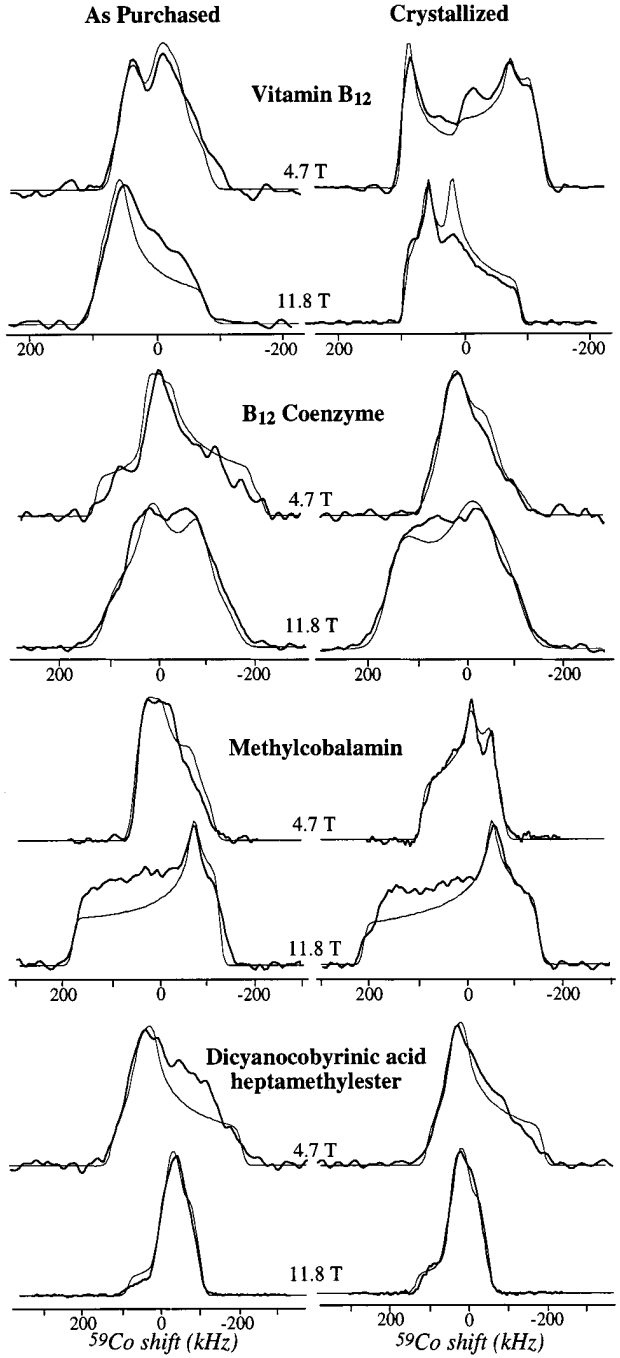

How can we remove second order quadrupole broadening to obtain high-resolution spectra?

Second Order Quadrupolar Interactions

MAS does not average the anisotropy to zero

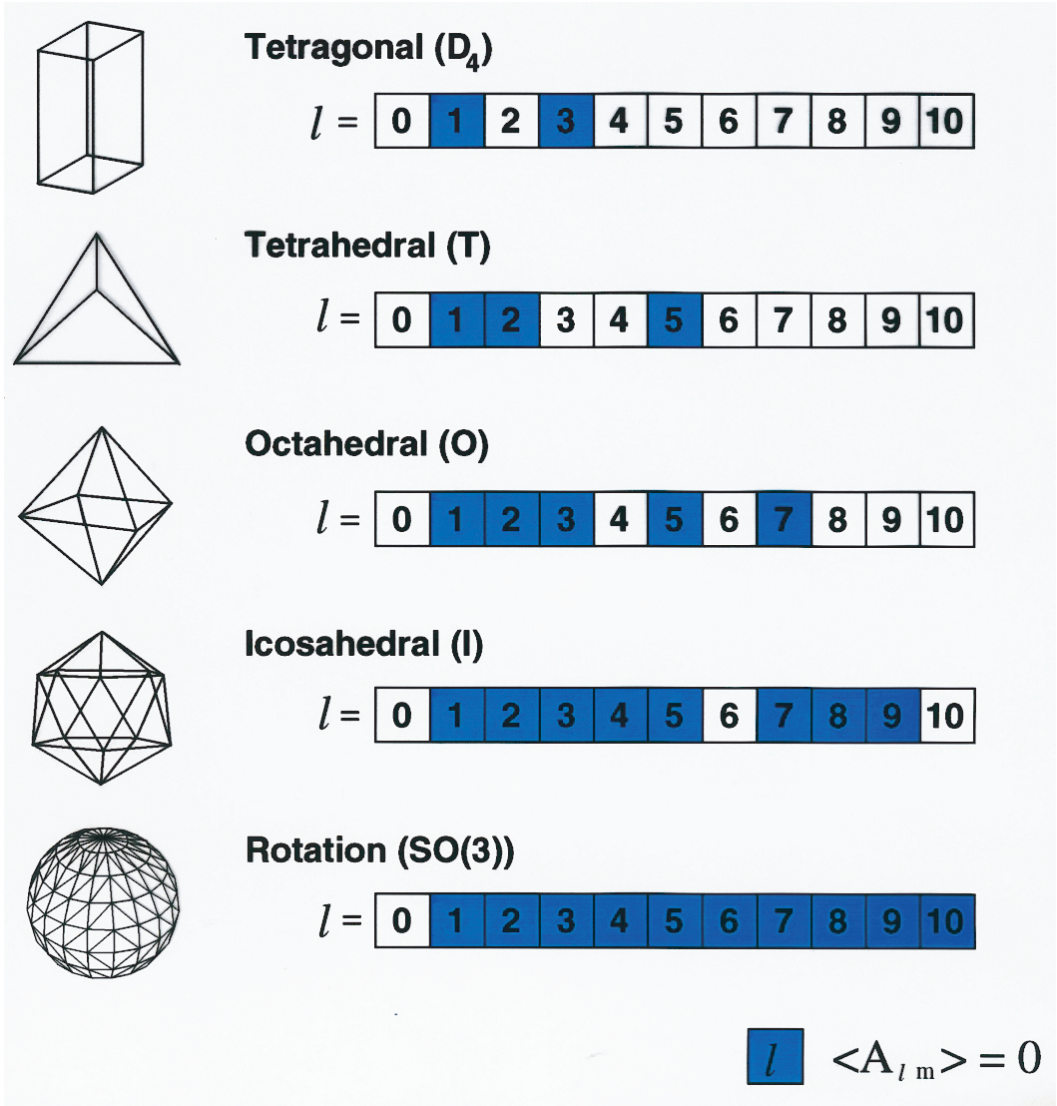

icosahedral motions are needed to average both second and fourth rank terms to zero

Second Order Quadrupolar Interactions

MAS does not average the anisotropy to zero

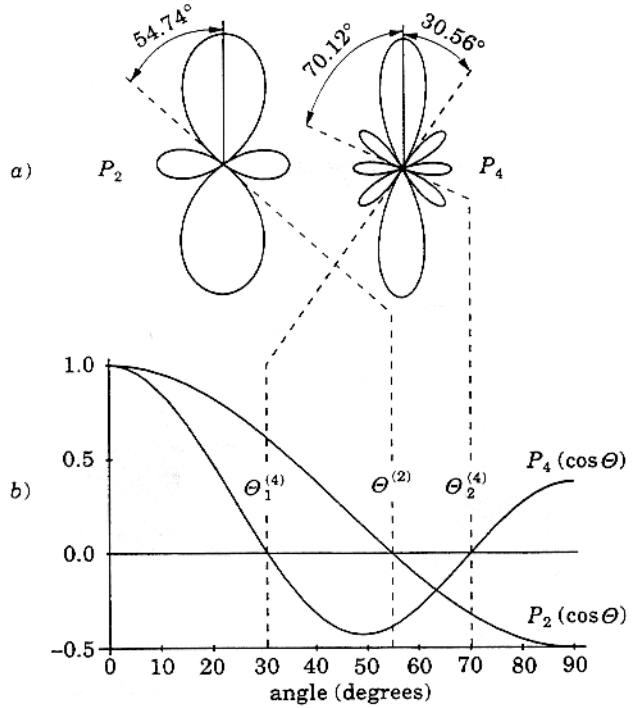

Fig. 5.9. – Plot of the second- and fourth-order Legendre polynomials, $P_2(\cos\theta)$ and $P_4(\cos\theta)$, *vs.* the angle of rotation in variable-angle spinning. *a*) Plot in polar coordinates, *b*) in Cartesian coordinates. The nodes of both functions are indicated by dashed lines. (Adapted from *Solid State Nucl. Magn. Reson.*, **1**, 267 (1992), with permission.)

rotation about both axes, $\beta_m(2)$ and $\beta_m(4)$, could remove all the anisotropy and yield narrow spectra of second order quadrupolar broadened systems....

Second Order Quadrupolar Interactions

Double Rotation yields isotropic spectra!

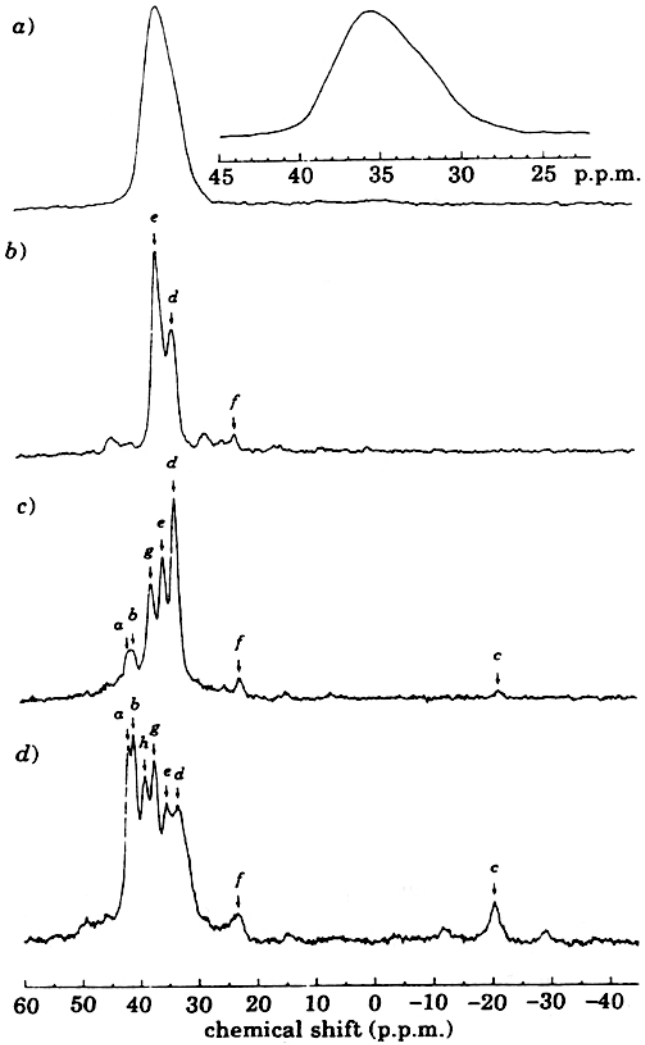

Fig. 2.6. – ^{27}Al NMR spectra of dehydrated and partially rehydrated VPI-5: *a*) MAS spectrum of dehydrated VPI-5, *b*) DOR spectrum of dehydrated VPI-5, *c*) DOR spectrum after two days of rehydration, *d*) DOR spectrum after 23 days of rehydration. (Adapted from *Nature* (*London*), **346**, 550 (1990), with permission.)

the sample is simultaneously rotated about both $\theta_m(2)$ and $\theta_m(4)$.

^{27}Al DOR spectra of dehydrated (b) and partially rehydrated (c,d) VPI-5

Second Order Quadrupolar Interactions

isotropic spectra at the magic angle

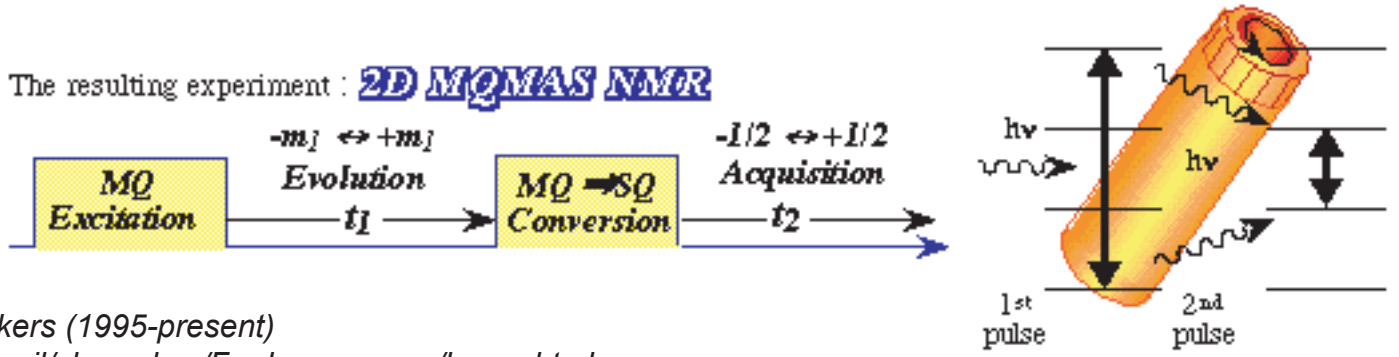

L. Frydman and coworkers (1995-present)
http://www.weizmann.ac.il/chemphys/Frydman_group/home.html

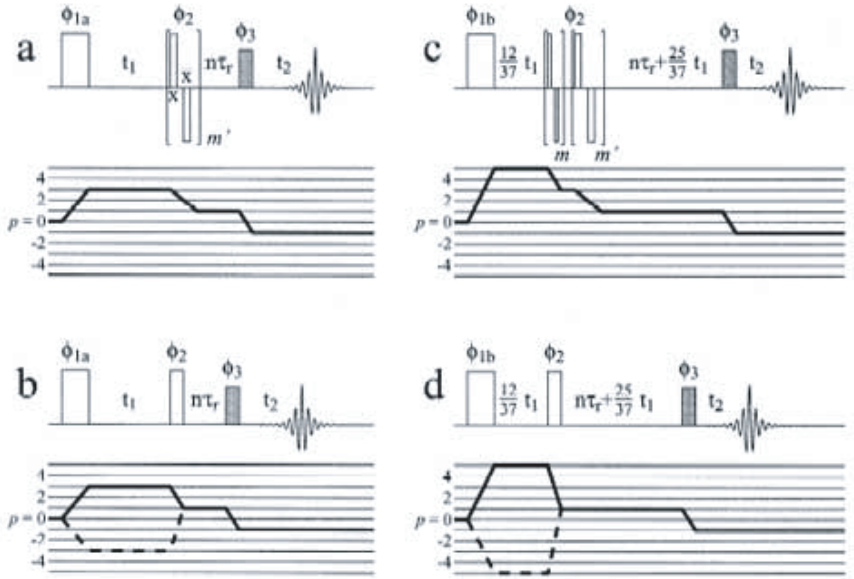

Fig. 1. Timing schemes and coherence transfer pathways for the 3Q-MAS (a,b) and 5Q-MAS (c,d) experiments employing modulated mixing (a,c) or single-pulse mixing (b,d). All sequences employ shifted-echo acquisition (and delayed acquisition [25] for the 5Q-MAS sequences) to ensure pure absorption-mode lineshapes. The three pulses are phase cycled as $\phi_{1a} = 0°, 60°, 120°, \ldots, 300°$ ($\phi_{1b} = 0°, 36°, 72°, \ldots, 324°$) and $\phi_2 = 0°$, supercycled by $\phi_3 = 0°, 180°$, and with the receiver phase adjusted to select the indicated pathways according to standard procedures [19], i.e., $\phi_{rec} = -3\phi_{1a} + 2\phi_3$ or $\phi_{rec} = -5\phi_{1b} + 2\phi_3$.

T.Vosegaard, D.Massiot, P.J.Grandinetti, 'Sensitivity enhancements in MQ-MAS NMR of spin-5/2 nuclei using modulated rf mixing pulses.', Chem. Phys. Letters, 326 pp454-460 (2000).

Second Order Quadrupolar Interactions

isotropic spectra at the magic angle

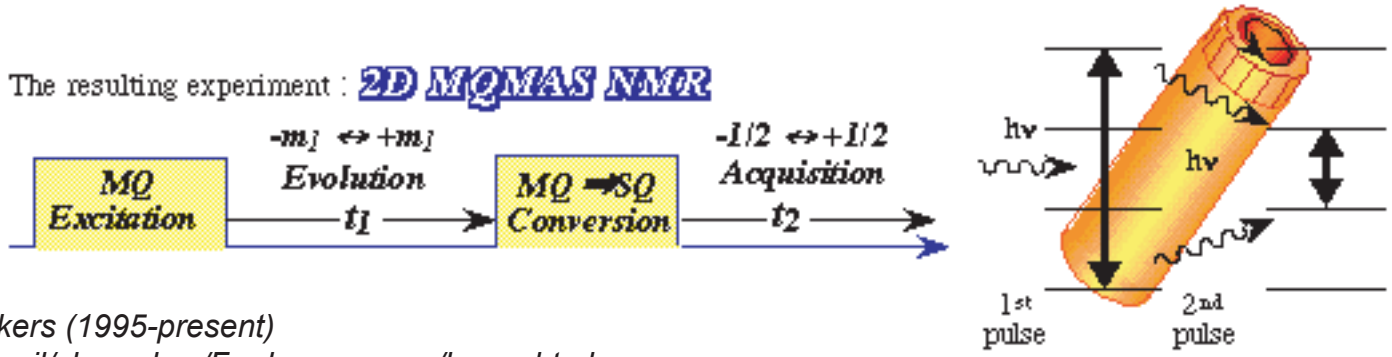

L. Frydman and coworkers (1995-present)
http://www.weizmann.ac.il/chemphys/Frydman_group/home.html

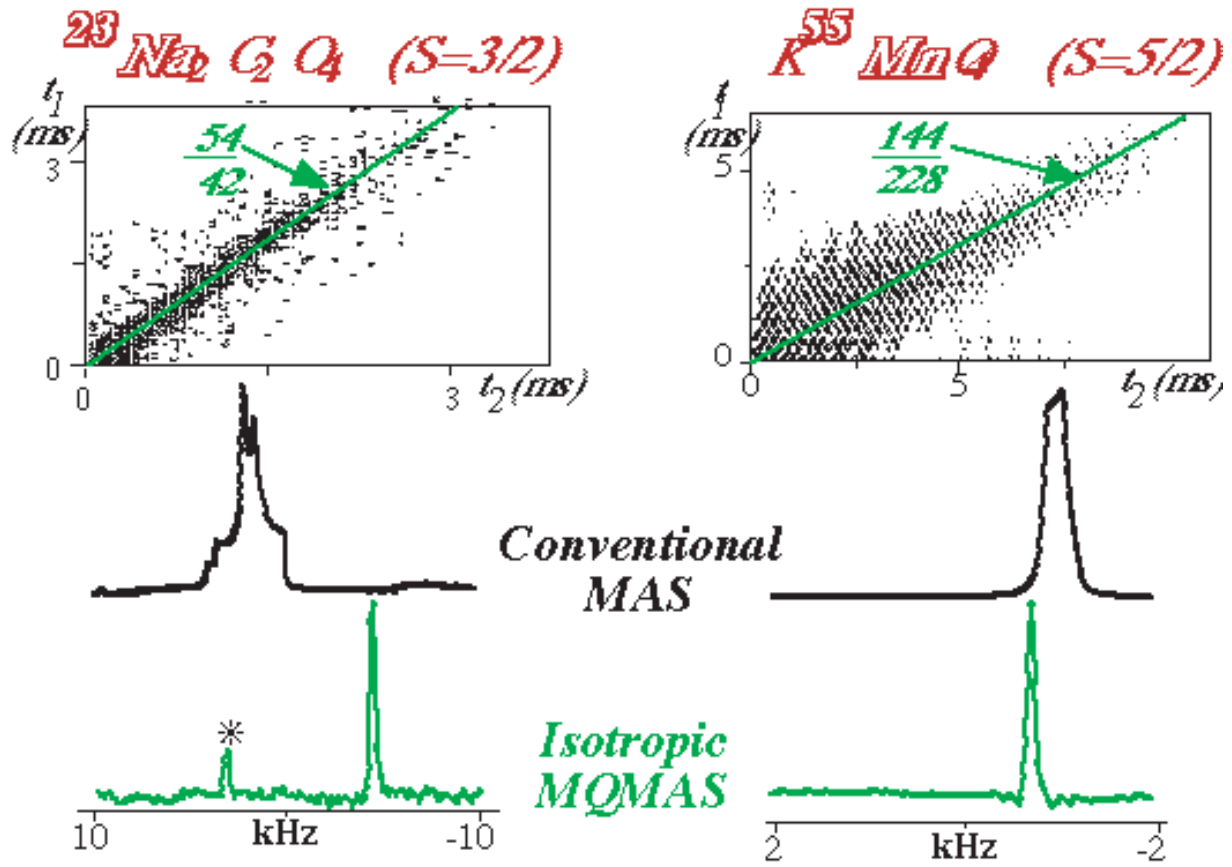

Second Order Quadrupolar Interactions

isotropic spectra at the magic angle

L. Frydman and coworkers (1995-present)
http://www.weizmann.ac.il/chemphys/Frydman_group/home.html

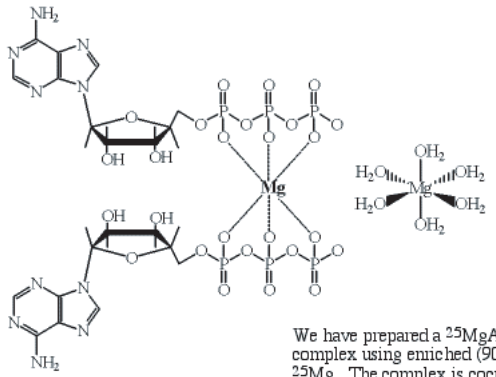

We have prepared a ^{25}MgATP complex using enriched (90%) ^{25}Mg. The complex is cocrystalized with bis(2-pyridyl)amine (BPA) and has been studied crystallographically by Cini et al. 1984.

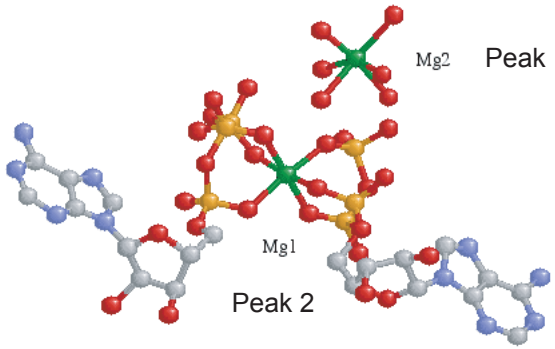

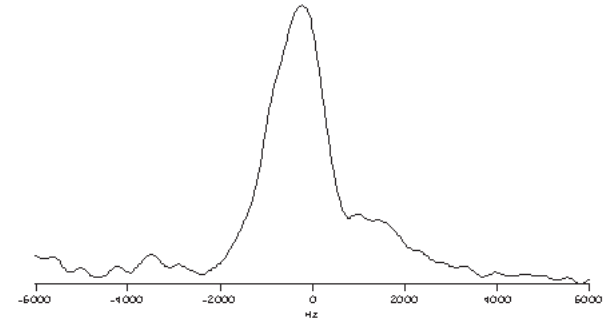

one-dimensional spectra do not give access to strucutral information

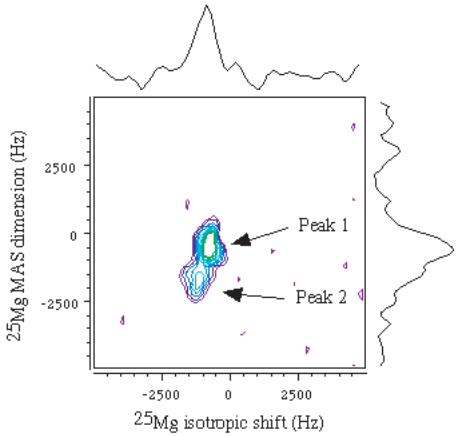

Simulation:

Peak 1:
$e^2qQ = 1.6$ MHz
$\eta = 1.0$
$\delta iso = -2.0$ ppm

Peak 2:
$e^2qQ = 2.3$ MHz
$\eta = 1.0$
$\delta iso = -9.0$ ppm

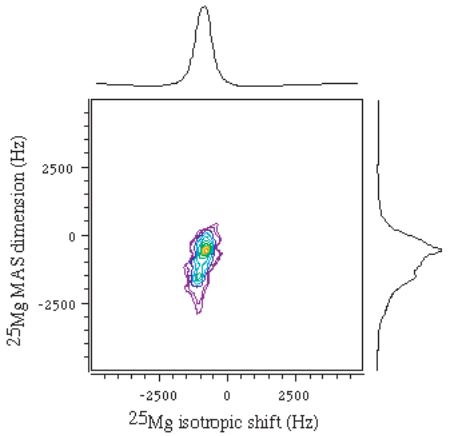

Arguably, the most important biological metal is magnesium. However, few techniques are available for the spectroscopic investigation of this closed shell, diamagnetic ion. Here the Frydman group illustrate the use of solid-state NMR to investigate the NMR properties of magnesium(II) in complex with adenosine 5'-triphosphate and bis(2-pyridyl)amine (BPA). This complex has been previously studied crystallographically and the BPA allows for high quality crystals.

Second Order Quadrupolar Interactions

isotropic spectra at the magic angle

A.Lafuma, F.Fayon, D.Massiot, S.Chodorowski Kimmes, C.Sanchez, 'Solid-state NMR characterization of oxygen sites in organically modified aluminosilicate xerogels.', Magnetic Resonance in Chemistry, 41 pp944-948 (2003).

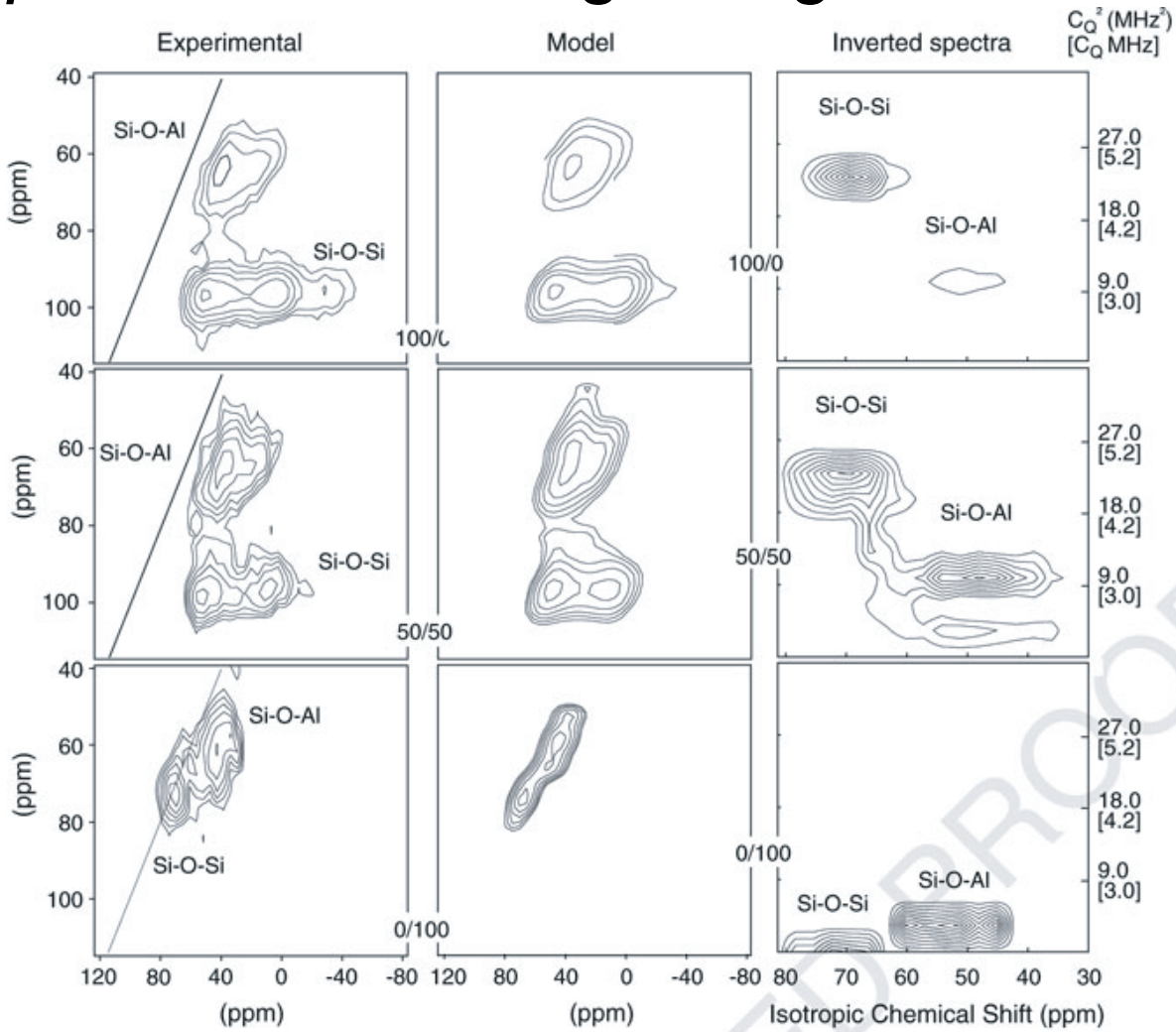

Figure 2. Experimental ^{17}O 3Q-MQMAS NMR spectra of TDA 100/0 (top), TDA 50/50 (middle) and TDA 0/100 (bottom) samples, with their respective inversion figures, and recomputed model spectra. The line drawn on the experimental spectra represents the 1/1 correlation of isotropic chemical shifts (where peak would reside for negligible quadrupolar coupling). Experimental and modelled MQMAS spectra are reported using bottom (F_2) and left (F_1) ppm scales, while inversion figures are given as correlation between isotropic chemical shift (δ) and squared quadrupolar coupling (C_Q^2), assuming $\eta_Q = 0$. Distributions of chemical shift and quadrupolar parameters can be directly obtained from the inversion figures whereas they give rise to spreading over the diagonal or away from the diagonal in the standard MQ-MAS experiments.

Second Order Broadening is Reduced at High Field

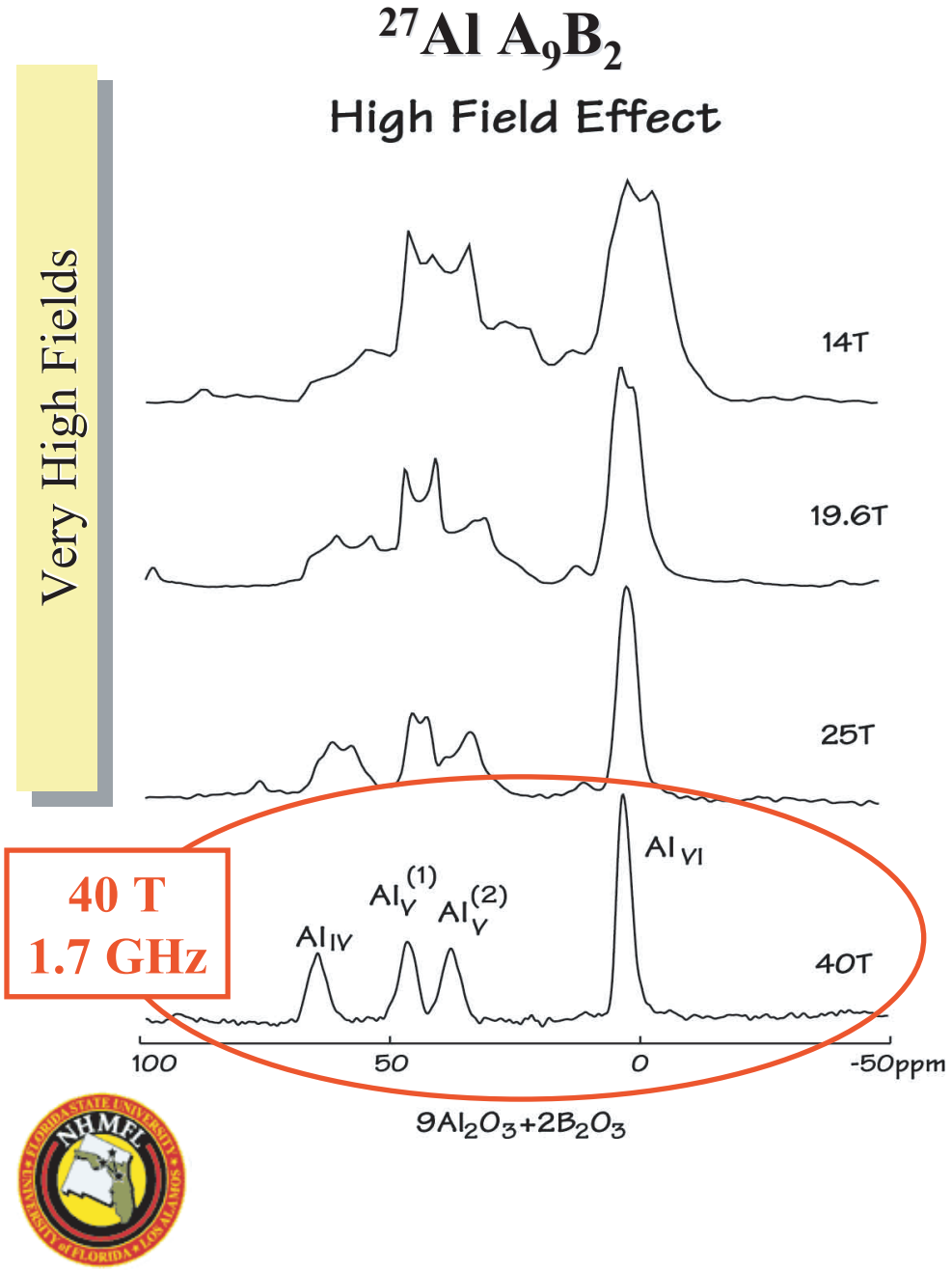

Second order quadrupolar broadening is proportional to B_0^{-2}

Gan, Gor'kov, Cross, Samoson, Massiot, JACS **124** 5634-5635 (2002)

- Q: Why don’t we see much solution-state NMR of quadrupoles?

- A: The quadrupolar integration is >100 times larger than the dipolar interaction: it usually leads to very efficient relaxation.

- Very fast relaxation leads to very broad lines and a consequent loss of resolution… less chemical information.

- (Some solution quadrupolar NMR is done, typically, on ^{23}Na, ^{27}Al, ^{14}N, ^{2}H…)

Conclusions

- Spins I > 1/2 have undergo the quadrupolar interaction: a coupling between the nuclear charge distribution and the electric field gradient at the nucleus.

- It leads to spectra with an isotropic centerband (for half-integer spins, to first order) and to anisotropic satellite transitions

- For most spins, the quadrupolar couplings are large (>MHz) and depend sensitively on the electronic structure.

- For ^{2}H, the quadrupolar coupling is around 200 kHz and does not depend much on structure. Observation of ^{2}H quadrupolar couplings yields a measure of local mobility.

nature reviews methods primers

Primer | Published: 14 January 2021

Solid-state NMR spectroscopy

Bernd Reif, Sharon E. Ashbrook, Lyndon Emsley & Mei Hong

Nature Reviews Methods Primers **1**, Article number: 2 (2021) | Cite this article

For a more detailed introduction to solid-state NMR methods and applications, read the primer available here: https://www.nature.com/articles/s43586-020-00002-1

and on Moodle

insoluble Alzheimer's proteins determined by MAS NMR

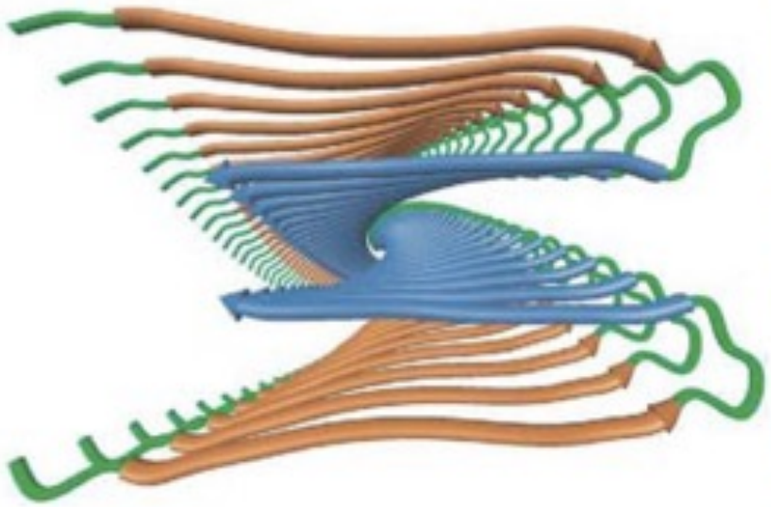

In the 1960s, the work of Andrew, Waugh, Pines, Stejskal and Shaeffer, provides high resolution spectra from solids with magic angle spinning (MAS). From 1994 onwards Griffin (MIT) provides increasingly detailed evidence for functional mechanisms in membrane proteins such as rhodopsin and bacteriorhodopsin, shining light on the primary steps in vision; in 2002 Tycko (NIH) uses NMR techniques to provide the first structure of the plaque forming amyloid proteins responsible for Alzheimer's disease; and in 2006 Oschkinat (Berlin) shows preliminary three-dimensional structures for membrane incorporated proteins obtained from 900 MHz NMR spectra.

JACS
JOURNAL OF THE AMERICAN CHEMICAL SOCIETY

Article

NMR Detection of pH-Dependent Histidine-Water Proton Exchange Reveals the Conduction Mechanism of a Transmembrane Proton Channel

Fanghao Hu, Klaus Schmidt-Rohr, and Mei Hong

J. Am. Chem. Soc., **Just Accepted Manuscript** • DOI: 10.1021/ja2081185 • Publication Date (Web): 05 Oct 2011

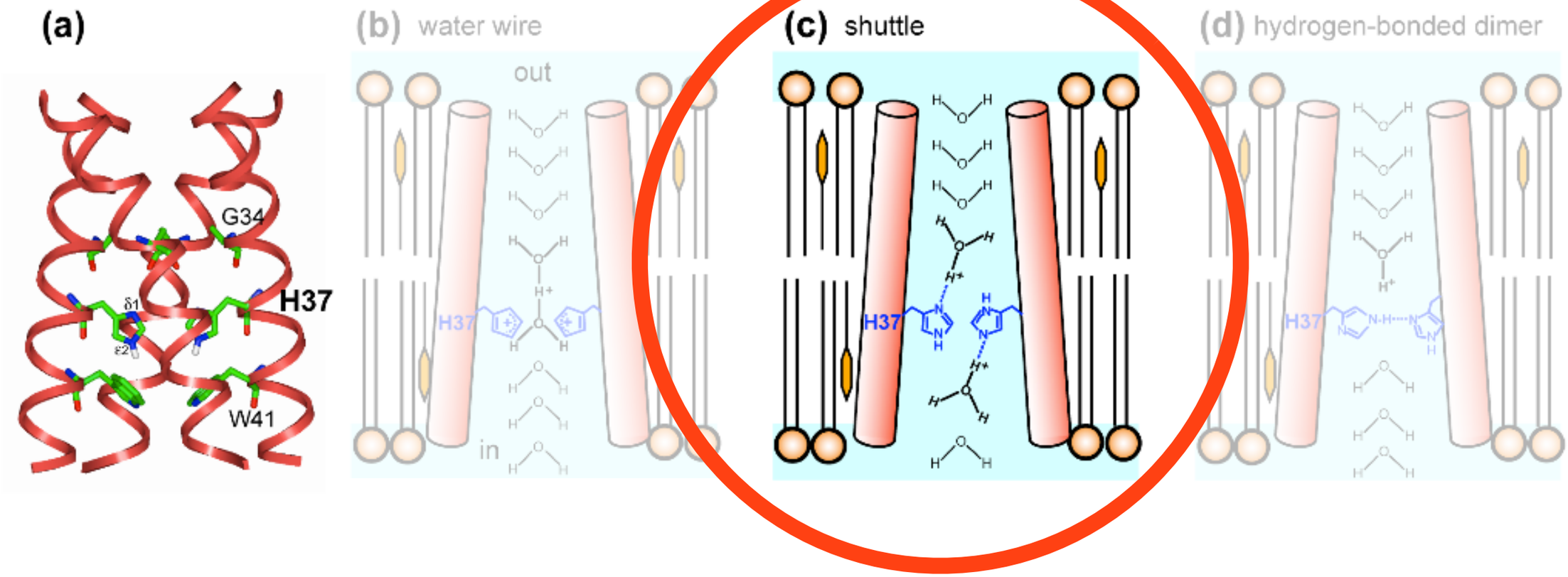

2015: ^{1}H Detected NMR with Fast MAS@1GHz

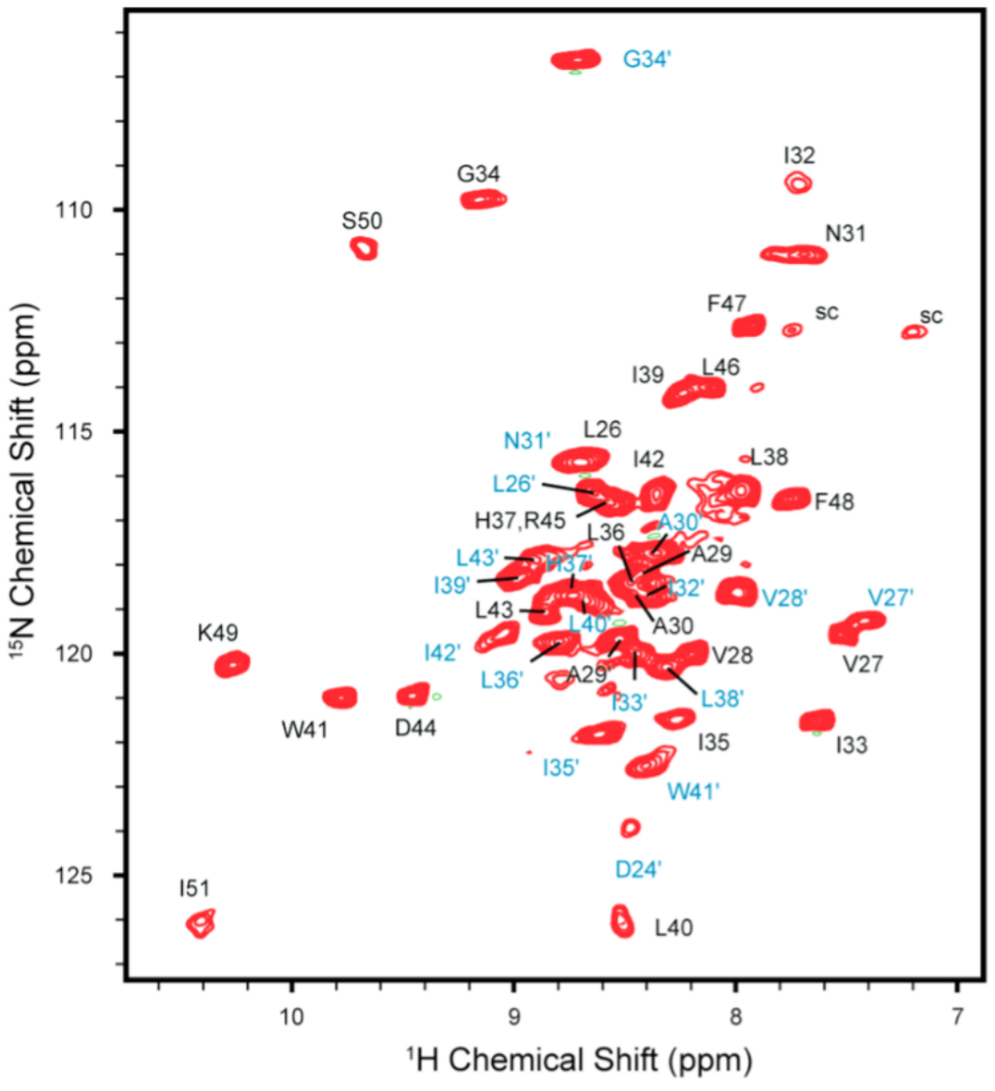

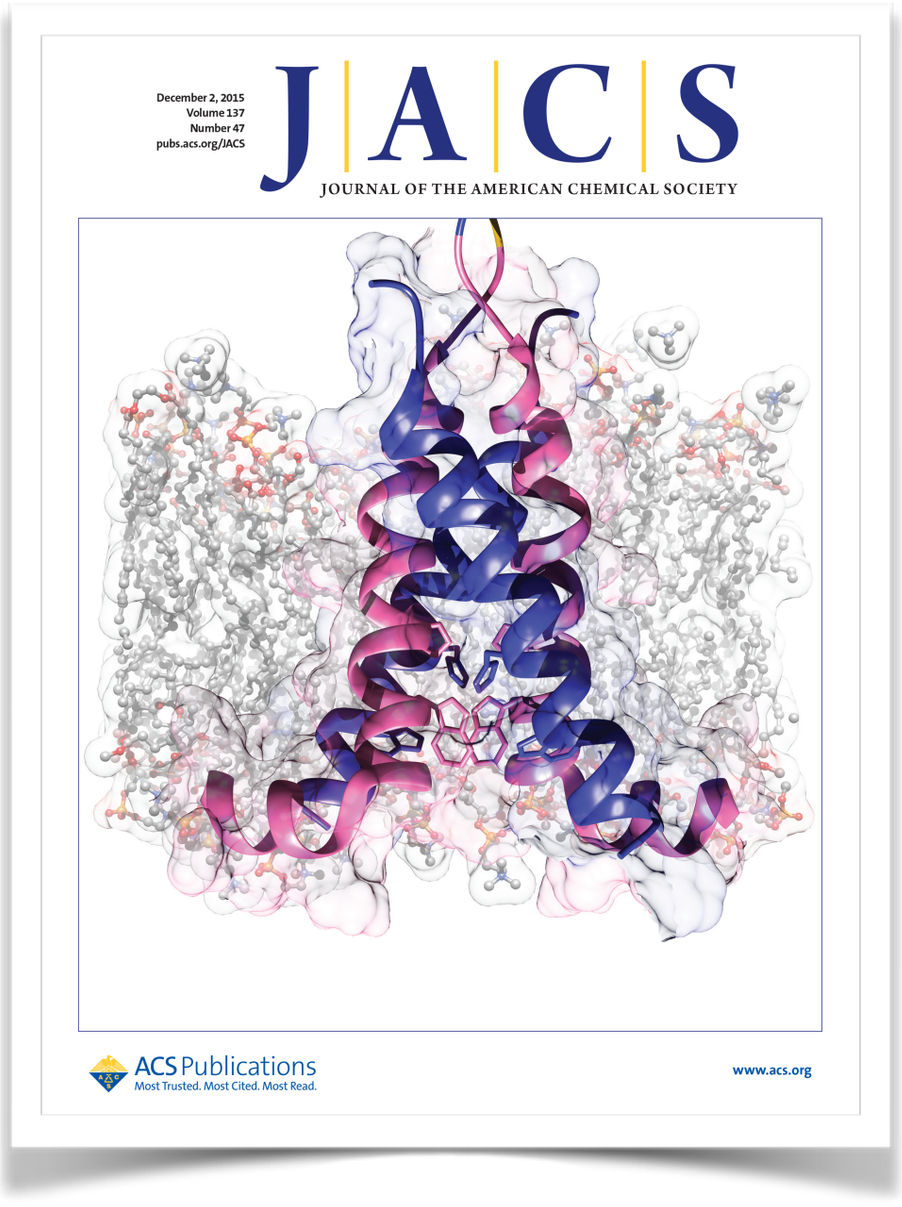

Structure and Mechanism of the Influenza A M2$_{18-60}$ Dimer of Dimers

Loren B. Andreas,[†] Marcel Reese,[†] Matthew T. Eddy,[†] Vladimir Gelev,[‡] Qing Zhe Ni,[†] Eric A. Miller,[†] Lyndon Emsley,[∥] Guido Pintacuda,[§] James J. Chou,[⊥] and Robert G. Griffin*[,†]

J. Am. Chem. Soc. **137**, 14877 (2015)

ÉCOLE POLYTECHNIQUE
FÉDÉRALE DE LAUSANNE

Carbon-13 Chemical Shifts

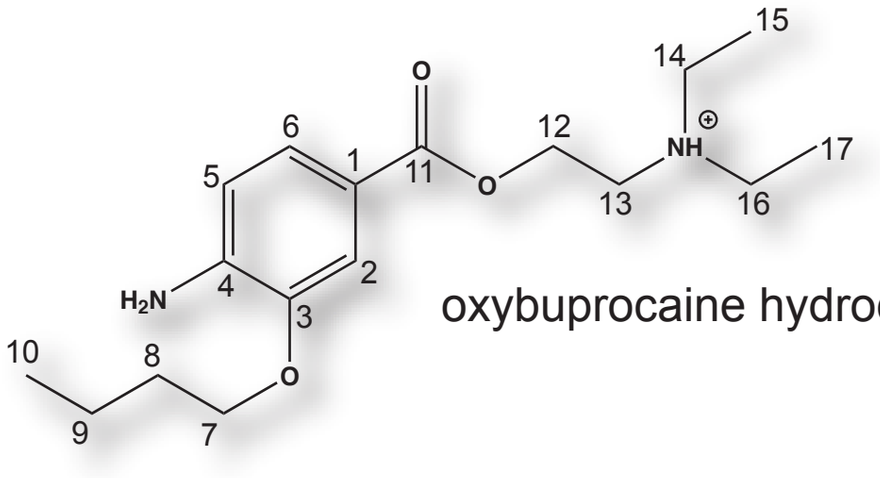

oxybuprocaine hydrochloride

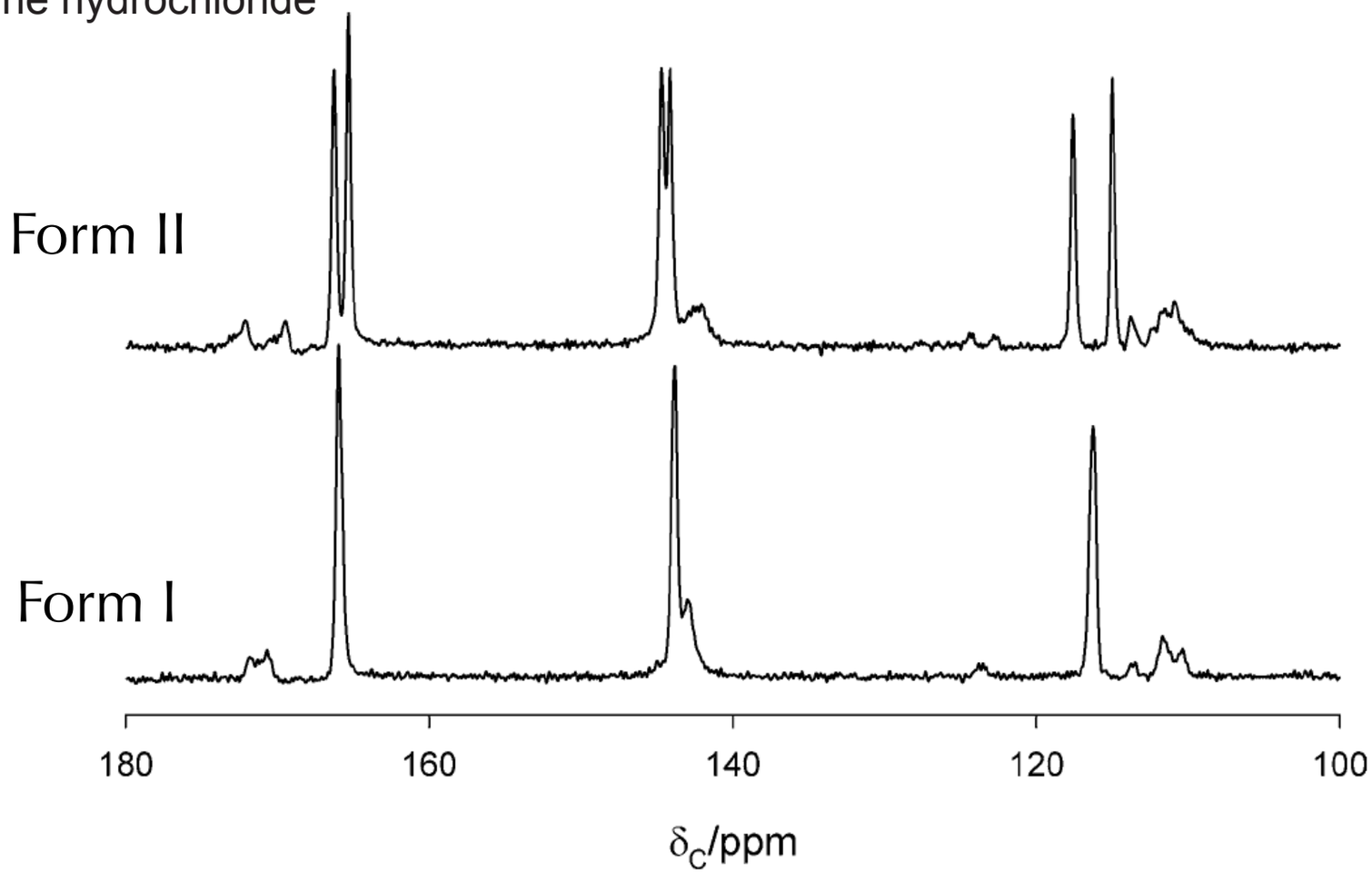

Solid-state chemical shifts reflect the precise crystalline environment

Harris, Sol. State. Sci. **6**, 1025 (2004)

Intermolecular ^{15}N-^{15}N *J* Couplings Across Hydrogen Bonds in the Solid-State

G-ribbon

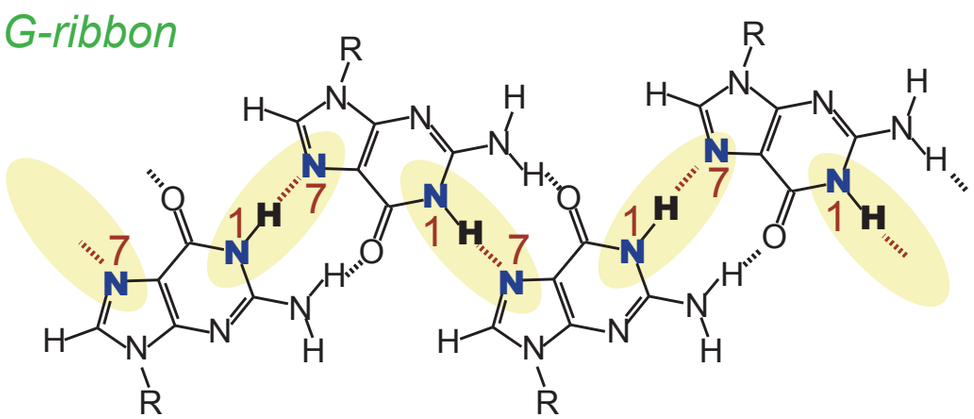

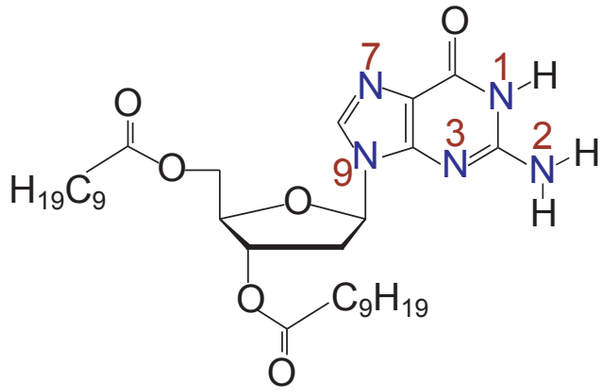

G-quartet

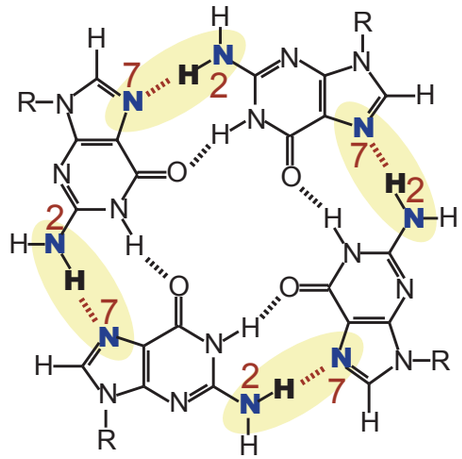

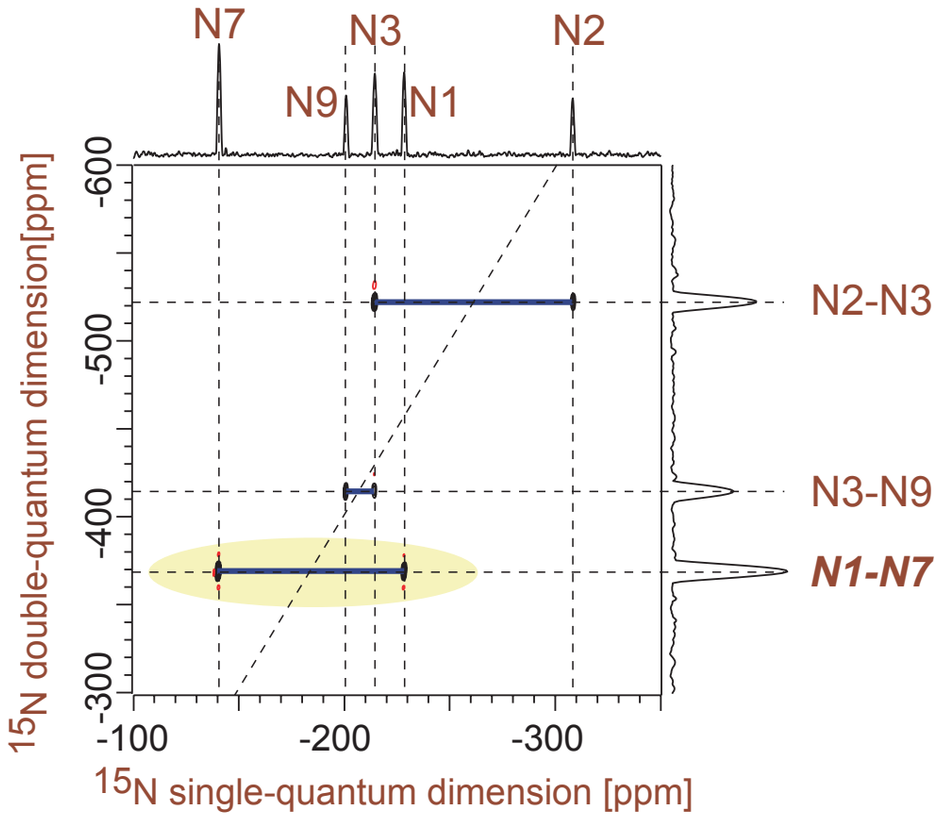

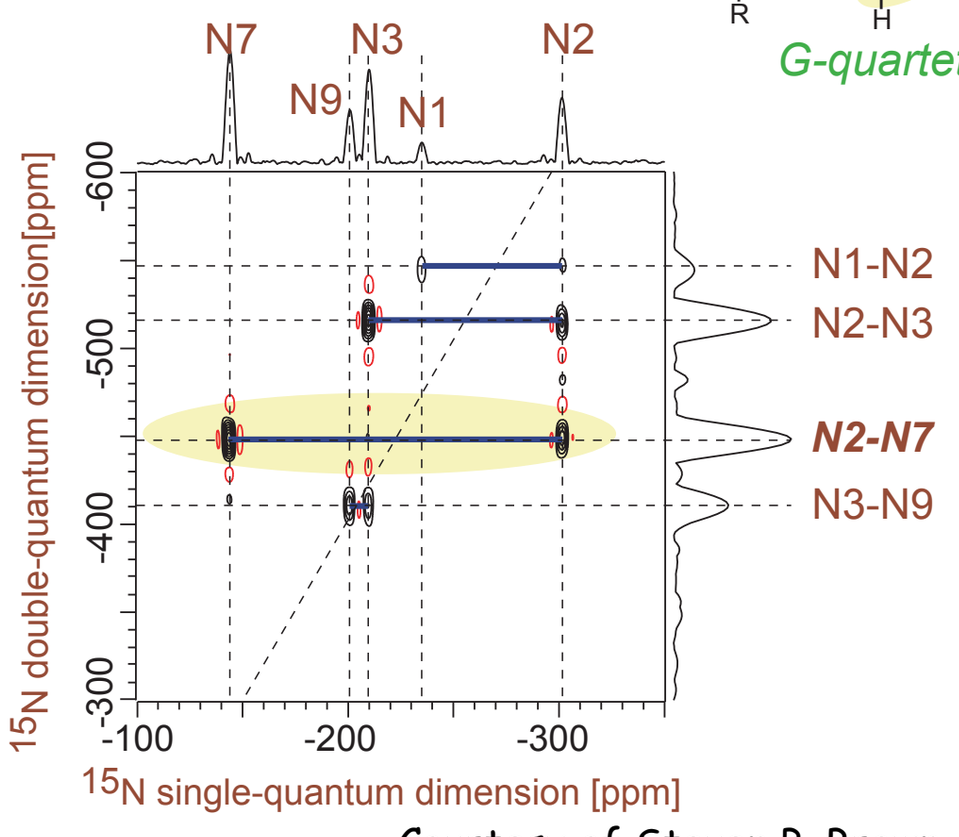

Courtesy of Steven P. Brown, Warwick

De Novo Determination of a Previously Unknown Structure

(Form 4 of AZD8329, a large drug molecule)

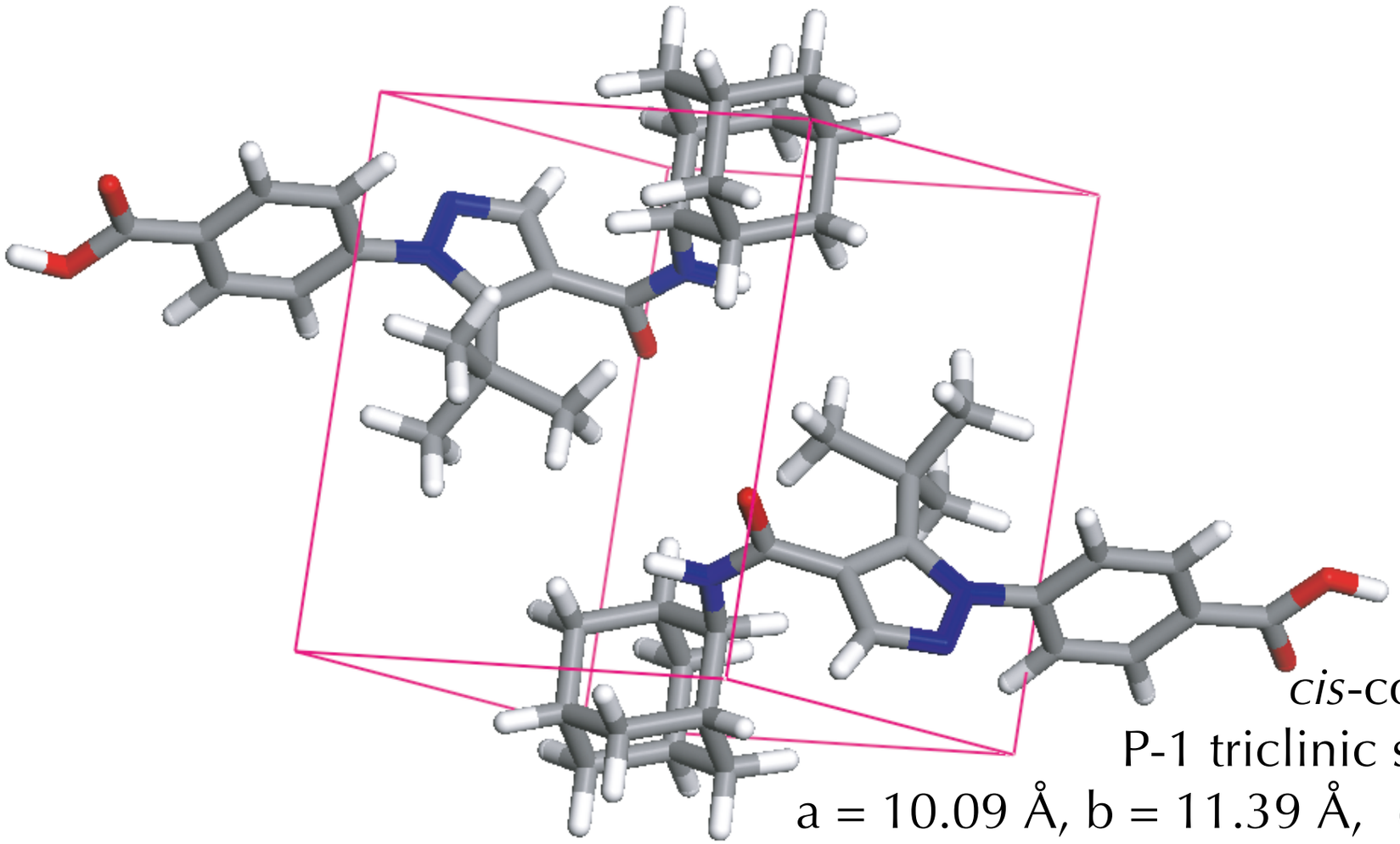

cis-conformation
P-1 triclinic space group
a = 10.09 Å, b = 11.39 Å, c = 13.17 Å
α = 99.1°, β = 59.5°, γ = 73.3°

First *de novo* determination of an unknown structure of an organic solid from NMR, DFT Chemical Shift Calculation and Computational Crystal Structure Prediction

J. Am. Chem. Soc. **135**, 17501 (2013)

(Multi-Dimensional) NMR Provides Atomic-Level Structures in Bulk Materials

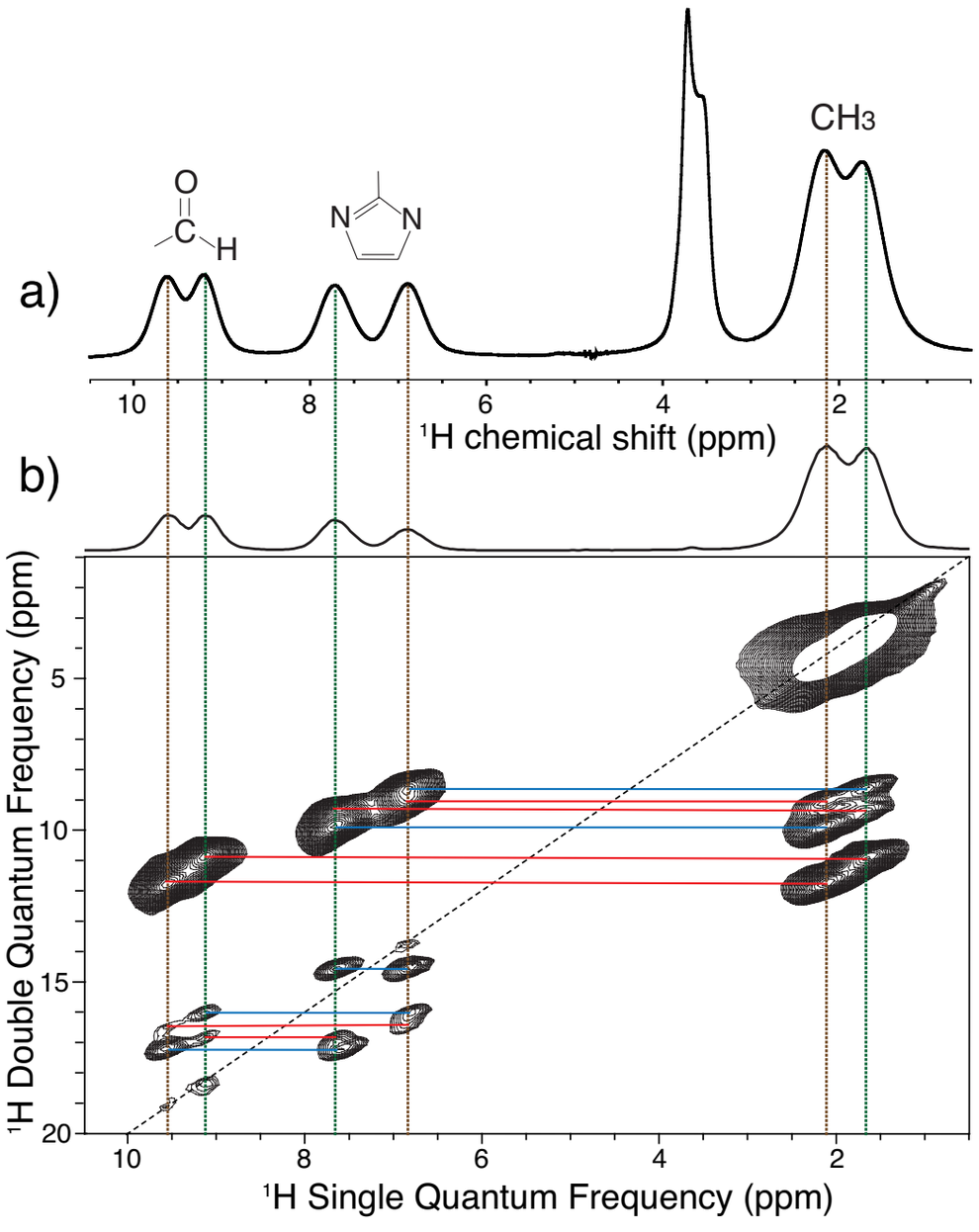

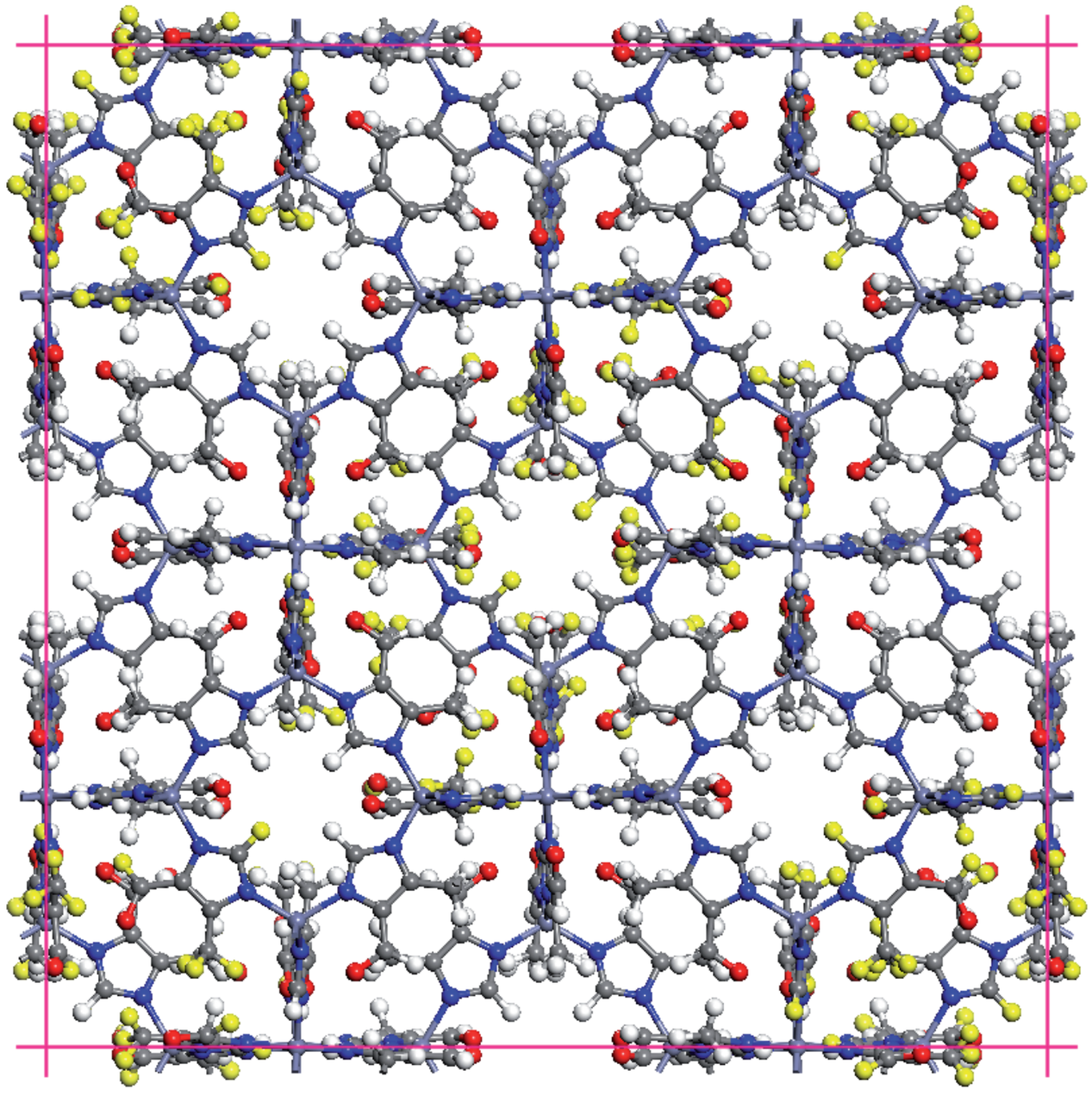

Here, 2D ^{1}H NMR in combination with DFT and PXRD yields the complete structure of the SIM-1 Metal Organic Framework

Angew. Chem. Intl. Ed. **54**, 5971 (2015)

J. AM. CHEM. SOC. 2004, *126*, 9425- 9432

Structure of a Surfactant-Templated Silicate Framework in the Absence of 3D Crystallinity

Niklas Hedin,[≤,] Robert Graf,[β] Sean C. Christiansen,[≤] Christel Gervais,[#] Ryan C. Hayward,[≤,] Juergen Eckert, [,|] and Bradley F. Chmelka*[,≤,]

Contribution from the Department of Chemical Engineering, UniVersity of California, Santa Barbara, California, 93106, Materials Research Laboratory, UniVersity of California, Santa Barbara, California, 93106, Max-Planck-Institute für Polymerforschung, Postfach 3148, D-55021 Mainz, Germany, Los Alamos National Laboratory, Los Alamos, New Mexico 87545, and Laboratoire de Chimie de la Matiere Condensee, UniVersite Pierre et Marie Curie, CNRS-UMR 7574, 4 Place Jussieu, 75252 Paris CEDEX 05 France

Abstract: The structure of a novel molecularly ordered two-dimensional (2D) silicate framework in a surfactant-templated mesophase has been established by using a combination of solid-state nuclear magnetic resonance (NMR) spectroscopy, X-ray diffraction, and quantum chemical and empirical force-field modeling. These materials are unusual in their combination of headgroup-directed 2D crystalline framework ordering, zeolite-like ring structures within the layers, and long-range mesoscopic organization without three-dimensional (3D) atomic periodicity. The absence of registry between the silicate sheets, resulting from the liquidlike disorder of the alkyl surfactant chains, has presented significant challenges to the determination of framework structures in these and similar materials lacking 3D crystalline order. Double-quantum ^{29}Si NMR correlation experiments establish the interactions and connectivities between distinct intra-sheet silicon sites from which the structure of the molecularly ordered inorganic framework is determined.

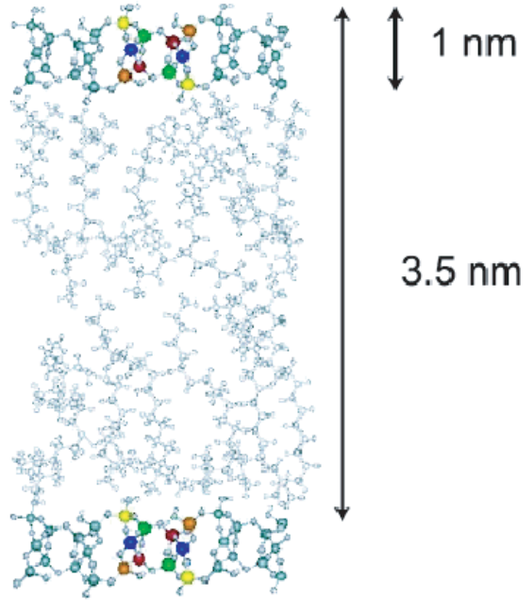

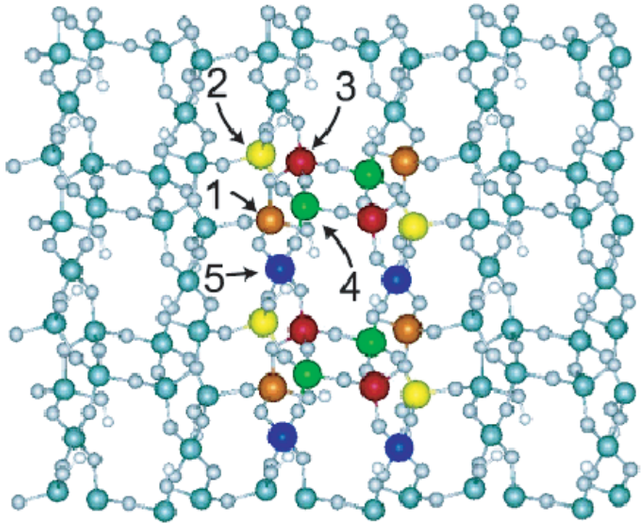

Figure 1. Energy-minimized structure of the molecularly ordered silicate sheets in the lamellar silicate- $C_{16}N^+Me_2Et$ mesophase. (a) Side-view, showing the layered structure in profile. The alkyl chains of the surfactant are disordered; their positions are not exact. (b) Top-view of the 2D silicate framework showing four- and six-membered silicate rings. The five different tetrahedrally coordinated silicon sites are highlighted, and the surfactant molecules are excluded for clarity. Two of the silicon sites are incompletely condensed Q^3 species, site 1 (orange) and site 2 (yellow), while site 3 (red), site 4 (green), and site 5 (blue) are fully condensed Q^4 moieties. The various Si sites correspond to the respectively labeled peaks in the 1D ^{29}Si MAS NMR spectrum of Figure 2.

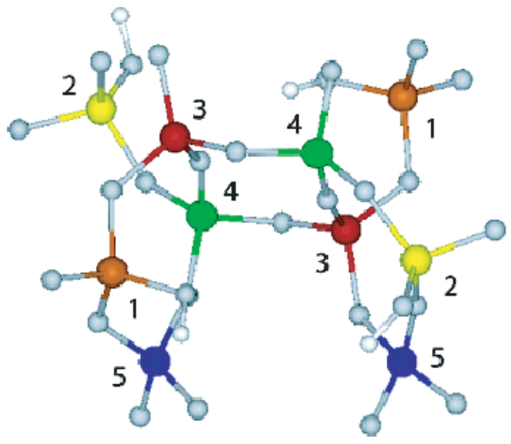

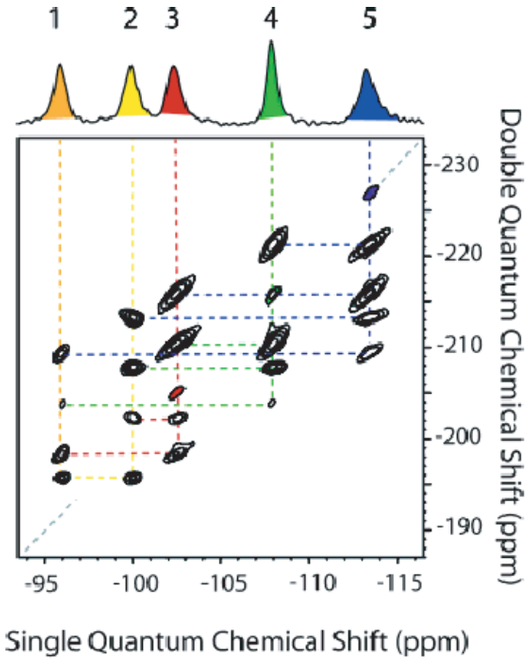

Figure 2. Dipole- dipole-mediated 2D Double-Quantum ^{29}Si{^{29}Si} MAS NMR spectrum from a lamellar silicate- $C_{16}N^+Me_2Et$ mesophase with a molecularly ordered framework, enriched 50% in ^{29}Si. A single-pulse ^{29}Si MAS NMR spectrum, with five resolved peaks of equal 1:1:1:1:1 integral intensities accompanies the contour plot along the horizontal single-quantum dimension, while the double-quantum dimension lies along the vertical axis. Spatial proximities between pairs of dipole- dipole-coupled ^{29}Si sites are established by correlated ^{29}Si signal intensities at identical double-quantum, chemical shifts. The lowest contour level is at 4% of the full intensity, and each new level corresponds to an intensity increase by a factor of 2. The molecular building unit from which the ordered silicate framework is constructed (see discussion below) accompanies the spectrum.

glasses, new materials, and nanosciences

Quadrupolar nuclei have always played a leading role in NMR. Since the 90s oxygen and aluminum NMR studies have continuously contributed to change the understanding we have of the structure and dynamics of glass forming materials and their related molten state. This is now changing the whole way we think about the formation and structure of disordered materials. In 2006 Grey and coworkers use understanding from NMR observations directly to improve the charging rate capacity of lithium nickel magnanese oxide in rechargeable batteries. In 2010 Emsley and coworkers introduce Dynamic Nuclear Polarisation Surface Enhanced NMR Spectroscopy (DNP SENS), and in 2014 they use this new method to solve the structure of core-shell nanoparticles.

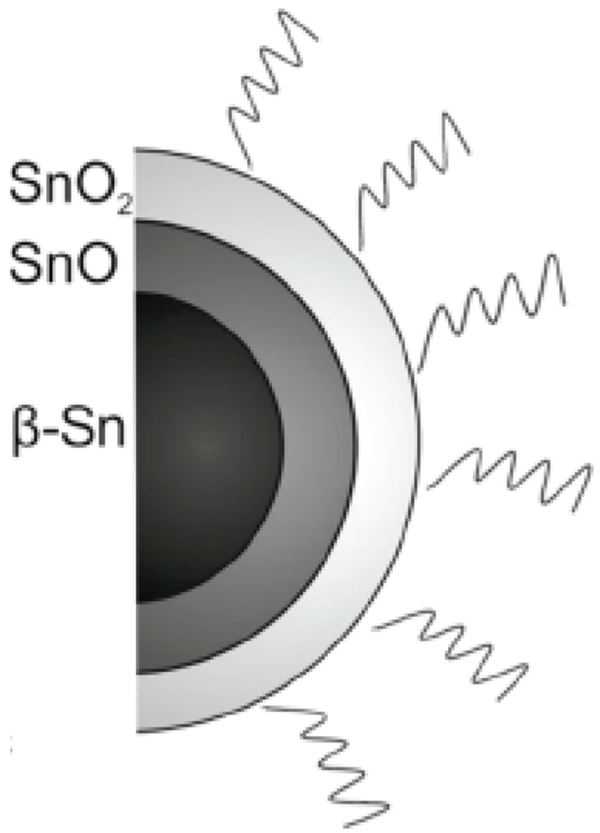

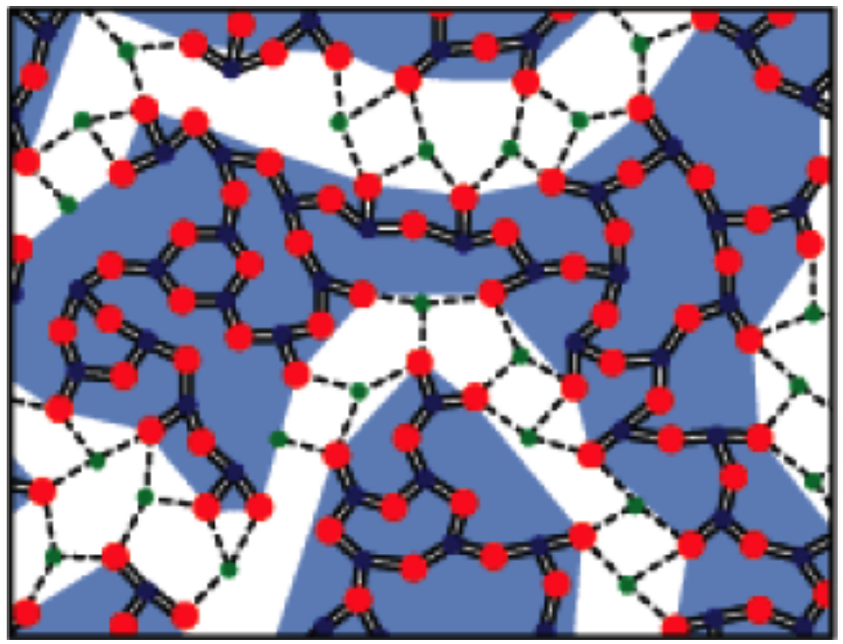

Quantification of actinide α-radiation damage in minerals and ceramics

Ian Farnan[1], Herman Cho[2] & William J. Weber[2]

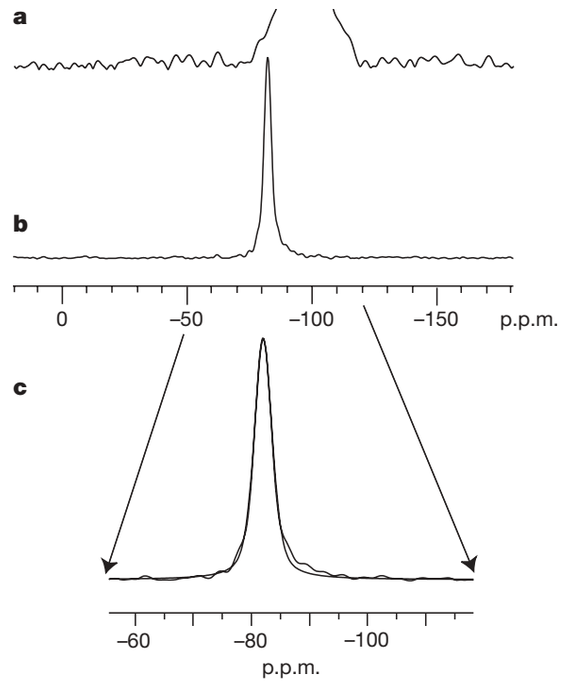

Figure 3 | The effect of plutonium α-self-irradiation on the local structure of Pu-doped ceramic zircons. ^{29}Si MAS NMR spectra of $^{238}Pu_{0.08}Zr_{0.92}SiO_4$ (**a**) and $^{239}Pu_{0.08}Zr_{0.92}SiO_4$ (**b**). The expansion in **c** of this high-resolution and high-sensitivity spectrum reveals the onset of internal radiation damage in the ^{239}Pu material. A damage fraction of 0.03 ± 0.02 can be computed by subtracting the fitted crystalline component.